RONALD BOOIJ

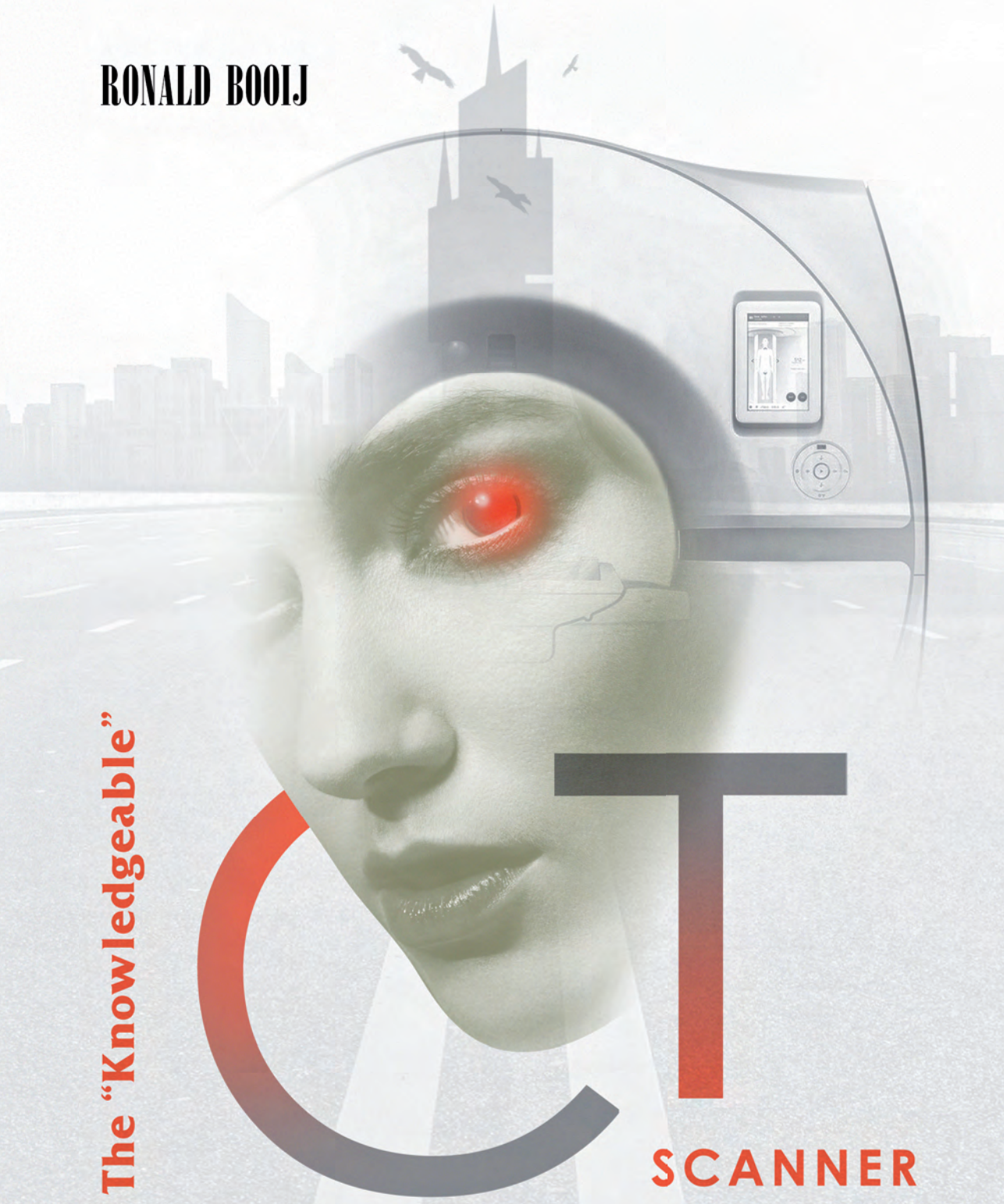

The "Knowledgeable"

CT SCANNER

Optimization by technological advancements

The “Knowledgeable” CT Scanner

Optimization by technological advancements

Ronald Booij

ISBN 978-94-6361-489-4
Layout and print by Optima Grafische Communicatie (www.ogc.nl)

The "Knowledgeable" CT Scanner

Optimization by technological advancements

De "intelligente" CT-scanner

Optimalisatie door technologische vooruitgang

Proefschrift

ter verkrijging van de graad van doctor aan de
Erasmus Universiteit Rotterdam
op gezag van de
rector magnificus

Prof.dr. F.A. van der Duijn Schouten

en volgens besluit van het College voor Promoties.

De openbare verdediging zal plaatsvinden op
dinsdag 23 februari 2021 om 13.00 uur

door

Ronald Booij

geboren te Rozenburg, Nederland

Erasmus University Rotterdam

PROMOTIECOMMISSIE:

Promotor:
Prof.dr. G.P. Krestin

Overige leden:
Prof.dr. A. van der Lugt
Prof.dr. M. Prokop
Prof.dr. H.A.W.M. Tiddens

Copromotoren:
Dr. R.P.J. Budde
Dr.ir. M. van Straten

Sandra, Julia en Timo, deze is voor jullie!

CONTENTS

PART I

Preface

CHAPTER 1

Introduction and outline

INTRODUCTION

A Computed Tomography (CT) scanner is a machine that provides cross-sectional images of a human body or scanned object, e.g. medical imaging phantoms, by the use of x-rays. After its introduction in the early seventies, CT has fundamentally changed the practice of medicine by expanding our knowledge about diseases and management of major health challenges [1]. With technological innovations, like high speed scanning, diagnostic capabilities improved in both adult and pediatric patients [2]. However, the associated radiation dose in CT scanning and the associated possible increase of the cancer risk in individuals are of concern. Especially when the radiation dose applied is high, or when imaging children as they are more sensitive to radiation effects [3]. Without doubt, CT scanning is the biggest contributor to the collective effective dose of medical examinations worldwide [2, 4-6]. Over the years, CT dose reduction strategies have been introduced, leading to a continuous decrease in radiation dose, but also an increase in complexity to determine the appropriate doses for specific diagnostic tasks and individual patients [7]. Even though the individual radiation dose decreases, there is an increase in the number of CT exams performed worldwide. Therefore, justification and optimization of a CT protocol is still important [8].

Changing CT scanning protocol parameters will influence both radiation dose and image quality (IQ).Therefore, optimization of a CT exam is not only about reducing the radiation dose, but also ensuring that diagnostic confidence of clinical tasks is retained. Objective and subjective IQ estimates do not necessarily correlate with diagnostic performance and this should be kept in mind within the optimization steps, especially when imaging various patient body types [9, 10]. Reducing radiation dose will lead to a decrease in lesion detectability, especially of more subtle lesions. This implies that a minimum dose level is required for a certain diagnostic accuracy [10]. Overall, technological developments resulted in a reduction of radiation dose per exam and improved IQ [11, 12]. In the meantime, the impact of technological developments was not restricted to optimizing a CT study itself, but played a role along the entire imaging chain: patient planning was digitized, digital application forms were introduced, and patients got easy access to their medical records. In addition, the image reconstruction, post-processing and reporting of medical images has fundamentally changed over the years through automation and artificial intelligence (AI) support.

"Knowledgeable" algorithms and tools may assist users with the deployment of new technologies and the processing of the increased amount of data. However, are the "knowledgeable" solutions beneficial and what does "knowledgeable" mean in this context? Knowledge is about understanding of something, Thereby, it should be supported by rationality and evidence, and not by chance [13-17]. Therefore, chance should be ruled out in CT imaging as much as possible by building a knowledge base on the

outcomes of validated studies, based on both human and phantom studies. Then, the knowledge obtained can be implemented by the team of radiographers, radiologists and medical physicists to benefit from its full potential for the optimization of a CT scan procedure. However, this can be quite a challenge because of several factors: interrelation of numerous scan and reconstruction parameters, increased workload and human error. In addition, updates within hardware and software requires verification and validation of (new) protocols and the variety of patients and referral questions necessitates different acquisition strategies. This ultimately leads to the need for a "knowledgeable" CT scanner that makes procedures more accurate, standardized and supports the users.

SCOPE AND OVERVIEW OF THIS THESIS

As developments were introduced to optimize a CT exam, the original steps within the imaging chain remain almost the same. A CT exam consists of several consecutive steps: Indication, logistics, the actual scan procedure and the image interpretation and advice (Fig. 1). The urgency in planning of the appropriate acquisition technique heavily depends on the indication. After a CT exam is ordered and planned, the patient can be seen and positioned on the CT scanner table. Once the scanning and contrast injection protocol is tailored to the needs of an individual patient and the clinical question, the data is acquired and the image is reconstructed, post-processed and archived by radiographers and interpreted by a radiologist. As ongoing technological developments are introduced into the diagnostic imaging chain, some of the reconstructions and data (post-)processing steps blend into both the "Scanning procedure" (performed by radiographers) and "Diagnosis & Advice" (performed by radiologists) categories (Fig. 1). In addition, AI is integrated more and more in most of the steps of the imaging chain as well. Even though AI is able to "learn" from analyzing more and more cases, it remains important to know and monitor their performance, as well as to determine their accuracy. This thesis focuses on evaluation and implementation of technological solutions to automate and / or improve distinct aspects of the CT imaging chain including: 1) patient positioning, 2) scan and contrast injection tailoring to the individual pediatric patient, 3) improved image reconstruction technique to facilitate dose reduction in coronary calcium scoring and 4) reduction of unused radiation exposure at the boundaries of the scan range as described below.

Patient positioning

Patient positioning in the isocenter of the CT scanner is essential for optimal imaging. The automatic exposure control (AEC) of a CT scanner continuously adapts the tube output to every individual patient to obtain consistent image quality. The AEC uses the localizer

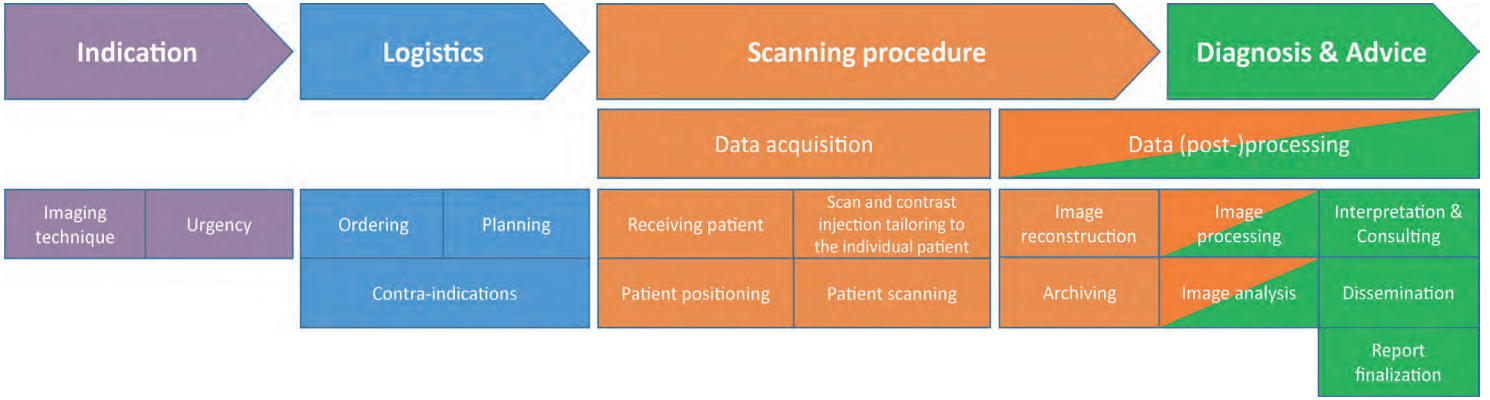

Figure 1. Graphical illustration of the steps in the diagnostic imaging chain for a CT exam. Each color represent a link in the imaging chain. Nowadays, the radiologist is able to perform additional post-processing within the "diagnosis & advice" category, for example image processing. An overlap between the "data acquisition" and "data (post-)processing" steps within the imaging chain are highlighted by the orange/green illustration.

radiograph, which is also used for planning of the scan ranges, as input to determine the patient's size and body composition. Optimal functioning of the AEC hence relies on the consistency and quality of this localizer radiograph. Therefore, proper patient positioning is required to overcome distortion of the localizer radiograph (Figs. 2a–c) with resultant incorrect adaptation of the tube output.

Bowtie filters are shaped filters placed directly after the tube that increase in thickness from the center to the periphery of the axial plane (resembling a bow tie, hence its name). The bowtie filter reduces radiation dose to the peripheries of a patient and helps to obtain a relatively uniform noise profile. For the bowtie filters to work optimally, patient positioning in the scanner isocenter is important as well as illustrated in Figures 2d–f.

Patients are positioned in the CT scanner by the radiographer using laser beams as guidance. However, proper positioning of a patient can be challenging, especially when imaging children, because of the wide variation in body proportions. Incorrect patient positioning directly affects the performance of the AEC and bowtie filter as described above. Technological advancements for automatic patient positioning by the use of a 3D camera for body contour detection (Fig. 3) claim to improve patient positioning when compared to manual positioning by a radiographer. However, the accuracy of the advancements are not yet clear and have to be investigated.

Scan and contrast injection tailoring to the individual pediatric patient

Not only can positioning of children in a CT scanner be quite demanding, several other parts within the imaging chain can be challenging too. First of all young patients can not be instructed and ideally sedation is avoided. Thus there is a need for fast scanning. Cardiovascular CT scans add additional challenges since there is a need for motion free imaging of the heart during optimal contrast enhancement. However, the often (very) high heart rates in pedicatric patients make motion free imaging of the heart difficult and the unpredictable contrast dynamics (especially in congentital heart disease) make timing of the scan cumbersome. New generation scanners are equipped with several technological features that, when appropriately applied, can solve these problems. However, practical guidelines on how to do this are not available or only available to a limited extent. Based on our extensive experience, we describe how to tailor the cardiovascular CT acquisition to the individual pediatric patient utilizing all available technological options with an optimal balance between image quality and radiation exposure.

Improved image reconstruction technique to facilitate dose reduction

Where cardiovascular imaging in pediatric patients is mainly suited for the investigation of congenital heart disease, in adults it is generally used for investigation of suspected coronary artery disease (CAD). A cardiac CT exam in adult patients normally starts with a

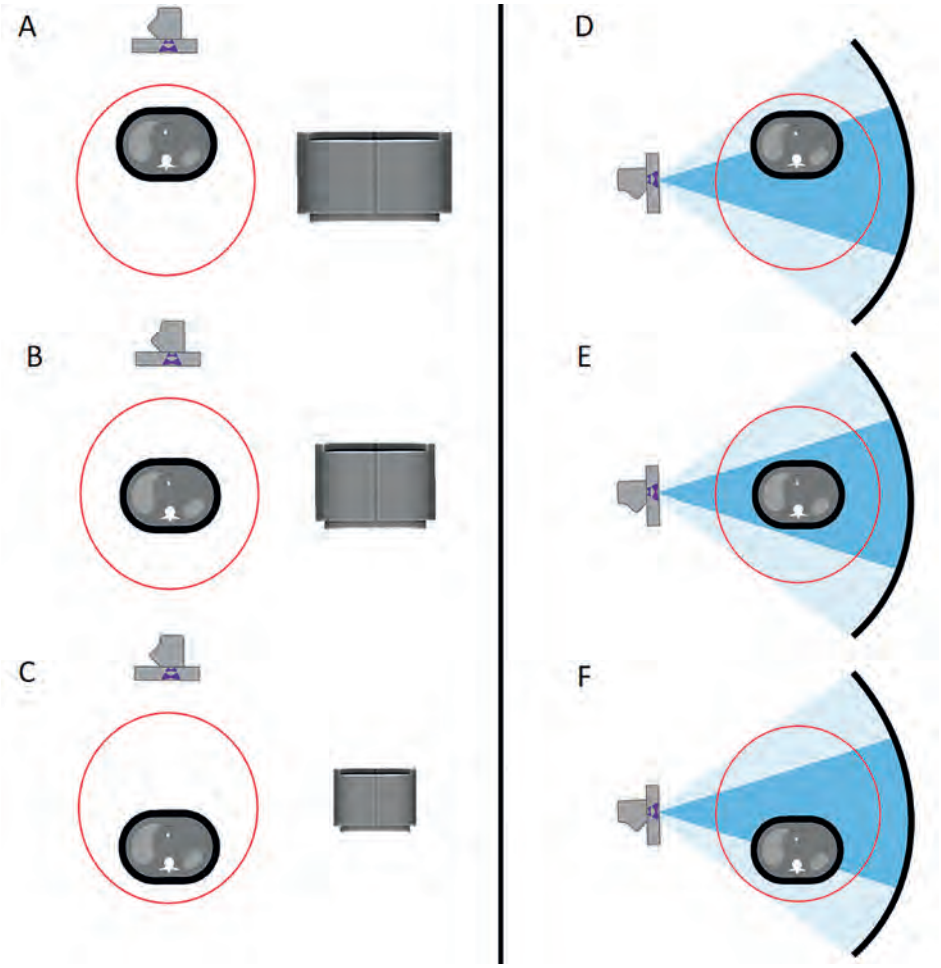

Figure 2 (a-f). The importance of proper patient positioning in CT. **(a-c)** Graphical illustration of localizer radiograph distortion: Phantom scans in isocenter **(b)** and away from the scanner isocenter with magnified **(a)** and reduced width of the localizer radiograph **(c)**. **(d-f)** Effect of table height position on radiation dose distribution due to the shape of the bowtie filter: Equal distribution of radiation dose for the upper and lower half of scanned object/patient when positioned in the scanner isocenter **(e)**. Upper part of the body is exposed to more radiation dose than the lower part of the body, with increased image noise for the lower part of the body when the object/patient is positioned below the scanner isocenter **(f)** and vice versa **(d)** when the object/patient is positioned above the scanner isocenter.

coronary artery calcium scoring, using the Agatston score as a common strategy for the quantification of coronary calcification. A limitation of the Agatston score is the need to acquire the images with a fixed peak tube voltage of 120 kV. Lowering the tube voltage potentially reduces the radiation dose which would be beneficial for calcium scoring scans as well. However, the CT numbers of calcium are tube voltage dependent. Lowering the tube voltage may result in inconsistent scores, impairing the risk assessment

Figure 3. 3D camera for body contour detection (white arrow and box) positioned above a dual source CT scanner of the Erasmus MC University Medical Center Rotterdam.

potential of the Agatston score. An improved reconstruction technique aiming at tube voltage independent CT numbers for calcium became available recently. This would be beneficial as it allows coronary calcium scans to be obtained at lower radiation dose whilst still providing an accurate coronary calcium score. The performance and dose reduction potential of this improved reconstruction technique remains to be determined.

Reduction of unused radiation exposure

One of the major developments in CT was the introduction of spiral CT and increased longitudinal coverage by wider detectors. A downside of these detectors is the increase of the so-called overranging effect in spiral CT. Due to this effect the radiation exposure range in spiral CT is longer than the actually depicted range. In order to reduce the overranging dose, technological improvements like dynamic collimators were introduced by all major CT manufactures. Dynamic collimators are mechanical blades that move in and out of the radiation area during the scan to block unused radiation at the boundaries of the scan range. Recently, a renewed dynamic collimator was introduced in a third-generation dual source CT (DSCT) scanner. However, the performance and efficacy of the dynamic collimators in different DSCT scanners is unknown.

The thesis is divided into four parts:

Part I: Preface

Chapter 1: introduction and outline of the thesis. **Chapter 2** gives an overview of technological developments in CT over half a century. In addition, the role of the associated acquisition and reconstruction parameters and the user's influence in the CT optimization process are highlighted. Hereby, the interrelation between radiation dose and image quality for many acquisition and reconstruction parameters is summarized.

Part II: Improvement of patient positioning by body contour detection with a 3D camera

Chapters 3–5 focus on the accuracy of automated patient positioning in a CT scanner with the aid of a 3D camera for body contour detection. The results for adult patients are presented in **Chapter 3** and the results for pediatric patients in **Chapter 4.** In **Chapter 5,** the influence of an inspiratory or an expiratory breathing state on the accuracy of the proposed patient positioning is demonstrated.

Part III: Improvement of acquisition and reconstruction techniques

Chapters 6–8 describe the use of several technological developments for improvement of CT protocols, some as part of automated algorithms, while other developments are directly adjustable by the user. **Chapter 6** reviews the steps in the protocol improvement of cardiovascular imaging in pediatric patients. Guidelines and the impact of technological features applied in cardiovascular imaging of pediatrics on image quality and radiation dose are given.

In **Chapter 7,** an improved reconstruction technique aiming at tube voltage independent CT numbers for calcium and its potential for radiation dose reduction is evaluated.

In **Chapter 8,** the efficacy of a dynamic collimator in a third-generation DSCT scanner was assessed and compared with the dynamic collimator used in the second-generation DSCT scanner.

Part IV: General discussion and summary

The general discussion of this thesis is presented in **Chapter 9** and the results presented in this thesis are summarized in **Chapter 10**.

REFERENCES

1. Rubin GD. Computed tomography: revolutionizing the practice of medicine for 40 years. Radiology. 2014;273(2 Suppl):S45-74.
2. Brenner DJ, Hall EJ. Computed tomography--an increasing source of radiation exposure. N Engl J Med. 2007;357(22):2277-84.
3. Brody AS, Frush DP, Huda W, Brent RL. Radiation Risk to Children From Computed Tomography. 2007;120(3):677-82.
4. Meulepas JM, Ronckers CM, Smets A, Nievelstein RAJ, Gradowska P, Lee C, et al. Radiation Exposure From Pediatric CT Scans and Subsequent Cancer Risk in the Netherlands. J Natl Cancer Inst. 2019;111(3):256-63.
5. Brugmans MJ, Buijs WC, Geleijns J, Lembrechts J. Population exposure to diagnostic use of ionizing radiation in The Netherlands. Health Phys. 2002;82(4):500-9.
6. European_Commission_Directorate-General_for_Energy. Radiation Protection No 180: Medical radiation exposure of the European population Part 1/2. EU Publications. Available from https://ec.europa.eu/energy/sites/ener/files/documents/RP180web.pdf. DOI: 10.2833/708119; 2015. Accessed 11-11-2020.
7. McCollough CH. Computed Tomography Technology-and Dose-in the 21st Century. Health Phys. 2019;116(2):157-62.
8. Brenner DJ, Hall EJ. Cancer risks from CT scans: now we have data, what next? Radiology. 2012;265(2):330-1.
9. Pickhardt PJ, Lubner MG, Kim DH, Tang J, Ruma JA, del Rio AM, et al. Abdominal CT with model-based iterative reconstruction (MBIR): initial results of a prospective trial comparing ultralow-dose with standard-dose imaging. AJR Am J Roentgenol. 2012;199(6):1266-74.
10. Solomon J, Marin D, Roy Choudhury K, Patel B, Samei E. Effect of Radiation Dose Reduction and Reconstruction Algorithm on Image Noise, Contrast, Resolution, and Detectability of Subtle Hypoattenuating Liver Lesions at Multidetector CT: Filtered Back Projection versus a Commercial Model-based Iterative Reconstruction Algorithm. Radiology. 2017;284(3):777-87.
11. Christe A, Heverhagen J, Ozdoba C, Weisstanner C, Ulzheimer S, Ebner L. CT dose and image quality in the last three scanner generations. World J Radiol. 2013;5(11):421-9.
12. Rehani MM. Radiation protection in newer imaging technologies. Radiat Prot Dosim. 2010;139(1-3):357-62.
13. Conee E, Feldman R. Evidentialism: Essays in Epistemology: Oxford University Press; 2004: 15-34.
14. Gettier EL. Is Justified True Belief Knowledge? Analysis. 1963;23(6):121-3.
15. Goldman A. What is Justified Belief. In: Pappas G, editor. Justification and Knowledge: D. Reidel; 1979. 1-25.
16. Russell S, Norvig P. Artificial Intelligence: A Modern Approach - 3rd Edition: Pearson Education, Inc.; 2016.
17. Chappell S. Plato on Knowledge in the Theaetetus: Metaphysics Research Lab, Stanford University; 2019. Available from: https://plato.stanford.edu/entries/plato-theaetetus/ Accessed on 11-11-2020.

CHAPTER 2

Technological developments of x-ray computed tomography over half a century: User's influence on protocol optimization

This chapter is based on the publication in Eur J Radiol. 2020;131:109261.

Ronald Booij, Ricardo P. Budde, Marcel L. Dijkshoorn, Marcel van Straten

ABSTRACT

Since the introduction of Computed Tomography (CT), technological improvements have been impressive. The number of adjustable acquisition and reconstruction parameters has increased accordingly. Overall, these developments led to improved image quality at a reduced radiation dose. However, many parameters are interrelated and part of automated algorithms. This makes it more complicated to adjust them individually and more difficult to comprehend their influence on CT protocol adjustments. Moreover, the user's influence in adapting protocol parameters is sometimes limited by the manufacturer's policy or the user's knowledge. Consequently, optimization can be a challenge. A literature search in Embase, Medline, Cochrane, and Web of Science was performed. The literature was reviewed with the objective to collect information regarding technological developments in CT over the past five decades and the role of the associated acquisition and reconstruction parameters in the optimization process.

INTRODUCTION

Computed tomography (CT) has fundamentally changed the practice of medicine and continues to expand our knowledge about diseases and management of major health challenges [1]. Consequently, the number of CT scans performed worldwide is constantly increasing. The number of CT exams obtained per year in the United States was around 3 million at the early eighties, increasing with approximately a factor of 20 to 62 million performed CT exams in 2007 [2]. The rapid increase of CT use was seen in European countries as well and where previously CT scans of mainly adults were performed, there is an increase of CT' scans performed in pediatric patients [3, 4]. Especially the latter are believed to benefit from technological innovations such as high-speed CT scanning that improve diagnostic capabilities in these patients. However, just like in adults, these scans should always be justified [2, 5]. Without a doubt, CT scanning is the biggest contributor of radiation exposure to the collective effective dose of medical examinations worldwide [3, 6]. Dutch researchers found that the increase in CT exams was not primarily due to the growth and aging of the Dutch population, but can be explained by its easy accessibility, associated technological developments and capabilities. In parallel with the increase of performed CT scans, public awareness and concerns about medical radiation exposure increased [7, 8]. The radiology community is aware of this fear and technological developments for radiation dose optimization have always been at their attention. However, optimization of a scanning protocol with respect to image quality (IQ) and radiation dose is a delicate procedure, mainly due to the interrelation of parameters. Furthermore, system properties and accompanying data acquisition techniques changed and expanded over the years. In this chapter, we present an overview of the technological developments during the evolution of CT and the accompanying user's influence for protocol optimization. Finally, a future outlook on technological developments is given.

SEARCH STRATEGY

Embase, Medline, Cochrane, and Web of Science were used for the literature search for this narrative review by combining synonyms for 'image quality', 'radiation dose', and 'CT' with English language restriction. The full search syntax is provided in the Appendix. Duplicates were removed and reference lists of included articles and review articles were searched for additional articles. First, articles were screened on title and abstract. Non-original research articles, e.g. case-reports, and original research articles not containing information on image quality and radiation dose regarding CT were excluded. Inclusion, exclusion and screening of all articles was performed by one author (RBo). Selection

criteria were articles containing information regarding key technological developments in CT and the accompanied influence of those developments on image quality and/or radiation dose. After the search, we continued to prospectively add recent articles of which we thought that they supported the text.

SYSTEM PROPERTIES

The user's influence and choices in protocol optimization depend on the CT scanner's technological capabilities and system properties. Main technological developments of system properties, acquisition, and reconstruction parameters are presented in table 1 and are discussed below. An overview of the evolution of CT scanners and the technical advances in CT is illustrated in Figure 1.

Translation-rotation and slip ring technology

Initially, CT images were acquired by the translation-rotation method in the "first- and second-" generation CT scanners. Within this method, data was acquired by the x-ray tube and detector moving in a linear translatory pathway and was repeated with small rotational increments [9]. The third-generation CT scanners have a wide fan beam and detectors that rotated slowly around the patient, requiring multiple breath holds to complete an axial CT exam. There was a high chance in missing abnormalities due to the multiple breath holds (Fig. 1a). Slip ring technology introduced in 1987 allowed continuous rotation of the tube and detectors by transferring electrical energy to the rotating gantry part and transmission of measured data to the computer system [10]. As the fourth-generation scanners, with a stationary detector ring, were not widely accepted, all currently available CT scanners are third-generation scanners by design. Therefore, we will only briefly comment on special scanner concepts like electron beam CT and dynamic spatial reconstructor.

Table 1. Timeline main technological developments of system properties, acquisition, and reconstruction parameters over the course of half a century of Computed Tomography.

Decades	`70s - `80s		`90s		`00s		`10s	
System properties	Gas detectors Translation-rotation	Fan beam Slip ring	Solid state detectors	Detector collimation	Dual source CT Wide area CT	Dynamic collimation	Electronic noise	Additional tin filtration
Acquisition properties	Constant tube voltage Constant tube current Sequential scanning	Rapid tube voltage switching dual energy ECG-gating	ECG-pulsing Spiral scanning	Automated tube current modulation Multi-detector spiral	Temporal resolution ECG-guided dose modulation	Dual energy 4DCT	Automatic tube voltage selection Routinely low tube voltage	
Reconstruction properties	Algebraic reconstruction Filtered back-projection	180- and 360-degree reconstruction	Reconstruction speed	Slice thickness	Noise & motion reduction	Temporal resolution	Increased matrix size Iterative reconstruction	Artificial intelligence Advanced beam hardening correction

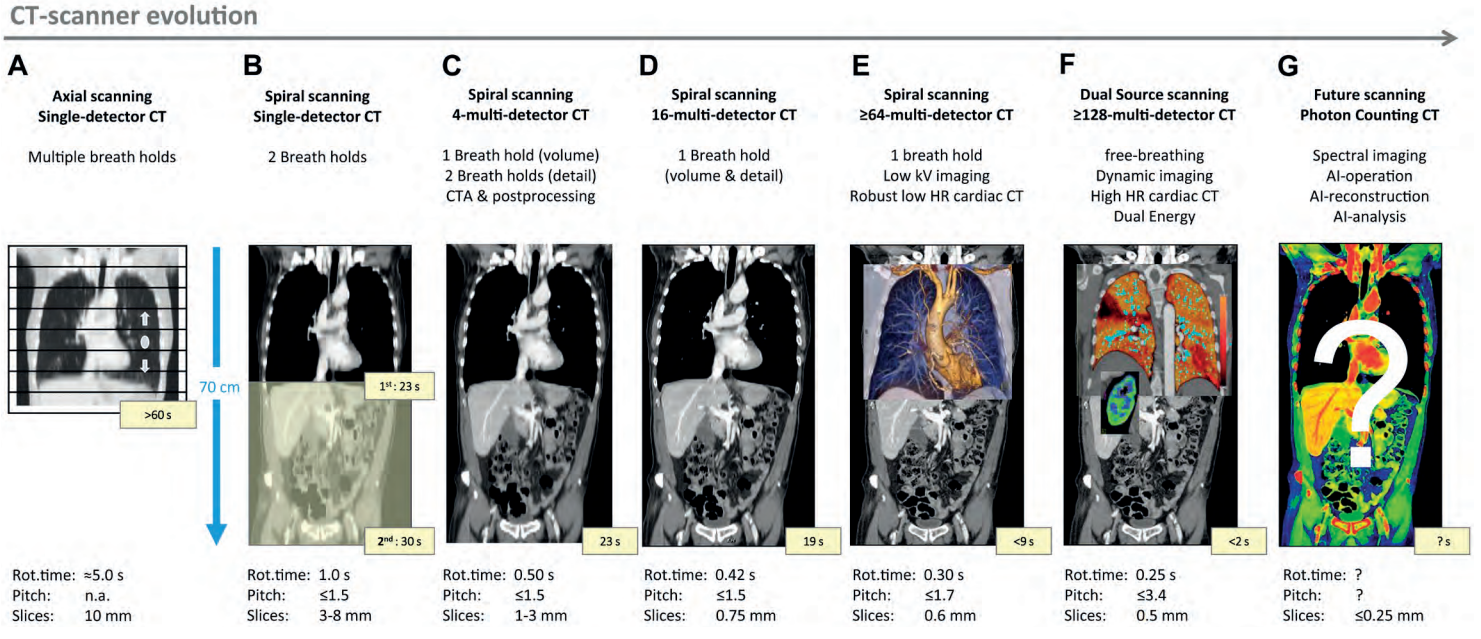

Figure 1 (a-g). Graphical representation of the evolution of third-generation CT scanner technology from a single detector row design to expected future technology. The coronal multiplanar reconstructions (MPR) of the thorax-abdomen that illustrate the improvements of MPR quality over time are based on a dataset of one patient (at one moment in time). **(a)** Single-detector (row) 10 mm axial scan. **(b)** Spiral single-detector scan needed at least two breath holds for a full thorax-abdomen scan. (**c**) Multi-detector CT. **(d)** Spiral CT with 16 detector rows allowed for volume scanning with isotropic datasets. **(e)** Faster rotation times and 64-detector CT allowed for robust cardiac CT exams. **(f)** Free-breathing and dual energy possibilities with dual source CT. **(g)** Future technologies. The color scale is used for illustrative purposes only and does not reflect true photon counting (PCCT) or spectral CT. See text for more details.

Detectors

The total beam collimation in the longitudinal, or z-direction, in the first-generation CT scanners was limited to one detector of 8 – 13 mm in width, but detector size decreased rapidly to 2 – 8 mm [11, 12]. With the introduction of spiral multi-detector CT (MDCT) in 1998 (also known as multi-slice CT), the individual detector elements became even smaller, down to 0.25 mm per detector element nowadays [13], resulting in improved spatial resolution. Moreover, it provided more and fast longitudinal coverage since multiple detector elements were combined (Fig. 1) [14]. Currently, for several CT manufacturers the total beam collimation is up to 160 mm with multiple detectors in the z-direction, allowing dynamic data acquisition of e.g. the entire brain or heart without table movement [15, 16]. Another positive outcome of an increased total collimation is the decrease of the overbeaming effect: The collimated x-ray beam is always wider than the total detector width because of the penumbra, which does not contribute to the image reconstruction, but does increase radiation dose. Although the impact of overbeaming on radiation dose was reduced with increased total collimation, overranging dose increases with increasing collimation and pitch values [17]. Therefore, a dynamic collimator was introduced in 2009 to reduce the amount of pre- and post-spiral dose, which are irrelevant for image reconstruction and is automatically applied [18].

Another approach to detector developments were improved detector efficiency to increase radiation dose efficacy, and the introduction of dual layer detectors. These detectors can measure x-ray attenuation for low and high-energy photons separately in two different detector layers, enabling material identification and quantification [19].

X-Ray Tube

With the introduction of spiral CT, the x-ray tubes had to be redesigned again to cope with overheating problems because of the need for increased tube output [20]. The introduction of a periodic motion of the focal spot in the z-direction resulted in doubling measurement positions in the longitudinal direction per rotation; thereby increasing spatial resolution and eliminating aliasing artifacts [21]. This multifan measurement technique is commonly known as z-flying focal spot and "double-dynamic" focus and applied by several vendors. Recent developments also include an additional tin filtration within the x-ray tube, which is of particular use in e.g. unenhanced CT high contrast studies of the chest and sinus [22, 23] and is currently applied by one vendor.

Dual source CT (DSCT)

CT scanners with multiple x-ray sources can provide fast imaging and improved temporal resolution (TR). The dynamic spatial reconstructor was one of the first attempts to introduce such a CT system but was never used in clinical routine [24]. In 2005, the first DSCT with two tubes and two corresponding detectors was introduced, demonstrating

improved TR and dual energy imaging capabilities in clinical practice, which was widely accepted [25].

ACQUISITION PARAMETERS

The main developments in acquisition parameters and how they influence image acquisition are discussed next.

Tube current

Within the first-generation CT scanners, the user could set tube current (mA value) depending on the accompanying tube voltage [26, 27]. Tube current was constant during a scan and this remained so for almost twenty years.

Automated tube current modulation (ATCM)

ATCM was introduced end '90s as part of the automatic exposure control (AEC) [28]. Early strategies consisted of online angular tube current modulation only, where nowadays it is often applied in combination with tube current adaptation in longitudinal directions. Some strategies enabled users to set customizable quality levels to achieve a constant noise level, whereby tube current is adjusted for the chosen scan and reconstruction parameters. Algorithms within the latest systems may suggest adjustments to average tube current and image noise based on a user defined dose index and patient diameter, accounting for the use of iterative reconstructions (IR) and used tube voltage. Another strategy was to have the ATCM system measure the attenuation from patients in a specific protocol, using this as a standard protocol body attenuation. The user can determine a noise reference or set the tube current to individual patient habitus. A different approach of fully ATCM is adaptation to different anatomical regions and patient sizes by setting a target tube current level for a standard-size reference patient [29]. The user may set different tube current modulation schemes for different patient sizes and anatomical regions.

A high level of awareness by the users for optimal positioning of the patient in the CT scanners is of utmost importance [30, 31]. Both radiation dose and IQ may be affected when the CT localizer radiograph, which is used by the AEC, is made with the patient positioned off-center [30, 31].

Tube voltage

Within the first- and second-generation CT scanners, the user was able to set the peak tube voltage in the range of 100 – 140 kilovolt peak (kVp) [27, 32, 33]. These high voltages are much appreciated when imaging thick patients, or to reduce metal implant

artifacts, however radiation dose is likely to be increased. Lowering the tube voltage requires tube current to be increased, and this was often limited by tube power early on.

Automatic tube voltage selection

Changing the tube voltage in predefined scan protocols, requires understanding of its influence on signal-to-noise ratio and contrast-to-noise ratio (CNR). Therefore, it could be challenging for users to understand how to perceive an improved IQ, or even the same IQ while reducing radiation dose, when changing the tube voltage. It was until the '10s that integrated automatic tube voltage selection and accompanying tube current adjustment became fully integrated into the AEC. Currently, it is available in most CT systems [34]. The main goal of automated tube voltage selection is to control the CNR and thereby minimize radiation dose. The user can define settings for the anatomical region and exam type with or without contrast.

Dual energy imaging

Dual energy, or so-called spectral imaging, can add tissue information to the CT image (e.g. discriminate bone from iodine-enhanced tissue). The possibility of determining the atomic number of the materials within a slice was already discussed by Sir Hounsfield in the seventies [12]. First attempts were done by a double scan: once with a high tube voltage, once with a low tube voltage and in parallel by a rapid kV switching technique. However, clinical use was rather limited due to needed technological improvements and high costs. The introduction of DSCT in 2005 allowed the acquisition of nearly simultaneous dual-energy data by using two tubes (Fig. 1f) [35]. A few years later, this was also made possible with the introduction of an improved rapid tube voltage switching technique [36]. TwinBeam CT and Dual layer spectral CT are the latest technologies to acquire dual energy datasets [19, 37].

Scan mode

Sequential scanning

Sequential CT imaging represents scanning with a stationary scanner table while the x-ray tube is rotated around the patient. After the scan, the patient is transported with a predefined incremental step. Then the next acquisition is performed and the process is repeated to the end of the scan range.

Spiral scanning

CT entered a new era with spiral CT (also known as helical scanning) in the late 1980s [38, 39]. The scanner table was able to travel at a constant speed through the gantry, i.e. the table feed, with the tube rotating, allowing the acquisition of volumetric data. It also

introduced the concept of pitch (the ratio between the table feed per full rotation and total beam collimation) which can be adjusted by the user. With single-detector spiral CT and a reduced rotation time, scan time was reduced. However, scans were restricted to single organs. A complete thorax-abdomen scan required at least two breath holds (Fig. 1b). The introduction of MDCT (Fig. 1c) gave the user the choice to scan with a small detector row width (e.g. 4 x 1 mm) to increase spatial resolution (=detail) or to scan with a large detector size, e.g. 4 x 2.5 mm, to reduce scan time (=volume). Spiral scanning with a 16-row MDCT allowed isotropic datasets of large volumes and an increase in quality of the post-processing images, as demonstrated in Figure 1b-f. DSCT made scanning at a pitch >2 possible by filling the sampling gaps of one detector with data of the second detector, providing clinical advantages in (cardio)vascular, trauma and pediatric patients due to increased scan speed (Fig. 1f) [40, 41].

Rotation time and temporal resolution

Gantry rotation time directly affects TR, as data from at least a 180-degree rotation are needed to reconstruct an image. Faster gantry rotation times result in improved TR with less motion artifacts and improved clarity of lung and cardiac imaging [42, 43]. Gantry rotation times have decreased from 5 – 40 seconds in rotation-translation systems in the seventies to 0.24 - 0.30 seconds for the current CT systems [26]. Until today, most single source scanners still cannot reach the 50 – 100 ms TR of electron beam CT scanners. Those scanners were especially proposed for cardiac CT because they were able to reach good TR thanks to its scanning without mechanical motion [44]. It was until the introduction of DSCT to achieve similar TR with up to 66 ms with third-generation CT systems [45].

Electrocardiogram (ECG) synchronization and ECG-guided dose modulation

Cardiac motion limited imaging of the heart in the early years of CT. However, in 1977 there were considerable achievements in technology reducing cardiac motion by ECG-gated reconstruction and provided "stop-action" cardiac CT scans [46, 47]. However, acquiring data for a single slice took up to 12 seconds. Multi-detector spiral CT reduced exam time, enabled reducing contrast volume, improved spatial resolution and ECG-gated coronary CT angiography became feasible in clinical practice. Especially from the 64-row MDCT on, robust low heart rate (HR) cardiac CT was possible (Fig. 1e) [48, 49]. At first, only a retrospective spiral scan mode with full dose, during the whole R-R interval at low pitch values was provided [50]. Later on, by introducing adaptive algorithms that can react to heart rate variability and simple arrhythmia, a dose reduction was achieved [51]. When the heart rhythm has complex arrhythmia, often a retrospective protocol is preferred for ECG-gated data editing possibilities. However, such a protocol requires a low pitch for oversampling to ensure enough data for reconstruction is available at the

expense of a high(er) radiation dose. While a prospective sequential scanning technique might have stack artifacts, a single heart beat scan mode such as a high-pitch prospective scan or a scan with a wide area detector does not. However, both single heart beat techniques require a low and stable heart rate [52].

RECONSTRUCTION PARAMETERS

Some of the steps in the reconstruction process are not, or to a less degree, adjustable by the user. All of the choices made within the reconstruction process directly influence IQ. We will highlight the main technological developments in reconstruction techniques.

Image reconstruction technique

Within the first CT systems, images were reconstructed with a simple iterative reconstruction method known as algebraic reconstruction [53]. However, due to the lack of computing power, this technique was soon replaced by filtered backprojection (FBP) [54]. FBP images are reconstructed by a convolution method or a direct Fourier algorithm. This second group incorporated interpolation in the Fourier plane, followed by inverse Fourier transformation. Convoluting the attenuation profiles with a so-called kernel and the backprojection of the modified profiles into the image plane to create the final image, is the method known as filtered backprojection. It is an analytical solution of the reconstruction problem. Where FBP was the most widely used CT image reconstruction technique for decades, nowadays mainly IR techniques are applied [55].

Iterative reconstruction technique

Computing power by the late '00 made IR techniques feasible in clinical routine [55]. IR techniques developed rapidly in three steps: Firstly, IR reconstruction was mainly done in the image domain on an initial image reconstructed from the raw data; secondly, it went to sinogram-based or so-called hybrid reconstructions. Thirdly, reconstruction algorithms developed to full model-based IR techniques [56]. However, most algorithms remain a "black-box" lacking specific details.

Matrix and FoV

Within the first-generation CT scanners, the image matrix size was limited to 80x80 pixels and one could only adjust the window level and width. Nowadays 512x512 is the most commonly used image matrix size but CT scanners with sizes up to 2048x2048 are available [57].

Extended field of view (FoV) reconstructions allow visualization of skin and tissue outside the primary FoV. This is of importance for PET-CT attenuation correction and radiotherapy CT dose calculations [58].

Cardiac reconstructions

The multiple ECG cycles acquired for cardiac CT in the late seventies were needed for acceptable effective TR with the aid of multi-segment reconstruction. Despite long acquisition time and extensive motion artifacts, the cardiac outline and fat grooves could be sharply visualized. Nowadays, mono-segment reconstruction is often used, but bi- or multi-segment reconstruction techniques are still available to make scanning of coronaries at higher heartrates feasible. These methods could improve the TR by a factor of 2 by combining two or more heartbeats for one reconstruction, but at the cost of a very low pitch value and consequently an increased radiation dose [50]. A disadvantage of multi-segment reconstruction is a possible creation of blurry images [59]. Even though vendors developed motion reduction algorithms, motion free imaging primarily depends on heart rate and gantry rotation time [60, 61].

Image enhancement tools

Several tools to improve IQ are developed and can be manually selected or are integrated into the reconstruction process. The most often used tools are noise and artifact reduction algorithms.

Noise reduction

Recently, noise reduction algorithms are implemented in several reconstruction processes, mostly running in the background e.g. in repeated low dose imaging during dynamic CT perfusion, in order to improve spatial resolution and CNR [62]. Sometimes it can be manually applied by the user e.g. to improve CNR in monoenergetic image reconstruction of dual energy data [63].

Artifact reduction

Artifacts are defined as artificial structures, which deviate from reality. Examples are artifacts occurring from voluntary and involuntary patient motion or beamhardening. Nowadays, motion correction algorithms are often used in CT perfusion of the head and body to correct for subtle head displacement or the breathing state during the acquisition times. The corrections are applied on already reconstructed image data and mainly done in post-processing software. Most of the algorithms for beam hardening correction or metal artifact reduction use iterative algorithms and therefore have to be applied on raw data [64].

SCANNING PROTOCOL OPTIMIZATION

Technological developments generally resulted in a reduction of radiation dose per exam and improved IQ [65, 66]. Both radiation dose and IQ are dictated by the ALARA (As Low as Reasonably Achievable) principle. With the introduction of diagnostic reference levels for CT in 1996, a practical tool came available to promote radiation dose optimization for specific diagnostic tasks [67]. With that, reference levels for CT exams were introduced around the globe [68-71]. Together with the technological developments, it contributed to the decrease of effective dose for a CT exam [72]. However, the diagnostic reference levels are general guidelines and do not apply to optimization for an individual patient. In the meantime, the user is one of the "protocol optimization factors" or may be even the most important factor in the optimization process. The user's contribution to the optimization process depends on the user himself and on the technological developments. All stakeholders, e.g. radiologist, medical physicist, and radiographer should work together and consider the whole optimization process as a team effort. In the next paragraph, we will discuss the optimization process. Some optimization steps are highlighted by a single case study (Fig. 2), which covers a wide

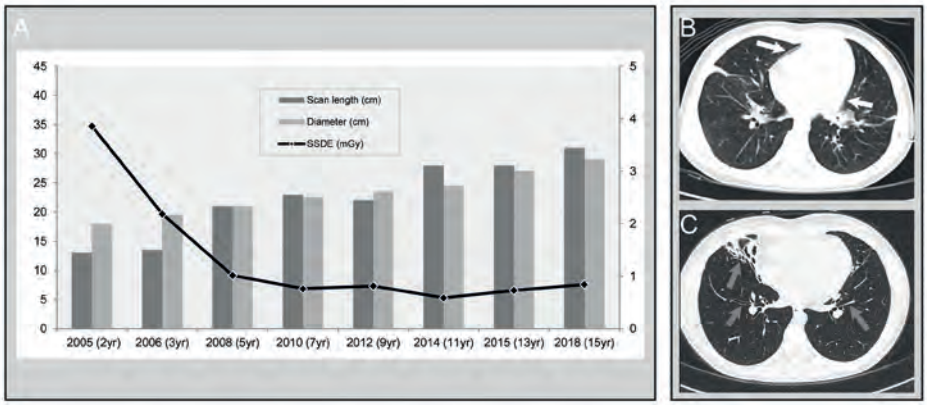

Figure 2 (a-c). Case presentation of a female child in the follow-up of cystic fibrosis. **(a)** Scan length and the chest diameter are shown as vertical bars on the left y-axis. The size-specific dose estimates (SSDE) are illustrated as diamonds on the secondary, right y-axis. At first, the patient was scanned with anesthesia on a 6-slice CT scanner with a slice width of 2.5 mm within the period 2005 – 2008. Tube voltage was fixed in this period and the scans in 2006 and 2008 were performed with a technician controlled breath hold. **(b)**. From 2010 – 2018, the patient was scanned with spirometry controlled breath hold on dual source CT, equipped with faster rotation time and thinner detector collimation. Within this period, scan protocol was optimized with iterative reconstruction technique, automatic tube voltage selection, and additional tin filtration. **(c)** CT scan (axial view) of the chest (2018) diameter increased from 18 cm to 29 cm and the scan length increased accordingly from 13 cm to 31 cm. SSDE dropped with almost 80%. Image noise was increased between **(b)** and **(c)** while increasing image quality due to improved temporal resolution and spatial resolution: White arrows in **(b)** show motion artifacts and the grey arrows in (**c**) show sharp delineation of the lung vessels and the airway wall.

area of technological developments over more than a decade. Note: As there are several CT manufacturers, so are (subtle) differences in their approaches in the technological developments in system, acquisition, and reconstruction parameters. Generalizations should come in only if features are significantly similar in all or most common vendors.

The whole scan protocol optimization process strives for optimization for an individual patient, taking the specific organ region and the referral question into account. Some technological developments have a direct effect on radiation dose applied to a patient (e.g. tube current). Other developments, like iterative reconstructions or automatic adaptation of tube voltage, are dependent on the user's motivation, acceptation and awareness. Benefits of the increased and evolved technologies are known, but the technological developments were and could be misunderstood or misused, leading to excessive radiation dose to the patient [73, 74]. Thereby, awareness of radiation dose and the possible risks are not always known [75].

Within the optimization process, the user's influence has increased, while automated tools were integrated to assist in the optimization process. This does not mean that changing a parameter will lead to an automatic compensation in other features/parameters, for example to maintain image quality. Many of the acquisition and reconstruction parameters are interrelated, making them more complicated to adjust individually and more difficult to comprehend, especially when they are part of automated algorithms and, likely, in the near future with artificial intelligence. Nevertheless, technological improvements and automated tools, combined with attention to the human side by the radiographer, will lead to the optimal scanning procedure. For example, automatization might speed up the scanning and reconstruction process, while the main focus of the radiographer is on the patient itself. In the meantime, adjusting parameters is like slotted dials: On the road to optimization, regardless of whether the adjustments have been made by humans or artificial intelligence, an adjustment of an acquisition or reconstruction parameter will have a direct influence on image quality and, directly or indirectly, on radiation dose as well due to their interrelation (Fig. 3). Within this light, it is mandatory to focus first on diagnostic optimization, which can be defined, and achieved, by the determination of the minimally acceptable IQ for diagnosis and thus of the lower limit of the diagnostic reference level. Minimally acceptable IQ is set by the desired image contrast, spatial resolution, and the amount of artifacts accepted [76, 77]. The second step will be technological optimization, defined as parameter selection to achieve this preferred lower limit IQ at the lowest reasonable dose. Figure 2 shows an example how a thoracic scanning protocol was technologically optimized. Users should be aware that diagnostic and technological optimization outcomes may vary between different CT scanners and institutions with different IQ preferences [71, 78]. The impact of a change in acquisition and reconstruction parameters on IQ and radiation dose, together with considerations for protocol optimization is illustrated in Table 2. This table

is used as a guidance for the next paragraphs to discuss the impact of adaptation of a single parameter on IQ and radiation dose.

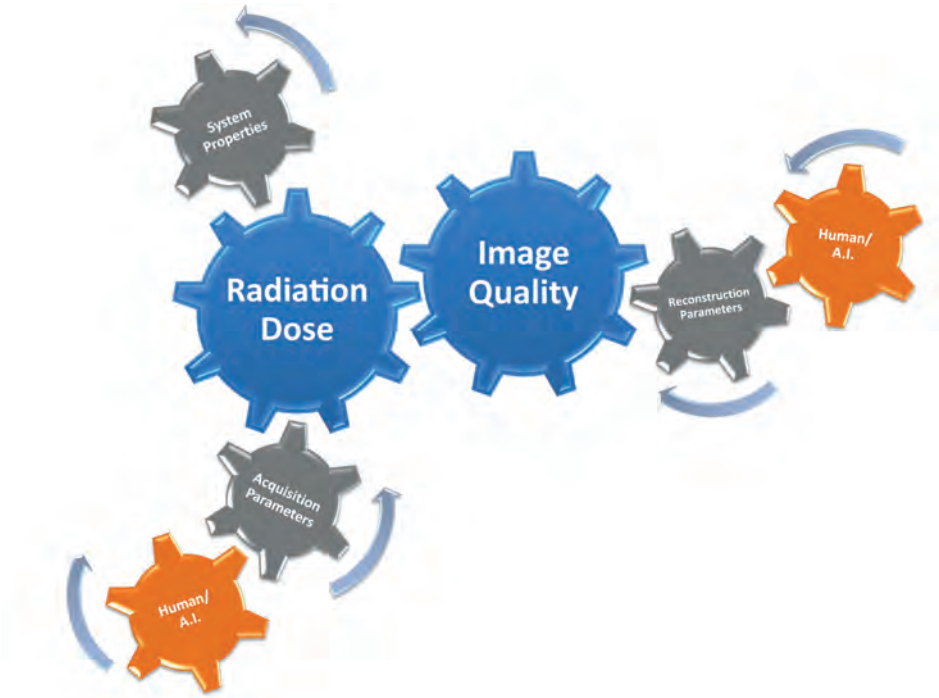

Figure 3. Graphical illustration by slotted dials, demonstrating the balance between optimization of a scanning protocol with respect to image quality and radiation dose. Changing system properties or parameters, input of human or artificial intelligence will influence both radiation dose and image quality.

Acquisition parameters

Protocol optimization for every individual patient can be obtained by adaptation of a single or multiple acquisition parameters. Every parameter demands its own consideration for optimization (Table 2, "considerations for CT protocol optimization"). For instance, when objects have slight attenuation differences such as in soft tissue studies, image noise impairs contrast resolution. So again, it is essential to determine the tolerance level of noise in the CT images as Sir Hounsfield already stated in 1976 [79]. An increase in noise is not problematic in objects with high intrinsic contrast, e.g. bone and air ways. [57, 79].

Adaptation of the tube voltage will have different effects and depends on whether or not iodinated contrast material is used (Table 2, "acquisition parameters", "image quality", "radiation dose") and on the general strategy for using automatic tube voltage selection [80]. X-ray attenuation by objects such as bone and iodine contrast strongly depends on

Table 2. Overview of general impact when adapting acquisition and reconstruction parameters currently used.

Acquisition Parameters	Image Quality			Radiation Dose	Considerations for CT Protocol Optimization
	Contrast Resolution	Spatial Resolution	Risk of Artifacts	Direct Absolute Effect	
Tube current increase	+	≈	≈	+ (linear)	Increase of contrast resolution and decrease of noise at the cost of increased radiation dose
Tube current decrease	–	≈	≈	– (linear)	Decrease of radiation dose at the cost of decrease of contrast resolution and increase of noise
Tube voltage increase (no iodinated contrast material applied)	soft tissue ≈ / - bone/fat	≈	– (1,2)	+ (non-linear)	Decrease of artifacts and noise at the cost of increased radiation dose and decreased contrast of bone/fat
Tube voltage decrease (no iodinated contrast material applied)	soft tissue ≈ / + bone/fat	≈	+ (1,2)	– (non-linear)	Increase of contrast bone/fat and decreased radiation dose at the cost of increase of artifacts and noise
Tube voltage increase (iodinated tissue)	soft tissue – / – bone/fat	≈	– (1,2)	+ (non-linear)	Decrease of artifacts and noise at the cost of increased radiation dose and decreased contrast of bone/fat, especially soft tissue (iodine)
Tube voltage decrease (iodinated tissue)	soft tissue ++ / + bone/fat	≈	+ (1,2)	– (non-linear)	Increase of contrast in soft tissue (iodine) and bone/fat with decreased radiation dose at the cost of increase of artifacts and noise
Sequential/ Axial (relative to spiral)	≈	–	– (3) / + (4)	– (non-linear)	No windmill/spiral artifacts and no overranging dose at the cost of increased stair-step artifacts and impaired scan speed
Multi-detector spiral (relative to sequential)	≈	+	+ (3) / - (4)	+ (linear)	Increased spatial resolution and scan speed at the cost of overranging dose and possible windmill/spiral artifacts
Pitch increase	–	–	+ (3) / - (5)	–	Decrease of motion artifacts, increase windmill/ spiral artifacts. Increase of noise when keeping tube current constant (strategies vary between vendors): Absorbed dose decrease. Overranging dose increase, but depends on the beam collimation, scanning range and the presence of dynamic collimation
Pitch decrease	+	+	– (3) / + (5)	+	Increase of motion artifacts, but decrease of noise and windmill/spiral artifacts and increase of contrast and spatial resolution. Increase of absorbed dose due to constant tube current (strategies may vary between vendors) and a decrease of overranging dose. Overranging depends on beam collimation and the presence of dynamic collimation as well.

Table 2. Overview of general impact when adapting acquisition and reconstruction parameters currently used. (continued)

Acquisition Parameters	Image Quality			Radiation Dose	Considerations for CT Protocol Optimization
	Contrast Resolution	Spatial Resolution	Risk of Artifacts	Direct Absolute Effect	
Longer rotation time	+	+ / ++ (a)	- (3,6) / ++ (5)	+ (linear)	Increase of contrast and spatial resolution with decrease of windmill/spiral artifacts with active flying focal spot and decrease of blooming at the cost of increased motion artifacts and radiation dose
Shorter rotation time	–	– / ≈ (a)	+ (3,6) / -- (5)	– (linear)	Decrease of motion artifacts and reduced radiation dose at the cost of increased windmill/spiral artifacts when no active flying focal spot is used, increase of blooming and noise with decreased contrast and spatial resolution
Iterative reconstruction technique (relative to filtered back-projection)	+	≈ / + (model based)	≈ / – (model based)	≈	Increase of contrast and spatial resolution with ability to reduce radiation dose and artifacts; probably user adaptation to different image impression
Matrix increase	–	+	– (6)	≈	Increase of spatial resolution; necessity to increase radiation dose to preserve the same SNR
Matrix decrease	+	–	+ (6)	≈	Increase of contrast resolution but increase of partial volume effect; ability to reduce radiation dose
dFoV increase	+	–	+ (6)	≈	Increase of contrast resolution but increase of partial volume effect; ability to reduce radiation dose
dFoV decrease	–	+	– (6)	≈	Increase of spatial resolution; necessity to increase radiation dose to preserve the same SNR
Slice thickness increase	+	–	– (3) / + (6)	≈	Increase of contrast resolution but increase of partial volume effect; ability to reduce radiation dose and windmill/spiral artifacts
Slice thickness decrease	–	+	– (6)	≈	Increase of spatial resolution with decrease of partial volume effect; necessity to increase radiation dose to preserve the same SNR

Note: Increase is demonstrated with the "+", decrease with the "–", and (almost) equal effect with the "≈". dFoV = display field of view. Data in paranthesis 1=beamhardening; 2=streak; 3=windmill/spiral; 4=stair-step; 5=motion/breathing/pulsation; 6=partial volume effect/ blooming; a=active flying focal spot.

the photon energy due to their high atomic number. Therefore, when iodine material is used, an improved CNR is possible, e.g. to better depict enhancing masses, at a low tube voltage with a dose similar to a high tube voltage (Figs. 4a-b) [81]. On the other hand, for scanning protocol optimization in e.g. young patients, the user may consider a reduction of radiation dose while maintaining CNR (Fig. 4c) [82]. While the main goal of automatic tube voltage selection is to control the CNR and thereby minimize radiation dose, sometimes the user should adjust the proposed parameters by the scanner software for an individual patient, instead of following the general strategy for automatic tube voltage selection. Thus, in some cases the referral question or individual patient demands for a higher radiation dose. For example, the user may also want to apply a higher contrast volume or flow since a high tube voltage decreases iodine contrast enhancement (Fig. 5a-b).

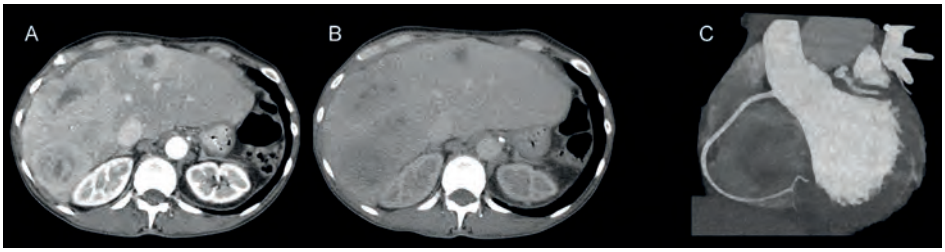

Figure 4 (a-c). Axial CT images of the same human abdomen acquired with equal CTDIvol and contrast injection protocol. Window width and level were 300/30. Images made with two days in between. **(a)** Demonstrating an increased contrast to noise ratio (CNR) when applying a lower tube voltage of 80 kVp compared to the CNR observed in **(b)** with 120 kVp. **(c)** CT image (maximum intensity projection, coronal view) of the heart of a thirteen-year-old boy. Reduced radiation dose in coronary CT angiography when applying low tube voltage (70 kV, a total dose length product of 8.2 mGy*cm, and a SSDE of 0.77 mGy).

The presence of high attenuating materials such as a hip prosthesis (Figs. 5c-d), warrants an increased tube voltage to decrease artifacts when no metal artifact reduction techniques are available (Table 2, "risk of artifacts").

Continuing with the parameter adaptation shown in Table 2: In general, tube current adaptation is not dependent on the use of iodine material, but rather on the noise tolerated in the images. Modulation of the tube current is used throughout most of the CT scanning protocols. Its use changes the relative dependencies in individual exposure parameters. For example, changing the pitch or rotation time often does not affect the patient's dose, as a change in tube current compensates for the change in other parameters [83]. However, when using ATCM, one should be aware that specific parameters, like slice thickness, kernel, and tube voltage, may affect the behavior of ATCM and that this differs between vendors [84].

Considerations to increase TR and the pitch mostly depend on the need of decreasing motion artifacts (Fig. 2b and 2c and 2c), mainly when imaging the heart or scanning

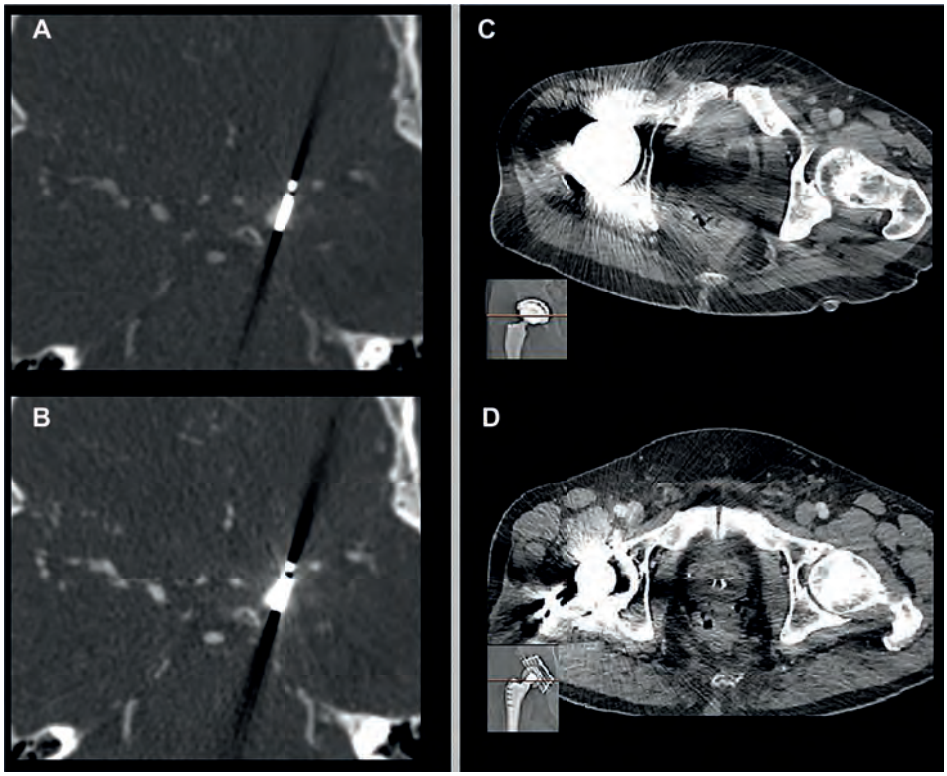

Figure 5 (a-d). Axial CT images demonstrating the influence of adjusting the tube voltage on metal artifacts and image quality in contrast enhanced CT scans. **(a-b)** Dual energy CT angiography of a clipped brain aneurysm with metal clip artifacts (a) 140 kV scan with low contrast HU, but with less beam hardening artifacts than in **(b)** 80 kV scan with high contrast HU. **(c-d)** CT of the abdomen of two different patients with hip prosthesis **(c)** Hip prosthesis with cobalt head causing disturbing beam hardening artifacts in the pelvic area. Not all metal type will cause disturbing beam hardening: **(d)** Hip prosthesis with a head made of titanium and a clear visualization of the pelvic area.

non-cooperative patients. However, a higher pitch value often demands a higher tube current, especially in scanners that keep the noise and dose level constant. Faster rotation times may increase artifacts. Therefore, in cooperative patients, the user may decrease the pitch to decrease the overranging effect. Moreover, this will also lead to increased IQ in e.g. bone exams, especially when the structures are angulated relative to scan plane [18, 85].

Reconstruction parameters

CT protocol optimization is also obtained by adaptation of single, or multiple, reconstruction parameters (Table 2). In image reconstruction, when selecting the level of smoothing (minimal, moderate, or maximum), the user can improve low contrast detectability by reducing the amount of noise. The other way around, edge-enhancement

filters improve spatial resolution, by "sharpening up" the CT image and are especially useful in bone or lung exams [86]. Other filters may increase metal to tissue transition such as stent lumen by reducing blooming effects [87]. An improved spatial resolution comes with an increased noise level and reduced soft tissue contrast.

Within iterative reconstruction techniques, careful considerations in iterative strength, also known as level or scale, and accompanied dose adjustments are mandatory [88, 89]. For instance, higher iterative strength can have an effect on contrast and spatial resolution, but also on image appearance [90]. The image texture might be blurred and a high iterative strength can give rise to a noiseless image appearance. These kind of images are often evaluated as too smooth or artificial and users often desire neither [91]. Reliable diagnostic quality and statistically significant dose reductions can be achieved in adult and pediatric patients using IR [92, 93]. However, negative effects as low contrast detectability are reported as well [94].

Spatial resolution may increase with increased matrix size thanks to a decrease of the voxel size. In general, this will be accompanied by an increase of noise (Table 2). Moreover, users should also be aware that image data size increases with increased matrix size.

Adaptation of the FoV is also related to the voxel size: Increasing or decreasing the FoV will directly influence voxel size. Thereby, it may affect IQ: a smaller FoV may increase spatial resolution, but decrease contrast resolution due to increase of noise. Balancing between optimization of a protocol with respect to IQ and radiation dose, e.g. the increase of spatial resolution, at the cost of image noise, the user may also want to adjust the slice thickness to restore the signal-to-noise ratio. For example, when an increase in contrast resolution is required, noise levels can be lowered by increasing slice thickness (Figs. 6a-b). Simultaneously, spatial resolution will decrease due to the partial-volume effect (Figs. 6c-d).

FUTURE OUTLOOK AND CONCLUSION

CT is still evolving, even in its middle age, and bringing new technological developments and new diagnostic strategies for healthcare. Users should not only be at the forefront in embracing latest technologies, but also be proactive on the road to highly optimized protocols.

Currently, photon counting CT (PCCT) and artificial intelligence (AI) promise to bring a new revolution in CT [55, 72] (Fig. 1g). PCCT is expected to provide intrinsic spectral sensitivity, high spatial resolution, less noise and artifacts with better low-signal performance, and less characteristic energy weighting [55, 95]. PCCT opens the possibility of achieving multi-energy imaging in every scan, similar to dual energy CT, but using

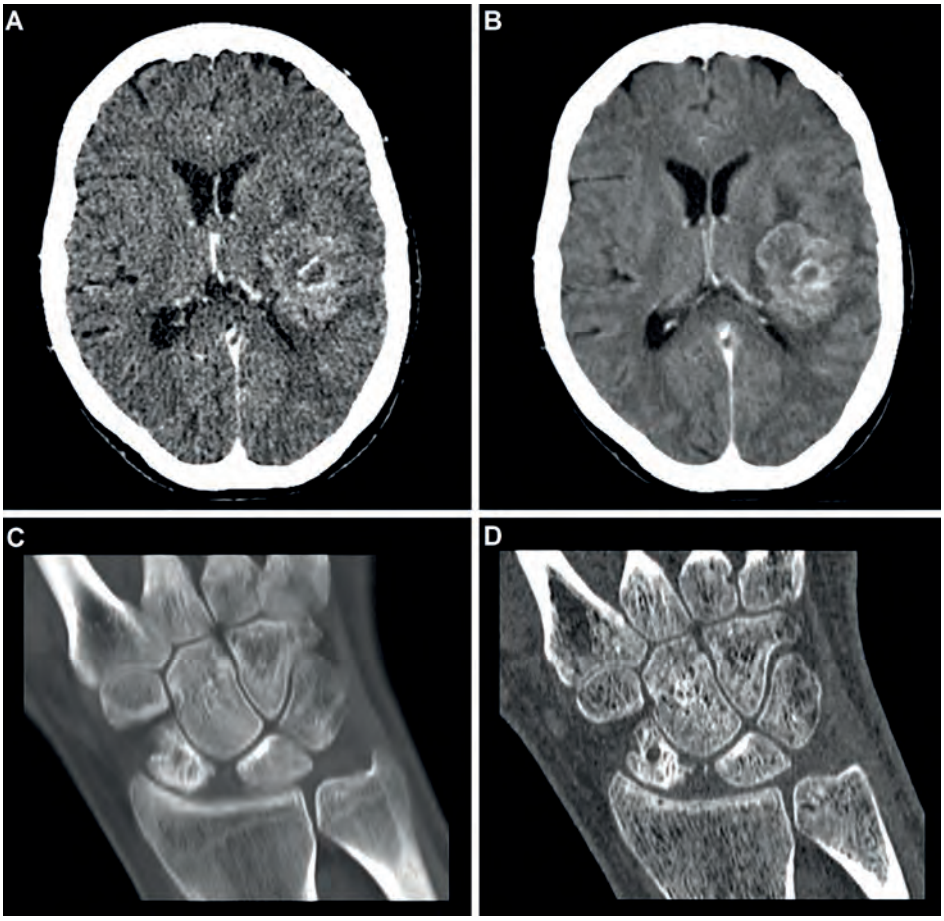

Figure 6 (a-d). CT images illustrating the influence of adjusting a reconstruction parameter (slice thickness) and its influence on contrast and spatial resolution. **(a-b)** CT images (axial view) of an adult brain (soft tissue) **(a)** 1.0 mm and b 5.0 mm. **(c-d)** CT images (multiplanar reconstruction, coronal view) of a wrist (bone). Contrast resolution is increased with thicker slices due to decrease of noise. **(c)** 5.0 mm and (d) 0.75 mm. Spatial resolution is increased with thinner slices due to decrease of the partial volume effect.

a single tube voltage. Where dual layer CT uses a single tube voltage too, PCCT is able to count the number of all incoming photons and measure its energy. Improved iodine contrast visibility may even require less radiation dose, or lower iodine contrast material injection [96, 97].

AI is already applied within clinical protocols for instance in artifact reduction and image reconstruction [95]. As such, the application of AI resembles IR: its application can be used to reduce radiation dose while maintaining IQ or increase IQ without increasing radiation exposure [55]. Both PCCT and AI are one of the latest technological developments in almost five decades of CT, but certainly will not be the last to be introduced and demanding an adjustment of the optimization process.

In conclusion, technological developments in CT have led to an increased number of processes for protocol optimization. Consequently, it is necessary that users are aware of those developments, their operation, and how they are interrelated with respect to image quality and radiation dose.

ACKNOWLEDGEMENTS

We would like to thank Wichor Bramer of the medical library Erasmus MC for his support in building the search syntax.

REFERENCES

1. Rubin GD. Computed tomography: revolutionizing the practice of medicine for 40 years. Radiology. 2014;273(2 Suppl):S45-74.
2. Brenner DJ, Hall EJ. Computed tomography--an increasing source of radiation exposure. N Engl J Med. 2007;357(22):2277-84.
3. Meulepas JM, Ronckers CM, Smets A, Nievelstein RAJ, Gradowska P, Lee C, et al. Radiation Exposure From Pediatric CT Scans and Subsequent Cancer Risk in the Netherlands. J Natl Cancer Inst. 2019;111(3):256-63.
4. Bosch de Basea M, Salotti JA, Pearce MS, Muchart J, Riera L, Barber I, et al. Trends and patterns in the use of computed tomography in children and young adults in Catalonia - results from the EPI-CT study. Pediatr Radiol. 2016;46(1):119-29.
5. Kalender WA. Dose in x-ray computed tomography. Phys Med Biol. 2014;59(3):R129-50.
6. Kaul A, Bauer B, Bernhardt J, Nosske D, Veit R. Effective doses to members of the public from the diagnostic application of ionizing radiation in Germany. Eur Radiol. 1997;7(7):1127-32.
7. Dauer LT, Thornton RH, Hay JL, Balter R, Williamson MJ, St Germain J. Fears, feelings, and facts: interactively communicating benefits and risks of medical radiation with patients. AJR Am J Roentgenol. 2011;196(4):756-61.
8. Power SP, Moloney F, Twomey M, James K, O'Connor OJ, Maher MM. Computed tomography and patient risk: Facts, perceptions and uncertainties. World J Radiol. 2016;8(12):902-15.
9. Hounsfield GN. Computed medical imaging. Nobel lecture, Decemberr 8, 1979. J Comput Assist Tomogr. 1980;4(5):665-74.
10. Kalender WA. X-ray computed tomography. Phys Med Biol. 2006;51(13):R29-43.
11. Ambrose J. Computerized transverse axial scanning (tomography): Part 2. Clinical application. The British Journal of Radiology. 1973;46(552):1023-47.
12. Hounsfield GN. The E.M.I. scanner. Proceedings of the Royal Society of London Series B Biological Sciences. 1977;195(1119):281.
13. Takagi H, Tanaka R, Nagata K, Ninomiya R, Arakita K, Schuijf JD, et al. Diagnostic performance of coronary CT angiography with ultra-high-resolution CT: Comparison with invasive coronary angiography. European Journal of Radiology. 2018;101:30-7.
14. Kalender WA. Computed Tomography - Fundamentals, System Technology, Image Quality, Applications. 3rd Revised ed: Publicis Publishing, Erlangen; 2011.
15. Klingebiel R, Siebert E, Diekmann S, Wiener E, Masuhr F, Wagner M, et al. 4-D Imaging in cerebrovascular disorders by using 320-slice CT: feasibility and preliminary clinical experience. Acad Radiol. 2009;16(2):123-9.
16. Rybicki FJ, Otero HJ, Steigner ML, Vorobiof G, Nallamshetty L, Mitsouras D, et al. Initial evaluation of coronary images from 320-detector row computed tomography. Int J Cardiovasc Imaging. 2008;24(5):535-46.
17. Tsalafoutas IA. The impact of overscan on patient dose with first generation multislice CT scanners. Physica medica : PM : an international journal devoted to the applications of physics to medicine and biology : official journal of the Italian Association of Biomedical Physics. 2011;27(2):69-74.
18. Booij R, Dijkshoorn ML, van Straten M. Efficacy of a dynamic collimator for overranging dose reduction in a second- and third-generation dual source CT scanner. Eur Radiol. 2017;27(9):3618-24.
19. Altman A, Carmi R. TU-E-210A-03: A Double-Layer Detector, Dual-Energy CT — Principles, Advantages and Applications. Medical Physics. 2009;36(6Part24):2750-.

20. Homberg R, & Koeppel, R. An X-ray tube assembly with rotating anode spiral groove bearing of the 2nd generation. Electromedica. 1997;66(2):65-6.
21. Kyriakou Y, Kachelriess M, Knaup M, Krause JU, Kalender WA. Impact of the z-flying focal spot on resolution and artifact behavior for a 64-slice spiral CT scanner. Eur Radiol. 2006;16(6):1206-15.
22. Gordic S, Morsbach F, Schmidt B, Allmendinger T, Flohr T, Husarik D, et al. Ultralow-dose chest computed tomography for pulmonary nodule detection: first performance evaluation of single energy scanning with spectral shaping. Invest Radiol. 2014;49(7):465-73.
23. May MS, Brand M, Lell MM, Sedlmair M, Allmendinger T, Uder M, et al. Radiation dose reduction in parasinus CT by spectral shaping. Neuroradiology. 2017;59(2):169-76.
24. Robb RA, Hoffman EA, Sinak L, Harris LD, Ritman EL. High-speed three-dimensional X-ray computed tomography: The dynamic spatial reconstructor. Proceedings of the Ieee. 1983;71:308 - 19.
25. Flohr TG, McCollough CH, Bruder H, Petersilka M, Gruber K, Suss C, et al. First performance evaluation of a dual-source CT (DSCT) system. Eur Radiol. 2006;16(2):256-68.
26. Gould R. Early Days of CT: Innovations (Both Good and Bad): 51st AAPM Annual Meeting; 200. Available from https://www.aapm.org/meetings/amos2/pdf/42-12236-29343-41.pdf. Accessed on 11-11-2020.
27. Cohen G. Contrast--detail--dose analysis of six different computed tomographic scanners. J Comput Assist Tomogr. 1979;3(2):197-203.
28. Kalender WA, Wolf H, Suess C, Gies M, Greess H, Bautz WA. Dose reduction in CT by on-line tube current control: principles and validation on phantoms and cadavers. Eur Radiol. 1999;9(2):323-8.
29. Ulzheimer S, Endt H, Flohr T. Computed tomography-patient dose and dose reduction technologies. Health Phys. 2011;100(3):325-8.
30. Kaasalainen T, Palmu K, Lampinen A, Kortesniemi M. Effect of vertical positioning on organ dose, image noise and contrast in pediatric chest CT--phantom study. Pediatr Radiol. 2013;43(6):673-84.
31. Toth T, Ge Z, Daly MP. The influence of patient centering on CT dose and image noise. Med Phys. 2007;34(7):3093-101.
32. Zatz LM. Image quality in cranial computed tomography. J Comput Assist Tomogr. 1978;2(3):336-46.
33. Southon FC. CT scanner comparison. Medical Physics. 1981;8(1):i-i.
34. Ramirez-Giraldo JC, Fuld M, Grant K, Primak AN, Flohr T. New Approaches to Reduce Radiation While Maintaining Image Quality in Multi-Detector-Computed Tomography. Curr Radiol Rep. 2015;3(2).
35. Johnson TRC, Krauß B, Sedlmair M, Grasruck M, Bruder H, Morhard D, et al. Material differentiation by dual energy CT: Initial experience. Eur Radiol. 2007;17(6):1510-7.
36. Marshall W, Hall E, Doost-Hoseini A, Alvarez R, Macovski A, Cassel D. An implementation of dual energy CT scanning. J Comput Assist Tomogr. 1984;8(4):745-9.
37. Almeida IP, Schyns LE, Ollers MC, van Elmpt W, Parodi K, Landry G, et al. Dual-energy CT quantitative imaging: a comparison study between twin-beam and dual-source CT scanners. Med Phys. 2017;44(1):171-9.
38. Kalender WA. Principles and applications of spiral CT. Nucl Med Biol. 1994;21(5):693-9.
39. Kalender WA, Vock P, Polacin A, Soucek M. [Spiral-CT: a new technique for volumetric scans. I. Basic principles and methodology]. Rontgenpraxis. 1990;43(9):323-30.
40. Achenbach S, Marwan M, Schepis T, Pflederer T, Bruder H, Allmendinger T, et al. High-pitch spiral acquisition: A new scan mode for coronary CT angiography. J Cardiovasc Comput Tomogr. 2009;3(2):117-21.

41. Flohr TG, Leng S, Yu L, Allmendinger T, Bruder H, Petersilka M, et al. Dual-source spiral CT with pitch up to 3.2 and 75 ms temporal resolution: Image reconstruction and assessment of image quality. Med Phys. 2009;36(12):5641-53.
42. Rubin GD, Leung AN, Robertson VJ, Stark P. Thoracic spiral CT: influence of subsecond gantry rotation on image quality. Radiology. 1998;208(3):771-6.
43. Montaudon M, Berger P, Blachère H, De Boucaud L, Latrabe V, Laurent F. Thin-section CT of the lung: Influence of 0.5-s gantry rotation and ECG triggering on image quality. Eur Radiol. 2001;11(9):1681-7.
44. P. Boyd D, J. Lipton M. Cardiac computed tomography1983. 298-307 p.
45. Carrascosa PM, Cury RC, García MJ, Leipsic J. Dual-Energy CT in Cardiovascular Imaging: Springer; 2015.
46. Harell G, Guthaner DF, Breiman RS. Stop-action cardiac computed tomography. Radiology. 1977;123: 515.
47. Sagel SS, Weiss ES, Gillard RG, Hounsfield GN, Jost GT, Stanley RJ, et al. Gated computed tomography of the human heart. Invest Radiol. 1977;12(6):563-6.
48. Nieman K, Oudkerk M, Rensing BJ, van Ooijen P, Munne A, van Geuns RJ, et al. Coronary angiography with multi-slice computed tomography. Lancet. 2001;357(9256):599-603.
49. Kachelrielß M, Ulzheimer S, Kalender WA. ECG-correlated image reconstruction from subsecond multi-slice spiral CT scans of the heart. Med Phys. 2000;27(8):1881-902.
50. Flohr T, Ohnesorge B, Bruder H, Stierstorfer K, Simon J, Suess C, et al. Image reconstruction and performance evaluation for ECG-gated spiral scanning with a 16-slice CT system. Med Phys. 2003;30(10):2650-62.
51. Bardo DME, Brown P. Cardiac multidetector computed tomography: Basic physics of image acquisition and clinical applications. Curr Cardiol Rev. 2008;4(3):231-43.
52. Neefjes LA, Rossi A, Genders TS, Nieman K, Papadopoulou SL, Dharampal AS, et al. Diagnostic accuracy of 128-slice dual-source CT coronary angiography: a randomized comparison of different acquisition protocols. Eur Radiol. 2013;23(3):614-22.
53. Beister M, Kolditz D, Kalender WA. Iterative reconstruction methods in X-ray CT. Phys Med. 2012;28(2):94-108.
54. Willemink MJ, De Jong PA, Leiner T, De Heer LM, Nievelstein RAJ, Budde RPJ, et al. Iterative reconstruction techniques for computed tomography Part 1: Technical principles. Eur Radiol. 2013;23(6):1623-31.
55. Willemink MJ, Noel PB. The evolution of image reconstruction for CT-from filtered back projection to artificial intelligence. Eur Radiol. 2018.
56. Shaqdan KW, Kambadakone AR, Hahn P, Sahani DV. Experience with Iterative Reconstruction Techniques for Abdominopelvic Computed Tomography in Morbidly and Super Obese Patients. J Comput Assisted Tomogr. 2018;42(1):124-32.
57. Hata A, Yanagawa M, Honda O, Kikuchi N, Miyata T, Tsukagoshi S, et al. Effect of Matrix Size on the Image Quality of Ultra-high-resolution CT of the Lung: Comparison of 512 × 512, 1024 × 1024, and 2048 × 2048. Academic Radiology. 2018;25(7):869-76.
58. Bruder H, Sedlmaier M, Stierstorfer K, Floh TG. High Definition Extended Field of View (HD FOV) Reconstruction in CT. RSNA (Radiological Society of North); Chicago2011.
59. Halliburton SS, Stillman AE, Flohr T, Ohnesorge B, Obuchowski N, Lieber M, et al. Do segmented reconstruction algorithms for cardiac multi-slice computed tomography improve image quality? Herz. 2003;28(1):20-31.

60. Schondube H, Allmendinger T, Stierstorfer K, Bruder H, Flohr T. Evaluation of a novel CT image reconstruction algorithm with enhanced temporal resolution. Medical Imaging 2011: Physics of Medical Imaging. Proceedings of SPIE. 7961. Bellingham: Spie-Int Soc Optical Engineering; 2011.
61. Rohkohl C, Bruder H, Stierstorfer K, Flohr T. Improving best-phase image quality in cardiac CT by motion correction with MAM optimization. Med Phys. 2013;40(3).
62. Pisana F, Henzler T, Schönberg S, Klotz E, Schmidt B, Kachelrieß M. Noise reduction and functional maps image quality improvement in dynamic CT perfusion using a new k-means clustering guided bilateral filter (KMGB). Med Phys. 2017;44(7):3464-82.
63. Marin D, Ramirez-Giraldo JC, Gupta S, Fu W, Stinnett SS, Mileto A, et al. Effect of a noise-optimized second-generation monoenergetic algorithm on image noise and conspicuity of hypervascular liver tumors: An in vitro and in vivo study. Am J Roentgenol. 2016;206(6):1222-32.
64. Wellenberg RHH, Hakvoort ET, Slump CH, Boomsma MF, Maas M, Streekstra GJ. Metal artifact reduction techniques in musculoskeletal CT-imaging. Eur J Radiol. 2018;107:60-9.
65. Christe A, Heverhagen J, Ozdoba C, Weisstanner C, Ulzheimer S, Ebner L. CT dose and image quality in the last three scanner generations. World J Radiol. 2013;5(11):421-9.
66. Rehani MM. Radiation protection in newer imaging technologies. Radiat Prot Dosim. 2010;139(1-3):357-62.
67. Brink JA, Miller DL. U.S. National Diagnostic Reference Levels: Closing the Gap. Radiology. 2015;277(1):3-6.
68. Boal TJ, Hedt JC, Einsiedel PF. A survey of patient dose and image quality factors for CT scanners in Victoria. Australas Phys Eng Sci Med. 1999;22(3):103-12.
69. Ekpo EU, Adejoh T, Akwo JD, Emeka OC, Modu AA, Abba M, et al. Diagnostic reference levels for common computed tomography (CT) examinations: results from the first Nigerian nationwide dose survey. J Radiol Prot. 2018;38(2):525-35.
70. Zhou DD, Sun P, Jia Z, Zhu W, Shi G, Kong B, et al. Multisection computed tomography: Results from a Chinese survey on radiation dose metrics. Journal of the Chinese Medical Association : JCMA. 2019;82(2):155-60.
71. Shrimpton PC, Jansen JT, Harrison JD. Updated estimates of typical effective doses for common CT examinations in the UK following the 2011 national review. Br J Radiol. 2016;89(1057):20150346.
72. McCollough CH. Computed Tomography Technology-and Dose-in the 21st Century. Health Phys. 2019;116(2):157-62.
73. Bogdanich W. Radiation overdoses point up dangers of CT scans. New York Times website (wwwnytimescom/2009/10/16/us/16radiationhtml). 2009.
74. Coakley FV, Gould R, Yeh BM, Arenson RL. CT Radiation Dose: What Can You Do Right Now in Your Practice? American Journal of Roentgenology. 2011;196(3):619-25.
75. Christoph IL, Andrew HH, Edward PM, James AB, Howard PF. Diagnostic CT Scans: Assessment of Patient, Physician, and Radiologist Awareness of Radiation Dose and Possible Risks. Radiology. 2004;231(2):393-8.
76. Goldman LW. Principles of CT: Radiation dose and image quality. J Nucl Med Technol. 2007;35(4):213-25.
77. Jurik A, Petersen J, Jessen KA, Bongartz G, Geleijns J, Golding SJ, et al. Clinical use of image quality criteria in computed tomography: A pilot study. Radiat Prot Dosim. 2000;90(1-2):47-52.
78. European_Commission_Directorate-General_for_Energy. Radiation Protection No 180: Medical radiation exposure of the European population Part 1/2. EU Publications. Available from https://ec.europa.eu/energy/sites/ener/files/documents/RP180web.pdf. DOI: 10.2833/708119; 2015. Accessed 11-11-2020.

79. Hounsfield GN. Picture quality of computed tomography. AM J ROENTGENOL. 1976;127(1):3-9.
80. Yu L, Li H, Fletcher JG, McCollough CH. Automatic selection of tube potential for radiation dose reduction in CT: a general strategy. Med Phys. 2010;37(1):234-43.
81. Tang K, Wang L, Li R, Lin J, Zheng X, Cao G. Effect of low tube voltage on image quality, radiation dose, and low-contrast detectability at abdominal multidetector CT: phantom study. J Biomed Biotechnol. 2012;2012:130169.
82. Blankstein R, Bolen MA, Pale R, Murphy MK, Shah AB, Bezerra HG, et al. Use of 100 kV versus 120 kV in cardiac dual source computed tomography: Effect on radiation dose and image quality. Int J Card Imaging. 2011;27(4):579-86.
83. Kalra MK, Maher MM, Toth TL, Schmidt B, Westerman BL, Morgan HT, et al. Techniques and applications of automatic tube current modulation for CT. Radiology. 2004;233(3):649-57.
84. Sookpeng S, Martin CJ, Gentle DJ. Investigation of the influence of image reconstruction filter and scan parameters on operation of automatic tube current modulation systems for different CT scanners. Radiat Prot Dosimetry. 2015;163(4):521-30.
85. Ney DR, Fishman EK, Magid D, Robertson DD, Kawashima A. Three-dimensional volumetric display of CT data: effect of scan parameters upon image quality. J Comput Assist Tomogr. 1991;15(5):875-85.
86. Fishman EK, Ney DR, Kawashima A, Scott Jr WW, Robertson DD. Effect of image display on the quality of multiplanar reconstruction of computed tomography data. INVEST RADIOL. 1993;28(2):146-9.
87. Seifarth H, Raupach R, Schaller S, Fallenberg EM, Flohr T, Heindel W, et al. Assessment of coronary artery stents using 16-slice MDCT angiography: Evaluation of a dedicated reconstruction kernel and a noise reduction filter. Eur Radiol. 2005;15(4):721-6.
88. Willemink MJ, Leiner T, De Jong PA, De Heer LM, Nievelstein RAJ, Schilham AMR, et al. Iterative reconstruction techniques for computed tomography part 2: Initial results in dose reduction and image quality. Eur Radiol. 2013;23(6):1632-42.
89. Noel PB, Fingerle AA, Renger B, Munzel D, Rummeny EJ, Dobritz M. Initial performance characterization of a clinical noise-suppressing reconstruction algorithm for MDCT. AJR Am J Roentgenol. 2011;197(6):1404-9.
90. Winklehner A, Karlo C, Puippe G, Schmidt B, Flohr T, Goetti R, et al. Raw data-based iterative reconstruction in body CTA: Evaluation of radiation dose saving potential. Eur Radiol. 2011;21(12):2521-6.
91. Baskan O, Erol C, Ozbek H, Paksoy Y. Effect of radiation dose reduction on image quality in adult head CT with noise-suppressing reconstruction system with a 256 slice MDCT. J Appl Clin Med Phys. 2015;16(3):5360.
92. Singh S, Kalra MK, Shenoy-Bhangle AS, Saini A, Gervais DA, Westra SJ, et al. Radiation dose reduction with hybrid iterative reconstruction for pediatric CT. Radiology. 2012;263(2):537-46.
93. Wu TH, Hung SC, Sun JY, Lin CJ, Lin CH, Chiu CF, et al. How far can the radiation dose be lowered in head CT with iterative reconstruction? Analysis of imaging quality and diagnostic accuracy. Eur Radiol. 2013;23(9):2612-21.
94. Mileto A, Guimaraes LS, McCollough CH, Fletcher JG, Yu L. State of the Art in Abdominal CT: The Limits of Iterative Reconstruction Algorithms. Radiology. 2019;293(3):491-503.
95. Lell MM, Kachelrieß M. Recent and Upcoming Technological Developments in Computed Tomography: High Speed, Low Dose, Deep Learning, Multienergy. Investigative Radiology. 9000;Publish Ahead of Print.
96. Yu Z, Leng S, Kappler S, Hahn K, Li Z, Halaweish AF, et al. Low-dose performance of a whole-body research photon-counting CT scanner: SPIE; 2016.

97. Pourmorteza A, Symons R, Reich DS, Bagheri M, Cork TE, Kappler S, et al. Photon-Counting CT of the Brain: In Vivo Human Results and Image-Quality Assessment. AJNR Am J Neuroradiol. 2017;38(12):2257-63.

APPENDIX

Literature search

Embase, Medline, Cochrane, and Web of Science were used for the narrative review by combining synonyms for 'image quality', 'radiation dose', and 'CT' with English language restriction. Duplicates were removed and reference lists of included articles and review articles were searched for additional articles. Inclusion, exclusion, and screening of all articles was performed by one author (RBo). Search strategy is provided in Appendix Table 1.

Table A1. Literature search syntax

Search strategy performed at 01 May 2020	Before de-duplication	After de-duplication
Embase.com	4522	4425
Medline Ovid	4207	1422
Web of science	3603	1290
Cochrane CENTRAL	233	52
TOTAL	**12565**	**7189**

Embase.com

('computer assisted tomography'/mj/de OR 'computed tomographic angiography'/mj/de OR 'cone beam computed tomography'/mj/de OR 'electron beam tomography'/mj/de OR 'four dimensional computed tomography'/mj/de OR 'high resolution computer tomography'/mj/de OR 'multidetector computed tomography'/mj/de OR 'spiral computer assisted tomography'/mj/de OR 'whole body CT'/mj/de OR 'x-ray computed tomography'/mj/exp OR 'computed tomography scanner'/mj/de OR 'cone beam computed tomography scanner'/mj/de OR 'portable computed tomography scanner'/mj/de OR (((compute* OR electron-beam*) NEAR/3 tomogra*) OR ct OR cbct OR mdct OR CTA OR msct OR ssct OR dsct):ti) AND ('image quality'/mj/exp OR 'image enhancement'/mj/de OR 'contrast enhancement'/mj/de OR 'contrast to noise ratio'/mj/de OR 'total quality management'/mj/de OR 'image reconstruction'/mj/de OR (((imag* OR contrast* OR scan OR scans) NEAR/3 (qualit* OR enhance* OR nois* OR denois* OR acquisition* OR reconstruct* OR performan*)) OR ((Signal OR reduc*) NEAR/3 noise)):ti) AND ('radiological parameters'/de OR 'radiation dose'/exp OR 'rotation'/de OR 'collimator'/de OR 'field of view'/de OR 'kernel method'/de OR 'filtered back projection'/de OR 'filtered backprojection'/de OR 'iterative reconstruction'/de OR parameters/de OR algorithm/de OR 'dosimetry'/de OR 'electric current'/de OR (((radiation OR effectiv* OR index OR level OR reduc*) NEAR/3 (dose OR dosage*)) OR parameter* OR rotation* OR collimation OR 'field of view' OR fov OR kernel* OR 'filtered back projection' OR 'filtered backprojection' OR (iterative NEAR/3 reconstruct*) OR pitch OR (slice NEAR/3 thick*) OR (table NEAR/3

feed) OR voltage OR ampere OR (current NEAR/3 (tube OR electric*)) OR ((tube OR bowtie) NEAR/3 filter*) OR algorithm* OR (automat* NEAR/3 exposure* NEAR/3 control*) OR aec OR atcm OR scout-view* OR topogram* OR scanogram* OR localizer*):ab,ti) NOT ([animals]/lim NOT [humans]/lim) NOT ([Conference Abstract]/lim OR [Letter]/lim OR [Note]/lim OR [Editorial]/lim) AND [english]/lim

Medline Ovid

(* Tomography, X-Ray Computed/ OR * Computed Tomography Angiography/ OR * Four-Dimensional Computed Tomography/ OR * Tomography Scanners, X-Ray Computed/ OR (((compute* OR electron-beam*) ADJ3 tomogra*) OR ct OR cbct OR mdct OR CTA OR msct OR ssct OR dsct).ti.) AND (* Image Enhancement / OR * Radiographic Image Enhancement/ OR * Quality Improvement/ OR * Total Quality Management/ OR (((imag* OR contrast* OR scan OR scans) ADJ3 (qualit* OR enhance* OR nois* OR denois* OR acquisition* OR reconstruct* OR performan*)) OR ((Signal OR reduc*) ADJ3 noise)).ti.) AND (Radiation Dosage/ OR rotation/ OR Radiometry/ OR Algorithms/ OR In Vivo Dosimetry/ OR Electricity/ OR (((radiation OR effectiv* OR index OR level OR reduc*) ADJ3 (dose OR dosage*)) OR parameter* OR rotation* OR collimation OR field of view OR fov OR kernel* OR filtered back projection OR filtered backprojection OR (iterative ADJ3 reconstruct*) OR pitch OR (slice ADJ3 thick*) OR (table ADJ3 feed) OR voltage OR ampere OR (current ADJ3 (tube OR electric*)) OR ((tube OR bowtie) ADJ3 filter*) OR algorithm* OR (automat* ADJ3 exposure* ADJ3 control*) OR aec OR atcm OR scout-view* OR topogram* OR scanogram* OR localizer*).ab,ti.) NOT (exp animals/ NOT humans/) NOT (letter OR news OR comment OR editorial OR congresses OR abstracts).pt. AND english.la.

Cochrane CENTRAL

((((compute* OR electron-beam*) NEAR/3 tomogra*) OR ct OR cbct OR mdct OR CTA OR msct OR ssct OR dsct):ti) AND ((((imag* OR contrast* OR scan OR scans) NEAR/3 (qualit* OR enhance* OR nois* OR denois* OR acquisition* OR reconstruct* OR performan*)) OR ((Signal OR reduc*) NEAR/3 noise)):ti) AND ((((radiation OR effectiv* OR index OR level OR reduc*) NEAR/3 (dose OR dosage*)) OR parameter* OR rotation* OR collimation OR 'field of view' OR fov OR kernel* OR 'filtered back projection' OR 'filtered backprojection' OR (iterative NEAR/3 reconstruct*) OR pitch OR (slice NEAR/3 thick*) OR (table NEAR/3 feed) OR voltage OR ampere OR (current NEAR/3 (tube OR electric*)) OR ((tube OR bowtie) NEAR/3 filter*) OR algorithm* OR (automat* NEAR/3 exposure* NEAR/3 control*) OR aec OR atcm OR scout-view* OR topogram* OR scanogram* OR localizer*):ab,ti)

Web of science

(TI=((((compute* OR electron-beam*) NEAR/2 tomogra*) OR ct OR cbct OR mdct OR CTA OR msct OR ssct OR dsct)) AND TI=((((imag* OR contrast* OR scan OR scans) NEAR/2

(qualit* OR enhance* OR nois* OR denois* OR acquisition* OR reconstruct* OR performan*)) OR ((Signal OR reduc*) NEAR/2 noise))) AND TS=((((radiation OR effectiv* OR index OR level OR reduc*) NEAR/2 (dose OR dosage*)) OR parameter* OR rotation* OR collimation OR "field of view" OR fov OR kernel* OR "filtered back projection" OR "filtered backprojection" OR (iterative NEAR/2 reconstruct*) OR pitch OR (slice NEAR/2 thick*) OR (table NEAR/2 feed) OR voltage OR ampere OR (current NEAR/2 (tube OR electric*)) OR ((tube OR bowtie) NEAR/2 filter*) OR algorithm* OR (automat* NEAR/2 exposure* NEAR/2 control*) OR aec OR atcm OR scout-view* OR topogram* OR scanogram* OR localizer*)))

PART II

Improvement of patient positioning by body contour detection with a 3D camera

CHAPTER 3

Accuracy of automated patient positioning in CT using a 3D camera for body contour detection

This chapter is based on the publication in Eur Radiol. 2019;29(4):2079-88

Ronald Booij, Ricardo P. Budde, Marcel L. Dijkshoorn, Marcel van Straten

ABSTRACT

Objective

To assess the accuracy of a 3D camera for body contour detection and patient positioning in CT compared to routine manual positioning by radiographers.

Methods and materials

Four hundred and twenty-three patients that underwent CT of the head, thorax and/or abdomen on a scanner with manual table height selection and 254 patients on a scanner with table height suggestion by a 3D camera were retrospectively included. Within the camera group, table height suggestion was based on infrared body contour detection and fitting of a scalable patient model to the 3D data. Proper positioning was defined as the ideal table height at which the scanner isocenter coincides with the patient's isocenter. Patient isocenter was computed by automatic skin contour extraction in each axial image and averaged over all images. Table heights suggested by the camera and selected by the radiographer were compared with the ideal height.

Results

Median (interquartile range) absolute table height deviation in mm was 12.0 (21.6) for abdomen, 12.2 (12.0) for head, 13.4 (17.6) for thorax-abdomen, and 14.7 (17.3) for thorax CT scans positioned by radiographers. The deviation was significantly less (p<0.01) for the 3D camera at 6.3 (6.9) for abdomen, 9.5 (6.8) for head, 6.0 (6.1) for thorax-abdomen, and 5.4 (6.4) mm for thorax.

Conclusion

A 3D camera for body contour detection allows for accurate patient positioning, thereby outperforming manual positioning done by radiographers, resulting in significantly smaller deviations from the ideal table height. However, radiographers remain indispensable when the system fails or in challenging cases.

INTRODUCTION

The applied dose in Computed Tomography (CT) should be as low as reasonable achievable. This makes scan acquisition protocol optimization important [1, 2]. Over the years many dose optimization techniques have been introduced, such as iterative reconstruction techniques, automated tube current modulation (ATCM) and automated tube voltage selection [3, 4]. However, little attention has been paid to proper patient positioning in the CT scanner. Proper patient positioning can be defined as choosing the ideal CT table height at which the scanner isocenter coincides with the patient's isocenter. This may at first sight seem to be a minor action. However, it is not, as patient positioning affects the patient's shape and size on a CT localizer radiograph, directly affecting ATCM behavior as well as the efficacy of bowtie filters [5-8].

Although radiographers can use laser beams to visually check the central positioning of the patient, this method is user-dependent and therefore patient positioning at a non-ideal table height is common [6, 7, 9, 10]. If the patient is positioned away from the isocenter (i.e. table positioned too high or too low), the localizer radiograph is either magnified or reduced in width and the radiation dose applied by the ATCM consequently increases or decreases, which might result in suboptimal image quality or an increase in dose [6-8, 10, 11]. In a study by Saltybaeva and Alkadhi, vertical off-centering by 20 mm in chest CT resulted in 7% organ dose differences, while off-centering of more than 40 mm was associated with significant dose differences of 20% and higher [12]. Other studies using a phantom demonstrated a substantial increase in radiation dose to the surface and periphery of the phantom [13], and an increase in image noise, or a considerable effect on eye-lens and skin dose by off-centering [8]. This was partly due to sub-optimal performance of the bowtie filter with inappropriate beam attenuation because of off-centering. Habibzadeh et al. (2012) found that patient positioning more than 10 mm from the ideal table height occurred in over 75% of patients in their sample [5]. Especially in challenging patients, it can be difficult for radiographers to estimate the ideal table height.

Body contour detection using advanced sensors and a virtual patient model [14, 15] may improve table height selection. Recently, a 3D camera for body contour detection based on these techniques was introduced that allows for automatic patient positioning in the CT gantry. The aim of our study was to assess the performance and accuracy of this system for patient positioning and compare it to routine manual positioning by the radiographer.

MATERIALS AND METHODS

Study Design and patient selection

The study was conducted in accordance with the declaration of Helsinki and international standards of Good Clinical Practice. The medical ethics committee of Erasmus MC waived the need for informed consent. Vertical patient positioning, i.e. CT table height selection, performance was assessed on two dual source CT scanners (DSCT) from Siemens Healthineers: SOMATOM Drive (software version Syngo CT VA62A) equipped with a 3D camera for body contour detection (prototype; Siemens Healthineers), and a SOMATOM Force (software version Syngo CT VA50A) with vertical patient positioning done manually by radiographers.

All consecutive adult patients that underwent a CT examination of the head, thorax and/or abdomen during routine clinical care on the two DSCT scanners in our institution mentioned above during a one-month period from February to March 2017 were retrospectively included.

Patient positioning using a 3D camera for body contour detection

The 3D camera was positioned above the patient, in front of the CT gantry and equipped with an infrared light source and sensor, as well as a visible light camera. The camera is connected to the scanner and integrated into the patient positioning workflow.

Once the patient is positioned on the table and assumes the target pose for the CT scan, the radiographer triggers a planning image by pressing a button on a touch display mounted at the gantry. The image analysis starts after taking this image and it happens independent from the target body region.

The 3D camera uses infrared light and the time-of-flight (TOF) principle [14] to measure the distance of object surfaces to the camera. The result is a scalar depth image, where the magnitude of each pixel represents a distance with respect to the camera in millimeters. Figure 1a shows a depth image visualized as greyscale image where brighter colors denote larger distances. Black means no measurements are available. This may happen at edges, e.g. those of the table, where the infrared light is not reflected back into the camera but scattered. Aligning of the depth image to the color image, which has a larger field-of-view, may lead to undefined areas at the border of the depth image. The depth image taken with the 3D camera is converted to a 3D point cloud (Fig. 1b) by inverting the perspective projection of the camera. The depth image/point cloud is the main source of input to the algorithm, which defines the patient isocenter. The algorithm consists of three steps that are described below: 1) Detection of the pose of the patient and body regions, such as head, thorax, and abdomen. 2) Fallback isocenter, and 3) Avatar fit [15].

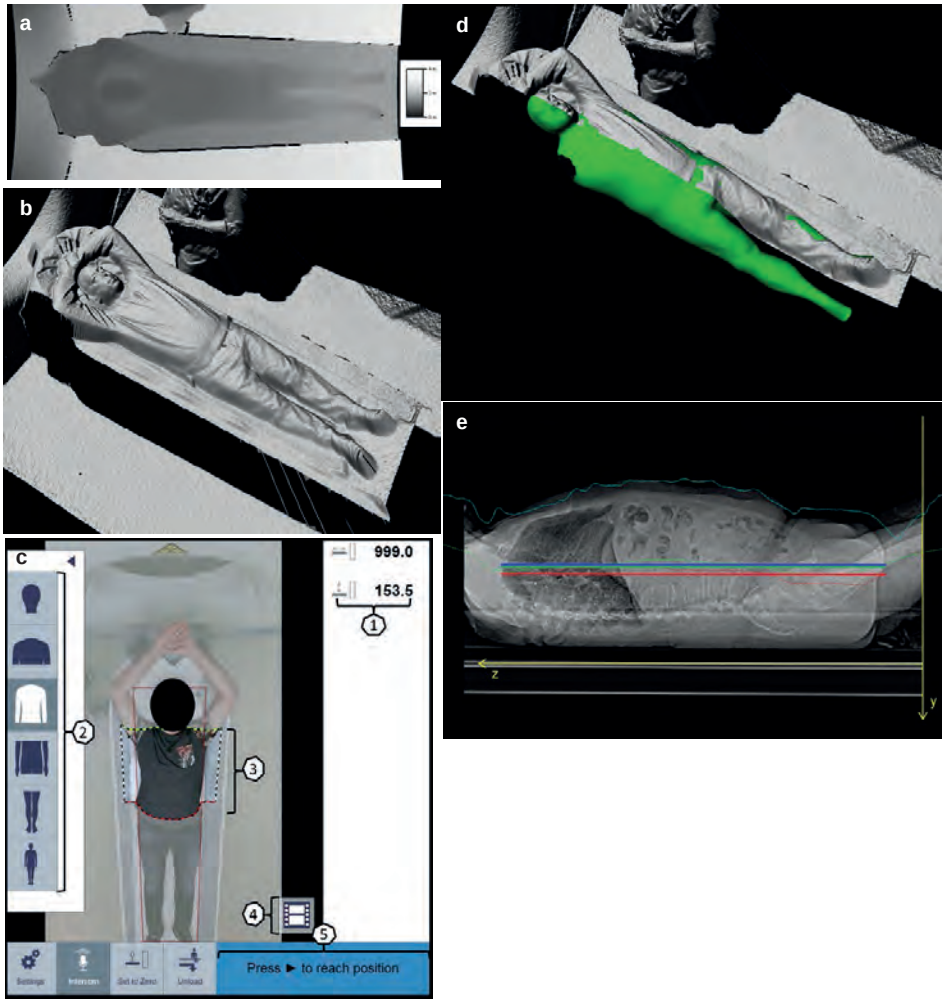

Figure 1 (a-e). **(a)** Measured depth values; **(b)** Depth surface after perspective correction; **(c)** User interface of touch panel on CT scanner: 1. Table position and table height; 2. Selectable body region; 3. Adjustable scan range; 4. Taking planning image; 5. Automatic position of the patient on base of selected scan range; **(d)** Virtual Patient Avatar; **(e)** Patient positioning accuracy: Red horizontal line: average patient isocenter, blue horizontal line: scanner isocenter, green horizontal line: average patient isocenter estimated by camera.

Within step 1, based on the detected body regions and the selected scan protocol, the system automatically defines the horizontal range for the scan. If necessary, the user can manually adjust the scan range on the touch panel to the preferred length and region by dragging the boundary overlays on the color image (Fig. 1c). Within step 2, a fallback isocenter is computed before step 3 because it is a fast method, and will be used when the Avatar fit in step 3 fails. The center between the point cloud and the table top is a reasonable approximation to the patient's isocenter when the patient is lying flat on the

table. Since the camera is calibrated to the gantry coordinate system of the CT scanner, the point cloud can be mapped into gantry space by a rigid transformation. In gantry space, the center is computed between the point cloud and the known position of the table top along the length axis of the table. This leads to a centerline curve. The curve is truncated to the target body region to be scanned and then averaged to obtain the isocenter of the patient. The deviation between this isocenter and the known isocenter of the scanner can then be applied to the table position at which the camera image was acquired in order to automatically align the body region to be scanned with the isocenter of the scanner.

Within the last step, an Avatar is fitted to the camera data. The Avatar is a statistical shape model (Fig. 1d) learnt from a training database and used to obtain the isocenter curve of the patient (Fig. 1e). During the fitting process, the Avatar assumes the pose and the body proportions of the patient as captured by the depth data and within the limits of the model. The Avatar currently does not model the arms, but the thorax shape still accounts for arms behind the head or arms at the side of the body. Since the 3D camera only sees the upward facing side of the patient, the known position and shape of the table top are used to constrain the backwards facing side of the patient. The center of the Avatar in the lateral direction is then computed for the target body region in order to obtain a robust estimate of the patient's isocenter. The Avatar model ensures a robust isocenter estimate is obtained also in case positioning aids such as head or knee rests are used or when blankets cover the patient. If an Avatar model cannot be fit, the previously described fallback isocenter (step 2) will be used. The isocenter is then estimated by averaging the depth data and the known table top. Once the move button on the gantry is pressed, the isocenter curve (either Avatar or fallback) computed for the whole patient will be truncated to the selected target scan region.

All described steps occur in milliseconds and only manually adjusting the scan range will add more time (seconds) to the procedure.

Manual patient positioning by radiographers

The radiographer is using laser beam guidance as routinely available on the CT scanner to position patients on the scanner. For vertical positioning, the scanner is equipped with laser beams that project a horizontal line through the isocenter of the gantry on the lateral side of the patient. All scans were acquired during routine clinical care by a team of dedicated CT radiographers.

Calculation of patient positioning accuracy

For each patient, the positioning accuracy is expressed as a single value in mm that represents the difference between the table height suggested by the camera or chosen by the radiographer and the ideal table height. The latter was defined as the height at

which the scanner isocenter coincides with the patient isocenter as calculated based on the axial images as described below. The distribution of patients positioned higher or lower than the ideal table height were expressed as negative or positive numbers, respectively.

In each axial slice of the acquired CT scan, the skin contour (representing the perimeter of the patient at that specific axial position) was extracted by thresholding. The vertical position of the patient isocenter in each slice was defined as the average of the lowest and highest skin contour position, i.e. the two points on the extracted perimeter closest to the top and bottom of the axial image (Figs. 2a-b). Finally, the patient isocenter for the total scan length was computed by averaging the vertical isocenter positions for each individual image over all images. The computations were performed with a mathematical computing software code developed in house (MATLAB R2008a, The MathWorks Inc., Natick, Massachusetts, USA). Reconstructed slice thickness was 3.0 mm, reconstruction increment 3.0 mm, and the reconstructed field of view (FoV) was chosen to include the entire skin surface by an additional reconstruction with the maximum possible FoV.

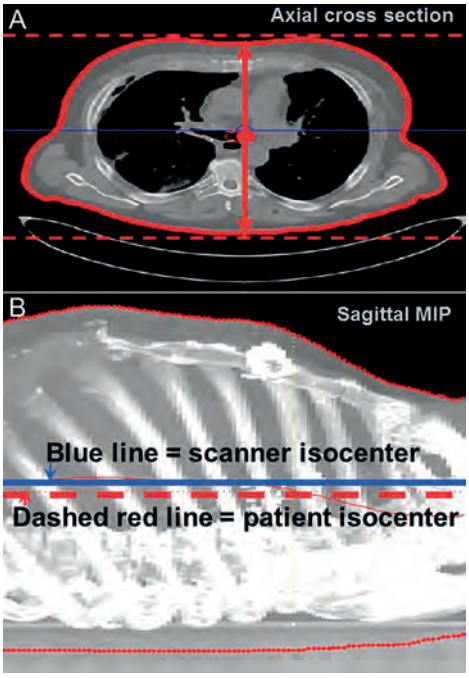

Figure 2 (a-b). 3D region growing to extract patient isocenter. **(a)** Axial view of region growing to extract patient isocenter for each slice, defined as the midpoint between the highest and lowest point (red dashed lines) of the extracted patient skin contour; **(b)** Lateral MIP is created to demonstrate vertical height measurement of consecutive axial images and demonstrate scanner isocenter does not coincide with patient isocenter (blue line=scanner isocenter; dashed red line=patient isocenter).

Exclusion of scans

In case of obvious impossibility to position the patient at the preferred table height, e.g., very bended knees or arms due to physical constraints and that could not be completely extended above the head, patients were excluded from analysis. In case of obvious patient movement after body contour detection by the 3D camera and before the CT scan, or in case of large objects blocking the camera sight, patients were excluded from analysis as well.

Statistical analyses

To determine whether there were significant differences in patient positioning between the radiographers and the 3D camera for body contour detection, we performed an analysis by means of normality and a nonparametric test. The absolute table height deviation is a continuous unpaired variable reported as median (interquartile range (IQR)), calculated with Microsoft Excel (Microsoft Office Professional Plus 2010). Data distribution was tested with Shapiro-Wilk test. The non-normally distributed data of the absolute table height deviation for the different body regions within and between the camera- and radiographer-group were compared with the Mann-Whitney U test. A two-sided p-value of <0.05 was considered statistically significant. Statistical analyses were performed using SPSS (version 22, IBM Corp, Armonk NY, USA). Continuous measures of isocenter deviation (mm) was calculated and evaluated with Microsoft Excel (Microsoft Office Professional Plus 2010).

RESULTS

Patient positioning accuracy of 3D camera for body contour detection

Two hundred and seventy-two scans were available for analysis. Eighteen (6.6%) scans were excluded from analysis due to obvious patient movement after body contour detection by the 3D camera or large objects blocking the camera sight. Consequently, 254 patients were included in the analysis: 58 (22.8%) abdomen, 45 (17.7%) head, 70 (27.6%) thorax-abdomen, and 81 (31.9%) thorax CT scans. Median (interquartile range (IQR)) absolute table height deviation was 6.3 (6.9) for abdomen, 9.5 (6.8) for head, 6.0 (6.1) for thorax-abdomen, and 5.4 (6.4) mm for thorax CT scans. Median table height deviation was largest for head CT (Fig. 3a and Table 1). A fallback was applied in three cases since no Avatar could be fitted.

A total of 201 (79.1%) of patients were positioned higher than the scanner isocenter. 53 (20.9%) of the patients were positioned lower than the scanner isocenter (Fig. 4a). Sub analyses of the different body parts demonstrated the same tendency, with the exception of head CT (Table 1).

Patient positioning accuracy of radiographers

Four hundred and twenty-six scans were available for analysis. In three cases, it was not possible to position the patient at the preferred table height and these patients were therefore excluded from analysis. The total study population of 423 patients comprised 115 (27.2%) abdomen, 73 (17.3%) head, 72 (17.0%) thorax-abdomen, and 163 (38.5%) thorax CT scans.

Median (IQR) absolute table height deviation was 12.0 (21.6) for abdomen, 12.2 (12.0) for head, 13.4 (17.6) for thorax-abdomen, and 14.7 (17.3) mm for thorax CT scans done by radiographers. Median table height deviation was largest for the thorax (Fig. 3a and Table 1).

A total of 133 (31.4%) patients were positioned higher than the scanner isocenter. 290 (68.6%) of the patients were positioned lower than the scanner isocenter (Fig. 4b). Sub analyses of the different body parts demonstrated the same tendency, with the exception of head CT (Table 1).

Comparison between radiographer and 3D camera

Figure 3a-b and Table 1 present the performance of radiographers and the 3D camera. Median table height deviation, for all body parts combined, was 13.2 mm (IQR: 17.0) for patients positioned by radiographers and 6.1 mm (IQR: 7.0) for patients from the CT scanner equipped with a 3D camera. Overall p-value for difference in positioning was $p<0.05$.

For each of the four body part areas that were scanned, the maximum absolute deviation from the ideal table height was largest for patients positioned by radiographers. Patient positioning accuracy for the 3D camera system and the radiographers differed significantly for all four body parts: abdomen ($p<0.05$), head ($p=0.039$), thorax-abdomen ($p<0.05$), and thorax scans ($p<0.05$).

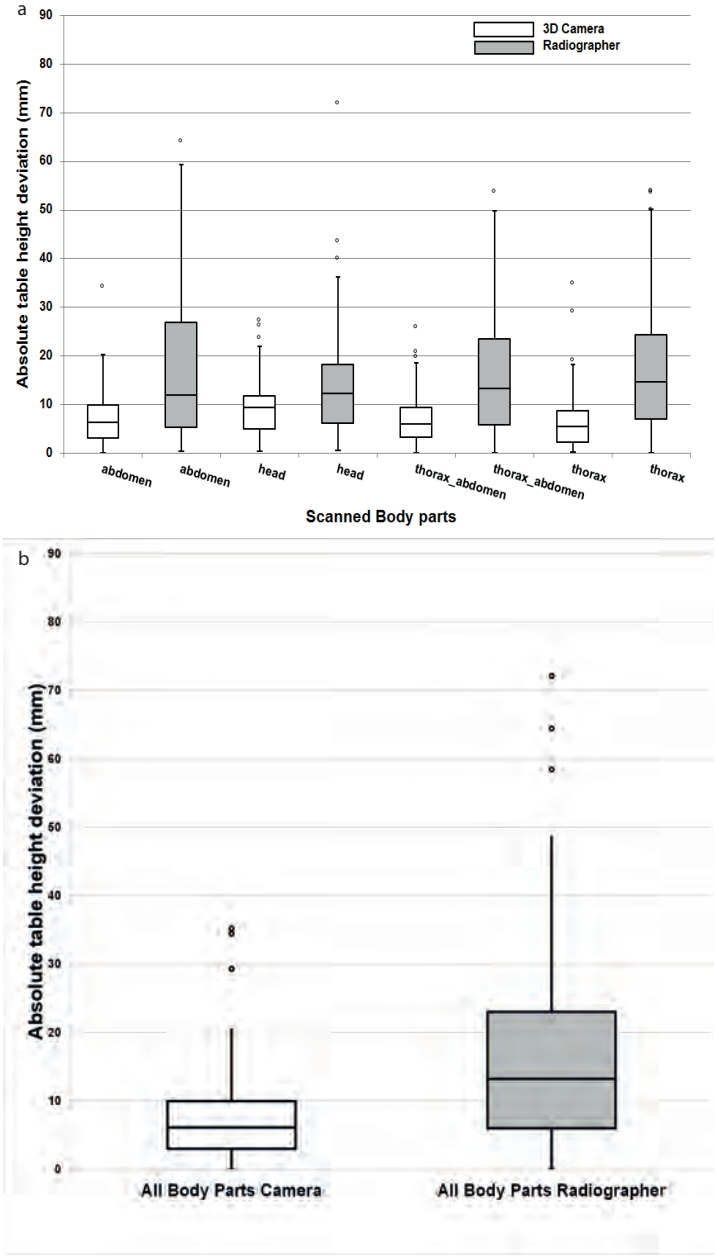

Figure 3 (a-b). (a) Box-and-whisker plots of patient positioning performance of all different body parts separately for the radiographers and the 3D camera; **(b)** Box-and-whisker plots of patient positioning performance of all different body parts combined for the radiographers and the 3D camera.
The median (horizontal line within box), interquartile range (box), and nonoutlier range (whiskers). The largest deviations from the scanner isocenter are plotted as open dots, and represent values outside the nonoutlier range of the IQR; the latter computed as 1.5 times interquartile range (i.e. 25—75%).

Table 1. Patient positioning performance in numbers (%), median, and interquartile range [IQR] for radiographers and the 3D camera and all four body parts individually and combined. Patient positioning data for absolute table height deviaton and higher/lower than the isocenter.

Body part	Abdomen	Head	Thorax-Abdomen	Thorax	Total body parts
Radiographers					
Patients, *n (%)*	115 (27%)	73 (17%)	72 (17%)	163 (39%)	423 (100%)
Median of absolute table height deviation, mm	12.0 [21.6]	12.2 [12.0]	13.4 [17.6]	14.7 [17.3]	13.2 [17.0]
Patients positioned higher than isocenter, *n (%)*	39 (34%)	34 (47%)	15 (21%)	45 (28%)	133 (31.4%)
Patients positioned lower than isocenter, n (%)	76 (66%)	39 (53%)	57 (79%)	118 (72%)	290 (68.6%)
Median of table height deviation, mm	10.08	1.95	10.44	10.23	9.47
Total	*115 (100%)*	*73 (100%)*	*72 (100%)*	*163 (72%)*	*423 (100%)*
3D Camera					
Patients, *n (%)*	58 (23%)	45 (18%)	70 (27%)	81 (32%)	254 (100%)
Median of absolute table height deviation, mm	6.3 [6.9]	9.5 [6.8]	6.0 [6.1]	5.4 [6.4]	6.1 [7.0]
Patients positioned higher than isocenter, n (%)	49 (84%)	28 (62%)	61 (87%)	63 (78%)	201 (79.1%)
Patients positioned lower than isocenter, n (%)	9 (16%)	17 (38%)	9 (13%)	18 (22%)	53 (20.9%)
Median of table height deviation, mm	-5.97	-3.99	-5.86	-4.27	-5.35
Total	*58 (100%)*	*45 (100%)*	*70 (100%)*	*81 (100%)*	*254 (100%)*
p value median absolute table height deviation	<0.05	0.039	<0.05	<0.05	<0.05

Data are numbers (%) and median [interquartile range]

DISCUSSION

We assessed the possible improvement of patient positioning in the CT gantry when using a 3D camera system with automated patient body contour detection over conventional manual positioning by radiographers with the aid of laser beams. We found that the 3D camera allowed for more accurate patient positioning than radiographers, resulting in significantly smaller median deviations from the ideal table height.

There have been previous initial attempts at automatic vertical position (AVP) such as described by Li et al. [16]. They assessed the effect of AVP software on radiation dose in CT, based on matching the patient's mean center of mass, calculated from the lateral

localizer radiograph. They showed vertical positioning by radiographers differed from automatic vertical positioning with an average of 33.2 mm (range 5.1 - 97 mm) [16]. Although their values were much higher than our results and no 3D camera was used, their AVP software also outperformed the radiographers. However, a major drawback of their approach was the inability to immediately use the recommendations given by the AVP software, which hampers routine clinical use. The 3D camera system in our study is fully integrated into the scanner system workflow.

We found a certain deviation from the isocenter not only for the radiographers, but also for the camera. Possible causes for this are inaccurate 3D depth data from the camera or inaccurate fitting of the Avatar model to this depth data. Apart from the visualizations like the one in Figure 1d, we did not have access to the Avatar data and thus were not able to investigate the latter possible cause any further. Nevertheless, we believe that the Avatar model and its registration algorithm can be improved by training and learning from clinical data.

Although we have no figures to proof this statement, we believe that automatic positioning might be an asset to help the radiographers speed up their routinely tasks. In clinical practice, we observed a more accurate positioning with the aid of the fast analysis of the 3D camera and in our opinion, the radiographers are supported in patient positioning with the aid of the camera, rather than visually checking only. Thereby they might be faster in determining of the ideal table height. Nevertheless, we believe it is rather the symbiosis of the human and the smart technology, which is making the difference: After the suggestion for the scan range and table height position done by the camera, the radiographer can easily check and adjust the proposals, while the main focus is on the patient itself. However, radiographers play an important role and remain indispensable in minimizing patient dose through optimized patient positioning [5], especially in challenging patients. Therefore, patient positioning deserves increased attention in clinical practice [10] and in education.

For the vast majority of patients different positioning was not a problem for the camera to perform adequately. For sixteen patients, the body contour appeared to be challenging including ten cases where folds in clothing, electronic wires and blankets gave rise to false interpretation of body shape, which would account for large deviations.

In two cases, the positioning of the head varied, as some parts of the head were not captured in depth measurements, or a bright white surface on the head such as a bandage led to erroneous protrusion of the forehead. This might explain the median absolute table height deviation for the camera being largest for the patient's head. In four cases, the patient was partly positioned in the gantry and the body parts were not in the full field of view of the camera. For these cases, it was possible to apply a fallback to the depth data and perform the analysis. In this way, the depth surface as seen by the camera and the curvature of the CT table is used, instead of the Avatar. With respect to

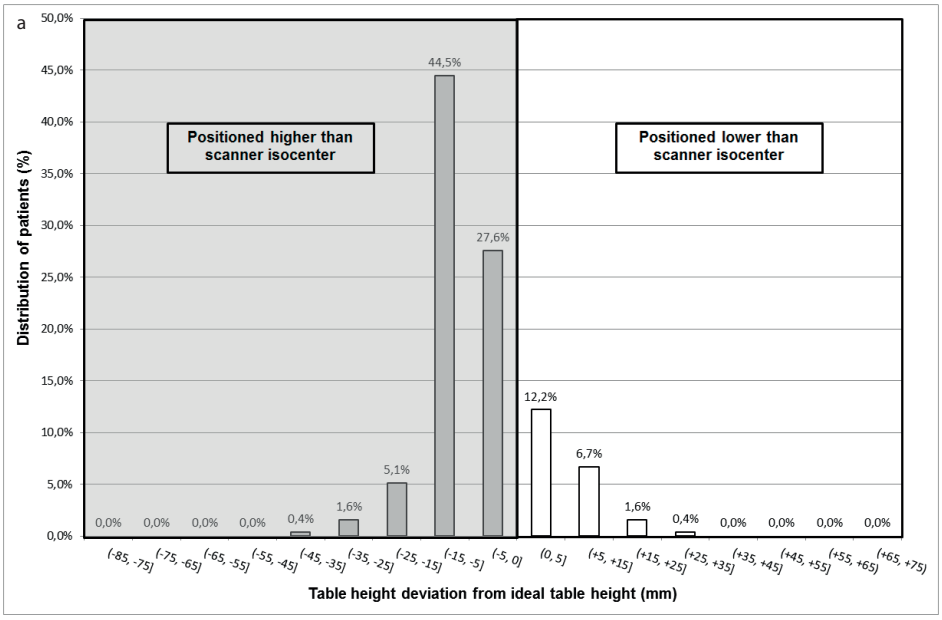

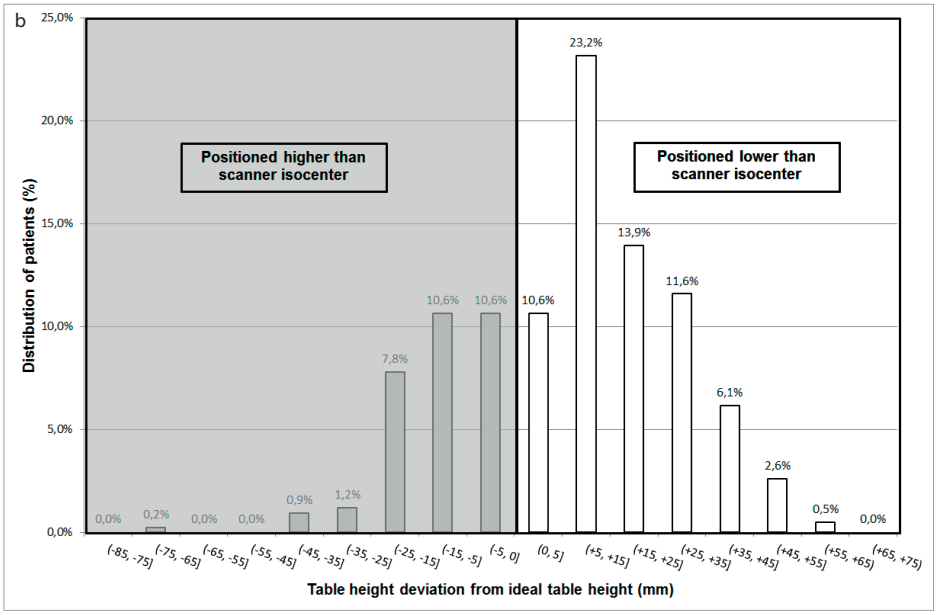

Figure 4 (a-b). (a) Distribution of patients positioned higher (negative numbers) and lower (positive numbers) from the ideal table height with table height suggestion by the 3D camera; **(b)** Distribution of patients positioned higher (negative numbers) and lower (positive numbers) from the ideal table height with manual positioning done by radiographers.

the false interpretation of body shape and applied fallback, we considered the data valid for analysis.

The difference in tendency of positioning of head CT (lower or higher than the isocenter) for radiographers and the 3D camera can probably be explained the same as for the challenges of the 3D camera: interpretation of the head was in some cases challenging. In addition, head CT positioning can be performed in different ways: soft cushion, carbon head holder, soft cushion head support or even no head holder at all, making isocentration complicated. For both radiographer and camera, it could be difficult to estimate the back of the head and to interpret the ideal table height whit varying head support. However, the overall deviation from the ideal table height was much less extreme with the 3D camera. This implies that most likely better dose management and image quality can be obtained with the use of the 3D camera system, compared to manual patient positioning by radiographers.

Positioning of the patient higher or lower than the scanner isocenter has a different effect on the distortion of the localizer radiograph. We did not evaluate the specific dose and image quality changes in the current study as they may be related to other factors as well. To evaluate the effect on dose and image quality of the distortion of the localizer radiograph, ideally each patient would be positioned and scanned twice: once with table height selection by the radiographer and once with selection by the camera. However, this would expose the patient to double the radiation dose. Saltybaeva and Alkadhi [12] reported in their phantom study no significant impact of off-centering on dose and image quality. However, off-centering with more than 4 cm resulted in increased radiation dose of 20%. Considering the median absolute table height deviation in our study, the more accurate positioning of the 3D camera has potential advantages in optimization of radiation dose and image quality.

Recently, Saltybaeva et al. [17] also demonstrated more accurate patient positioning with the aid of a 3D camera system similar to the one described here. They also found a significant improvement in patient centering when using automatic positioning with the 3D camera compared to manual positioning by radiographers. However, their study was limited to abdominal and thoracic CT scans. Our data included thorax-abdominal and head CT scans as well. Moreover, the number of patients included was higher in our study: 423 patients versus 52 patients positioned by radiographers, and 254 patients versus 68 patients with the camera. Also, we evaluated the number of patients positioned either lower or higher than the scanner isocenter for both radiographers and the camera.

The definition of the ideal table height was based on the idea to center the patient around the scanner's isocenter for optimal performance of the automatic exposure control (AEC). However, it might be preferable to place the examined organ, e.g., the spine or heart in the isocenter, because the scanner's image quality and temporal resolution are best near the isocenter. Therefore, a cardiac subset (n=63) was analyzed to assess how much the isocenter of the heart differs from the patient's body isocenter (Appendix

- Fig. A1). We think that the information obtained from the fitted avatar model allows for such organ-based table height selection and could be a topic of further investigation. The AEC algorithm should take this off-center positioning into account, for example, as described by McMillan et al. [18].

There are limitations to this study that require consideration. Because of the retrospective nature of the study, multiple radiographers performed the CT scans on the two different DSCT scanners. However, the scanners, patient groups, and radiographers were comparable. In addition, the study took place within the same hospital department. All radiographers had been trained to use the equipment and were experienced in performing CT scans and positioning of patients. This reflects daily clinical practice at our department.

For purpose of the analysis, we used all longitudinal positions of the scanned range to calculate the algorithm isocenter. This differs from routine operation of the camera system, whereby two-dimensional visible light information was used for automatic planning of the scan range and was manually adjustable to preferences of length and region before performing a localizer radiograph. The radiographer can adjust the scan length after performing the localizer radiograph. Consequently, the suggested table height by the, automatic or manually, planned scan range may differ. We did no further analyses on these differences but updating of table height suggestion after performing of a localizer radiograph would be of interest.

In conclusion, the 3D camera for body contour detection made patient positioning in CT at the ideal table height more accurate with less extreme deviations compared to manual positioning by radiographers. Radiographers will continue on playing an important role and remain indispensable for optimization of radiation dose and image quality through optimized patient positioning, especially in challenging patients.

ACKNOWLEDGEMENTS

We would like to thank Andreas Wimmer and Thomas Boettger (Siemens Healthineers, Forchheim, Germany) for providing information on the technical details of the 3D camera algorithm and for assisting in the analysis of the data.

REFERENCES

1. Brenner DJ, Hall EJ. Computed tomography--an increasing source of radiation exposure. N Engl J Med. 2007;357(22):2277-84.
2. Meulepas JM, Smets A, Nievelstein RAJ, Gradowska P, Verbeke J, Holscher HC, et al. Trends and patterns of computed tomography scan use among children in The Netherlands: 1990-2012. Eur Radiol. 2017;27(6):2426-33.
3. Willemink MJ, Leiner T, de Jong PA, de Heer LM, Nievelstein RA, Schilham AM, et al. Iterative reconstruction techniques for computed tomography part 2: initial results in dose reduction and image quality. Eur Radiol. 2013;23(6):1632-42.
4. Raman SP, Johnson PT, Deshmukh S, Mahesh M, Grant KL, Fishman EK. CT Dose Reduction Applications. Available Tools on the Latest Generation of CT Scanners. Journal of the American College of Radiology. 2013;10(1):37-41.
5. Habibzadeh MA, Ay MR, Asl ARK, Ghadiri H, Zaidi H. Impact of miscentering on patient dose and image noise in x-ray CT imaging: Phantom and clinical studies. Phys Med. 2012;28(3):191-9.
6. Kaasalainen T, Palmu K, Lampinen A, Kortesniemi M. Effect of vertical positioning on organ dose, image noise and contrast in pediatric chest CT--phantom study. Pediatr Radiol. 2013;43(6):673-84.
7. Kaasalainen T, Palmu K, Reijonen V, Kortesniemi M. Effect of patient centering on patient dose and image noise in chest CT. AJR Am J Roentgenol. 2014;203(1):123-30.
8. Perisinakis K, Seimenis I, Tzedakis A, Papadakis AE, Damilakis J. The effect of head sizeshape, miscentering, and bowtie filter on peak patient tissue doses from modern brain perfusion 256-slice CT: how can we minimize the risk for deterministic effects? Med Phys. 2013;40(1):011911.
9. Harri PA, Moreno CC, Nelson RC, Fani N, Small WC, Duong PA, et al. Variability of MDCT dose due to technologist performance: impact of posteroanterior versus anteroposterior localizer image and table height with use of automated tube current modulation. AJR Am J Roentgenol. 2014;203(2):377-86.
10. Toth T, Ge Z, Daly MP. The influence of patient centering on CT dose and image noise. Med Phys. 2007;34(7):3093-101.
11. Marsh RM, Silosky MS. The effects of patient positioning when interpreting CT dose metrics: A phantom study. Med Phys. 2017;44(4):1514-24.
12. Saltybaeva N, Alkadhi H. Vertical off-centering affects organ dose in chest CT: Evidence from Monte Carlo simulations in anthropomorphic phantoms. Med Phys. 2017;44(11):5697-704.
13. Li J, Udayasankar UK, Toth TL, Seamans J, Small WC, Kalra MK. Automatic patient centering for MDCT: effect on radiation dose. AJR Am J Roentgenol. 2007;188(2):547-52.
14. Remondino F, Stoppa D. TOF Range-Imaging Cameras: Springer, Berlin, Heidelberg. DOI:10.1007/978-3-642-27523-4; 2013.
15. Singh V, Ma K, Tamersoy B, Chang Y-J, Wimmer A, O'Donnell T, et al. DARWIN: Deformable Patient Avatar Representation With Deep Image Network. In: Descoteaux M, Maier-Hein L, Franz A, Jannin P, Collins DL, Duchesne S, editors. Medical Image Computing and Computer-Assisted Intervention – MICCAI 2017: 20th International Conference, Quebec City, QC, Canada, September 11-13, 2017, Proceedings, Part II. Cham: Springer International Publishing; 2017: 497-504..
16. Li J, Udayasankar UK, Toth TL, Small WC, Kalra MK. Application of automatic vertical positioning software to reduce radiation exposure in multidetector row computed tomography of the chest. Invest Radiol. 2008;43(6):447-52.

17. Saltybaeva N, Schmidt B, Wimmer A, Flohr T, Alkadhi H. Precise and Automatic Patient Positioning in Computed Tomography: Avatar Modeling of the Patient Surface Using a 3-Dimensional Camera. Invest Radiol. 2018.
18. McMillan K, Bostani M, Cagnon CH, Yu L, Leng S, McCollough CH, et al. Estimating patient dose from CT exams that use automatic exposure control: Development and validation of methods to accurately estimate tube current values. Med Phys. 2017;44(8):4262-75

APPENDIX

For optimal performance of automated exposure control (AEC), accurate centering of the patient's body in the CT scanner is mandatory because patient positioning affects the body size on a CT localizer radiograph. On the other hand, the optimal temporal resolution is obtained when the patient's heart is centered in the scanner. Possible differences in the ideal table height with respect to exposure control and temporal resolution were analyzed.

The ideal table height for optimal temporal resolution performance was defined as the table height at which the scanner isocenter coincides with the center of the patient's heart. In the axial image centrally through the heart, the position of the heart relative to the patient isocenter was calculated (MATLAB R2008a, The MathWorks Inc., Natick, Massachusetts, USA).

On average, the table height for optimal temporal resolution (heart isocenter in scanner isocenter) of the cardiac subset (n=63) was 37.8 (IQR 8.2) mm lower than the height for optimal ATCM performance.

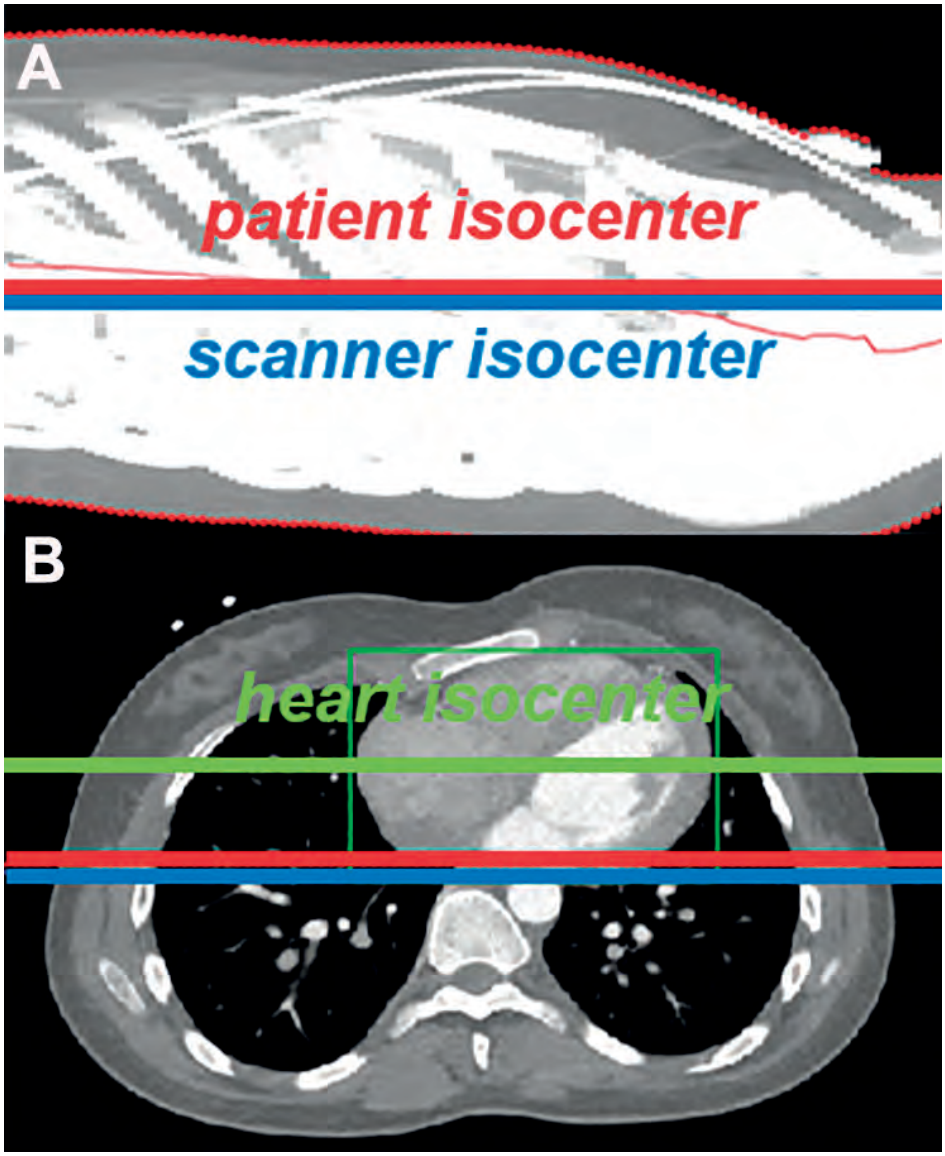

Figure A1 (a-b). Table height for proper patient positioning **(a, lateral MIP)** and proper heart positioning **(b, axial view)**. Blue line=scanner isocenter; red line=patient isocenter; green line=heart isocenter.

CHAPTER 4

Automated patient positioning in CT using a 3D camera for body contour detection: accuracy in pediatric patients

This chapter is based on the publication in Eur Radiol. 2019;DOI 10.1007/s00330 020-07097-w

Ronald Booij; Marcel van Straten; Andreas Wimmer; Ricardo P. Budde

ABSTRACT

Objective

To assess the accuracy of a 3D camera for body contour detection in pediatric patient positioning in CT compared with routine manual positioning by radiographers.

Methods and materials

One hundred and ninety-one patients, with and without fixation aid, which underwent CT of the head, thorax, and/or abdomen on a scanner with manual table height selection and with table height suggestion by a 3D camera were retrospectively included. The ideal table height was defined as the position at which the scanner isocenter coincides with the patient's isocenter. Table heights suggested by the camera and selected by the radiographer were compared with the ideal height.

Results

For pediatric patients without fixation aid like a baby cradle or vacuum cushion and positioned by radiographers, the median (interquartile range) absolute table height deviation in mm was 10.2 (16.8) for abdomen, 16.4 (16.6) for head, 4.1 (5.1) for thorax-abdomen and 9.7 (9.7) for thorax CT scans. The deviation was less for the 3D camera: 3.1 (4.7) for abdomen, 3.9 (6.3) for head, 2.2 (4.3) for thorax-abdomen and 4.8 (6.7) for thorax CT scans ($p < 0.05$ for all body parts combined).

Conclusion

A 3D camera for body contour detection allows for automated and more accurate pediatric patient positioning than manual positioning done by radiographers, resulting in overall significantly smaller deviations from the ideal table height. The 3D camera may be also useful in the positioning of patients with fixation aid; however, evaluation of possible improvements in positioning accuracy was limited by the small sample size.

INTRODUCTION

Technological developments in Computed Tomography (CT) enhanced the clinical imaging possibilities in pediatric patients, sparking off a growth in the number of CT scans performed within this population [1; 2]. Over the years, considerable efforts have been made to optimize radiation dose and image quality (IQ) [3; 4]. Several techniques are used to optimize pediatric CT scanning protocols such as automated tube current and tube voltage adaptation, as well as the use of iterative reconstruction techniques [5-8]. For an ideal working of the automatic exposure control (AEC) and to achieve ideal IQ, it is important to position the patient exactly in the center of the CT gantry [9]. Vertical patient positioning is determined by setting the table height. Ideal positioning is defined as the table height at which the patient's and scanner's isocenter coincide. Patient positioning lower or higher than the scanner isocenter (i.e., table set too low or too high) affects the patient's shape and size on a CT scan localizer radiograph, which is of direct effect on the behavior of the AEC. Positioning of pediatric patients is quite challenging, because of the wide variation in body proportions. Furthermore, when they have to be positioned in fixation aids such as a baby cradle or vacuum cushion due to lack of cooperation, it is more difficult to estimate the center of the patient. Recent studies have exhibited the benefits of using a 3D camera and a body contour detection algorithm for the accurate positioning of adult patients, resulting in smaller deviations from the ideal table height compared with manual positioning done by radiographers [10; 11]. The camera algorithm is described in detail in our paper with regard to (adult) patient positioning [11]. It was not yet applicable to pediatric patients due to their different body proportions compared with adults [10; 11]. The algorithm was improved to account for the pose and body proportions of pediatric patients, too. The aim of this study was to determine the accuracy of the new improved version of the algorithm in the positioning of pediatric patients in comparison to manual positioning done by radiographers.

MATERIALS AND METHODS

Study design and patient selection

The study was conducted in accordance with the Declaration of Helsinki and international standards of Good Clinical Practice. The medical ethics committee of our hospital waived the need for informed consent. All consecutive pediatric (<18 years old) patients that underwent a CT examination of the head, thorax and/or abdomen during routine clinical care in our hospital during a five-month period from September 2018 to February 2019 were retrospectively included. All scans were performed on a dual source CT scanner (DSCT) (SOMATOM Drive (software version Syngo CT VA62A), Siemens

Healthineers) that was also equipped with a commercially available 3D camera for body contour detection (Siemens Healthineers).

Manual patient positioning by radiographers

Positioning and scanning of the pediatric patients were done by a team of dedicated CT radiographers as per normal clinical routine. Patients were positioned by the radiographer with the aid of laser beams within the gantry of the CT scanner. A horizontal laser line was projected on the lateral side of the patient and the table height was adjusted by the radiographer so that the laser line was assumed to align the center of the body region to be examined with the scanner isocenter. In our hospital, radiographers are trained to pay special attention to the position of the patient. Scanning was performed after this manual positioning done by radiographers.

Patient positioning using a 3D camera for body contour detection

3D camera images of children were collected and retrospectively used for the evaluation of the accuracy in patient positioning. The 3D camera is part of the CT system (SOMATOM Drive, Siemens Healthineers) and is attached to the ceiling and in front of the CT scanner, facing down onto the patient table. To start the 3D camera patient positioning process, the radiographer triggers a planning image with the camera when the patient is lying down on the scanner table in the target pose for the CT examination. The camera obtains two images: a color image and a depth image. Each pixel in the depth image describes the distance from the camera to the closest object surface. First, the algorithm detects the pose of the patient and body regions using the depth measurements and the known table position and shape [12]. After selection of the scan range, the ideal table height for the individual patient and the scheduled examination is proposed by the 3D camera such that the isocenter of the selected body region and the scanner isocenter align. Therefore, a virtual patient Avatar is fitted to the camera data in order to cope with areas that cannot be seen by the camera, e.g., through clothing or blankets or to handle positioning aids. The Avatar is a statistical shape model that in the fitting process assumes the pose and body proportions of the patient found in the depth data. The isocenter curve of the Avatar is finally averaged across all slices of the body region selected on the localizer radiograph. If Avatar fitting is not possible, then the isocenter curve is automatically obtained as the geometric center between the camera depth data and the central part of the scanner table. This is the same fallback as described before [11]. For adult patients, the camera images are processed by an algorithm [12], as described in detail before [10; 11]. However, the algorithm installed on the scanner that was used in the (adult) reference study was not optimized for pediatric patients. Therefore, prior to the start of the inclusion for this study, an algorithm training was performed on a separate large dataset of pediatric patients (n=267) to improve the landmark detection and

to adjust the Avatar shape model to the different body proportions found in pediatric patients. With the adaptations made, the new version of the algorithm was expected to work for adult and pediatric patients, but was not yet installed at the scanner during the inclusion. Therefore, the algorithm was applied retrospectively without the need of additional data and no user input was required afterwards. By doing so, off-line system performance is equal to the real-world situation. When the algorithm was not able to fit the Avatar, the regular and automatic fallback was applied for patients positioned with and without a fixation aid, such as a baby cradle (Fig. 1) or a vacuum cushion (Fig. 2). The algorithm is currently not commercially available.

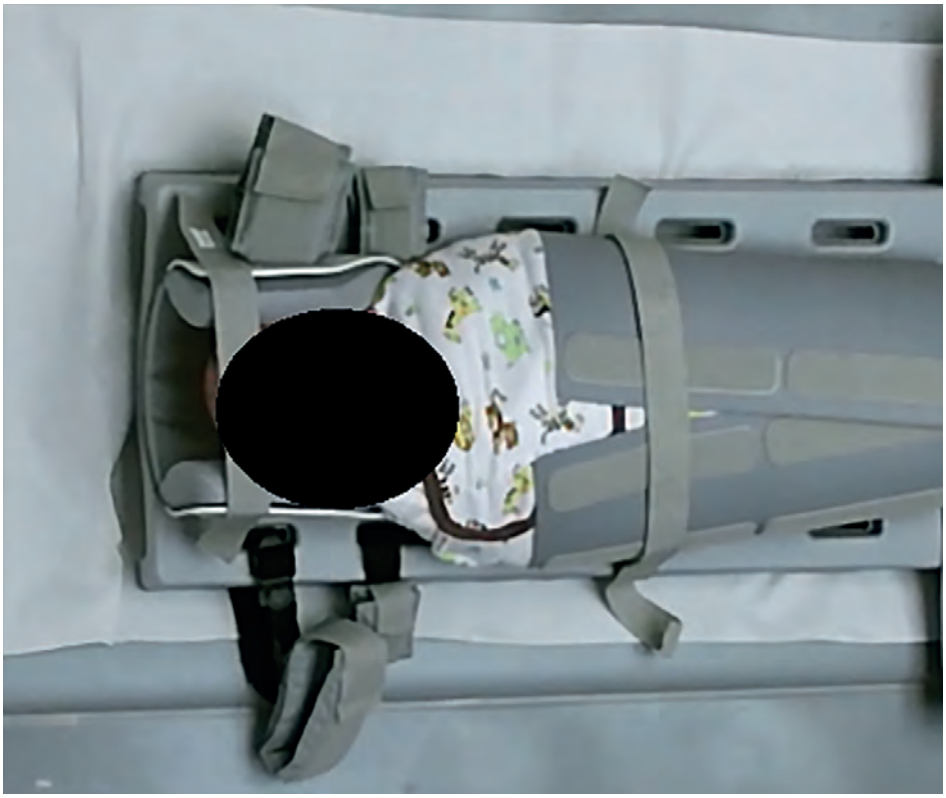

Figure 1. A child under the age of 1 year positioned in a (vendor specific) baby cradle.

Figure 2. A child under the age of 1 year positioned in a vacuum cushion.

Calculation of patient positioning accuracy

CT image reconstructions with a slice thickness of 3.0 mm and a reconstruction increment of 3.0 mm were used. The reconstructed field-of-view included the entire skin surface. The skin surface was extracted from the CT data in each axial slice and used to calculate the middle of the patient in the anterior-posterior direction. These values were averaged over all slices along the z-axis, providing the patient isocenter, to determine the ideal table height as described in detail before [11]. Accuracy in patient positioning is demonstrated as the difference between this ideal table height and the table height proposed by the camera algorithm or the radiographer. The accuracy is expressed as a single and absolute value in millimeter. The distribution of patients with a table height deviation lower or higher than the ideal table height is expressed as positive or negative numbers, respectively.

Exclusion of scans

Cases with obvious patient movement or repositioning between the body contour detection by the 3D camera and the CT scan or with large items blocking the camera sight were excluded.

Statistical analyses

Significant differences in patient positioning between the radiographers and the 3D camera were analyzed by means of normality and a nonparametric test. The absolute

table height deviation is a continuous paired variable reported as median (interquartile range (IQR)), calculated with Microsoft Excel (Microsoft Office Professional Plus 2016). Data distribution was tested with the Shapiro-Wilk test. Wilcoxon signed-rank test was used for comparison of the absolute table height deviation for the different body regions within and between the camera- and radiographer-group. A two-sided *p*-value of < 0.05 was considered statistically significant. Statistical analyses were performed using SPSS (version 25, IBM Corp). Continuous measures of absolute table height deviation (mm) were calculated and evaluated with Microsoft Excel (Microsoft Office Professional Plus 2016). A post hoc power analysis was performed with G*Power (version 3.1.9.6) for the patients positioned with a fixation aid to determine the effect size, given the power to be achieved (80%) and the sample size available [13; 14]. The purpose of this test is to estimate the smallest possible difference in patient positioning accuracy between the 3D camera and the radiographer that can be detected in this study.

RESULTS

Patient groups

After exclusion of sixteen scans from the analysis due to patient repositioning after body contour detection by the 3D camera or because of large objects blocking the camera sight, one hundred and ninety-one scans were available for analysis. Of which, 149 pediatric patients were without, and 42 patients were with a baby cradle or vacuum cushion. Within the group without fixation aids, the median age (IQR) was 11 years (6) and ranged between three months and seventeen years old. For patients positioned in the baby cradle or the vacuum cushion, the median age (IQR) was 0.8 years (1.4) and ranged between 1 day and 6 years.

Patient positioning accuracy of radiographers

Within the group without fixation aids, median (IQR) absolute table height deviation was 10.2 (16.8) for abdomen, 16.4 (16.6) for head, 4.1 (5.1) for thorax-abdomen, and 9.7 (9.7) mm for thorax CT scans positioned by radiographers (Fig. 3 and Table 1). A total of 41 (28%) patients were positioned higher than the scanner isocenter. The majority of patients were positioned lower than the scanner isocenter (Table 1).

For the 42 patients positioned in the baby cradle or the vacuum cushion, the median (IQR) absolute table height deviation was 8.7 (1.1) for abdomen, 9.1 (12.9) for head, 8.0 (3.1) for thorax-abdomen, and 15.3 (15.8) mm for thorax CT scans (Table 2). A total of 12 (29%) patients were positioned higher than the scanner isocenter. Within this group, the majority of patients were also positioned lower than the scanner isocenter (Table 2).

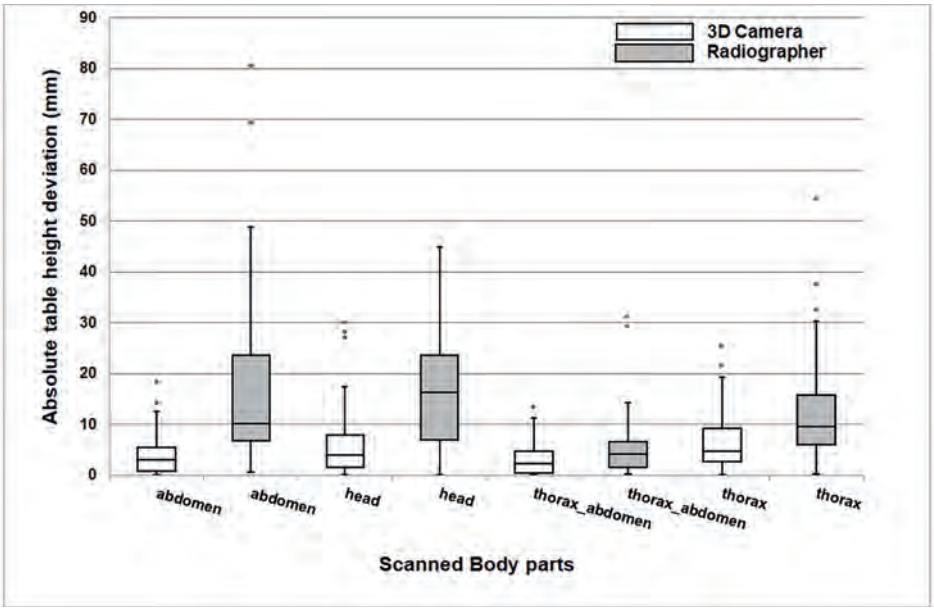

Figure 3. Box-and-whisker plots of patient positioning performance of all different body parts separately for the radiographers and the 3D camera for pediatrics positioned without fixation aid.
The median (horizontal line within box), interquartile range (box), and nonoutlier range (whiskers) which is defined as 1.5 times interquartile range (i.e. 25—75%). The largest deviations from the scanner isocenter, outside the nonoutlier range, are plotted as open dots.

Patient positioning accuracy of 3D camera

Within the group without fixation aids, median (IQR) absolute table height deviation in millimeter was 3.1 (4.7) for abdomen, 3.9 (6.3) for head, 2.2 (4.3) for thorax-abdomen, and 4.8 (6.7) for thorax CT scans (Fig. 3; Table 1). A small majority of the patients were positioned lower than the scanner isocenter (Table 1).

Within the patient group positioned in the baby cradle or vacuum cushion, the median (IQR) absolute table height deviation was 10.8 (8.3) for abdomen, 10.2 (15.3) for head, 17.4 (16.0) for thorax-abdomen, and 15.2 (15.0) mm for thorax CT scans. Within this group, the majority of patients were also positioned lower than the scanner isocenter (Table 2). An Avatar could be used in three out of nine cases when a patient was positioned in a baby cradle and the fallback had to be applied for all cases positioned in a vacuum cushion.

Table 1. Pediatric patient positioning performance, without a baby cradle or vacuum cushion, in median and interquartile range (IQR) for radiographers and the 3D camera and all four body parts individually, and for all body parts combined.

Table 1. Pediatric patient positioning without a baby cradle or vacuum cushion: Comparison of table height deviation for radiographers and 3D Camera					
Body part	**Abdomen**	**Head**	**Thorax-Abdomen**	**Thorax**	**All body parts combined**
Total number of patients without a baby cradle or vacuum cushion	22 (15%)	46 (31%)	14 (9%)	67 (45%)	149 (100%)
Table height determined by: Radiographers					
Median of absolute table height deviation, mm	10.2 [16.8]	16.4 [16.6]	4.1 [5.1]	9.7 [9.7]	10.3 [12.6]
Patients positioned higher than isocenter, *n (%)*	5 (23%)	15 (33%)	2 (14%)	19 (28%)	41 (28%)
Patients positioned lower than isocenter, n (%)	17 (77%)	31 (67%)	12 (86%)	48 (72%)	108 (72%)
Largest deviation, mm {age in years}	80.5 {13yr}	44.9 {3yr}	31.1 {12yr}	54.3 {11yr}	
Table height determined by: 3D Camera					
Median of absolute table height deviation, mm	3.1 [4.7]	3.9 [6.3]	2.2 [4.3]	4.8 [6.7]	3.7 [5.8]
Patients positioned higher than isocenter, n (%)	8 (36%)	22 (48%)	6 (43%)	33 (49%)	69 (46%)
Patients positioned lower than isocenter, n (%)	14 (64%)	24 (52%)	8 (57%)	34 (51%)	80 (54%)
Largest deviation, mm {age in years}	18.2 {15yr}	-30.1 {10yr}	-13.5 {13yr}	-25.4 {3yr}	
p value median absolute table height deviation (3D camera versus radiographer)	<0.05	<0.05	0.064	<0.05	<0.05

Data are numbers (%) and median [interquartile range]
Negative deviaton numbers: patient positioned higher than isocenter
Positive deviation numbers: patient positioned lower than isocenter

Comparison between radiographer and 3D camera

For patients positioned without the baby cradle or vacuum cushion, the median absolute table height deviations were higher for all four body parts when positioned by the radiographer compared with table height suggestion by the 3D camera (Table 1). For each of the four body parts, the largest deviation from the ideal table height was also higher for patients positioned by the radiographer. The largest deviation was 80.5 mm for an abdominal scan with the pediatric patient positioned lower than the isocenter by the radiographer. For the 3D camera the largest deviation was 30.1 mm. Patient posi-

tioning accuracy for the 3D camera system and the radiographers differed significantly for all body parts (p <0.05) with the exception of thorax-abdomen scans (p = 0.064). Figure 4 shows a case presentation with small deviations from the ideal table height of 0.13 mm and -0.82 mm for the 3D camera and radiographer, respectively.

For patients positioned with the baby cradle and vacuum cushion, the deviation from the ideal table height by the 3D camera was up to 46.4 mm for a thoracic scan (Table 2). For the radiographer, the largest deviation was 42.4 mm below the isocenter. Difference between patient positioning accuracy of the 3D camera system and the radiographers was not significant (Table 2). For both groups, the mean and standard deviation (SD) of the table height deviation for all body parts combined (n = 42) was calculated for the post hoc power analysis. The mean (SD) was 17.1 (15.6) mm and 12.2 (9.4) mm for the 3D camera and radiographers group, respectively, with a correlation coefficient between groups of 0.2. The effect size or Cohen's d corresponding with a power of 80% was 0.45. This is equivalent to a difference of 8.2 mm between camera and radiographers.

Positioning of young patients with lots of cabling, vital monitoring devices, or blankets was challenging for accurate positioning by both the 3D camera and the radiographers. Such a case presentation is presented in Figure 5 with an ideal table height deviation of -10.3 mm and 23.8 mm for the 3D camera and radiographer, respectively.

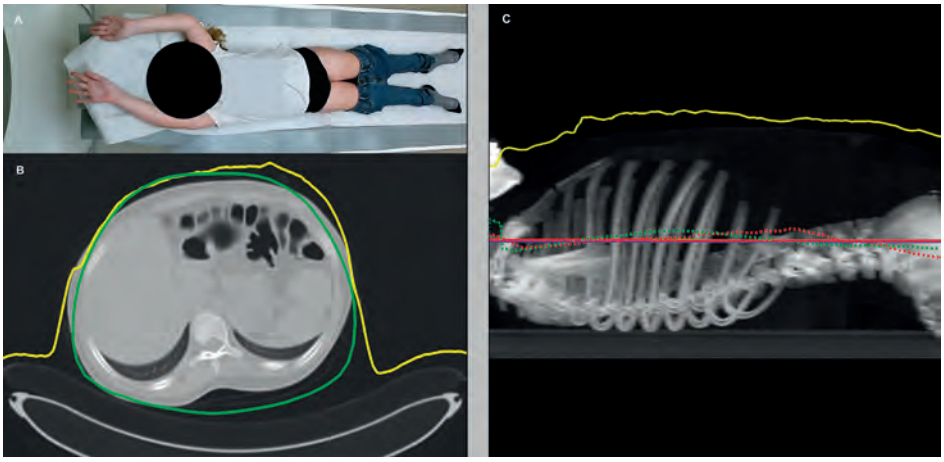

Figure 4 (a-c). Case presentation of a 12-year old child. **(a)** Color image taken by the 3D camera system. **(b)** Axial image of the abdomen with depth measurements (yellow line) by the 3D camera and the body contour (green) estimated by the algorithm. **(c)** Sagittal image of the thorax-upper abdomen with patient positioning accuracy: Blue horizontal line: patient isocenter estimated by the radiographer, green horizontal line: average patient isocenter estimated by the camera, green dotted line: Avatar isocenter curve, red horizontal line: average patient isocenter (ideal table height), red dotted line: patient isocenter per axial cross-section, yellow line: depth measurements. Note: The red, green, and blue straight lines are hard to distinguish from each other due to almost similar values as the ideal table height.

Table 2. Pediatric patient positioning performance, with a baby cradle or vacuum cushion, in median and interquartile range (IQR) for radiographers and the 3D camera and all four body parts individually, and for all body parts combined.

Table 2. Pediatric patient positioning with a baby cradle or vacuum cushion: Comparison of table height deviation for radiographers and 3D Camera					
Body part	**Abdomen**	**Head**	**Thorax-Abdomen**	**Thorax**	**All body parts combined**
Total number of patients with a baby cradle or vacuum cushion	3 (7%)	20 (48%)	2 (5%)	17 (40%)	42 (100%)
Table height determined by: Radiographers					
Median of absolute table height deviation, mm	8.7 [1.1]	9.1 [12.9]	8.0 [3.1]	15.3 [15.8]	9.2 [13.7]
Patients positioned higher than isocenter, *n (%)*	1 (33%)	4 (15%)	1 (50%)	6 (41%)	12 (29%)
Patients positioned lower than isocenter, n (%)	2 (67%)	17 (85%)	1 (50%)	10 (59%)	30 (71%)
Largest deviation, mm {age in months}	10.3 {12M}	-32.8 {3M}	11.1 {2M}	-42.4 {48M}	
Table height determined by: 3D Camera					
Median of absolute table height deviation, mm	10.8 [8.3]	10.2 [15.3]	17.4 [16.0]	15.2 [15.0]	10.9 [16.6]
Patients positioned higher than isocenter, n (%)	2 (67%)	18 (85%)	1 (50%)	7 (47%)	28 (67%)
Patients positioned lower than isocenter, n (%)	1 (33%)	3 (15%)	1 (50%)	9 (53%)	14 (33%)
Largest deviation, mm {age in months}	-23.3 {72M}	-67.1 {23M}	33.4 {2M}	-46.4 {5M}	
p value median absolute table height deviation (3D camera versus radiographer)	0.593	0.167	0.655	0.850	0.105

Data are numbers (%) and median [interquartile range]
Negative deviation numbers: patient positioned higher than isocenter
Positive deviation numbers: patient positioned lower than isocenter

DISCUSSION

We assessed the accuracy of pediatric patient positioning with the aid of a body contour detection system (3D camera) and compared it with manual positioning by radiographers. We found that positioning with the 3D camera of pediatric patients without a fixation aid allows for more accurate patient positioning than manual positioning by radiographers. This outcome is similar to the findings in adult patients [10; 11]. Differences in positioning accuracy between the 3D camera and radiographers were not statistically significant for patients positioned in a baby cradle or a vacuum cushion. In virtually all

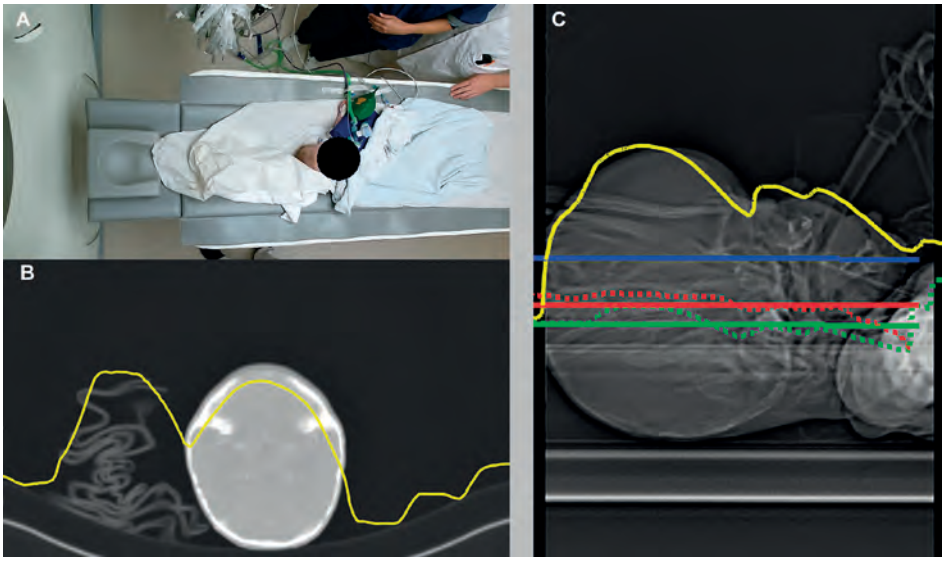

Figure 5 (a-c). Case presentation of a 3-month old child wrapped in a blanket with a breathing support and wires where accurate positioning is challenging for both the 3D camera and the radiographers. **(a)** Color image taken by the 3D camera system. **(b)** Axial image of the brain with depth measurements (yellow line) by the 3D camera. **(c)** Sagittal image of the head with patient positioning accuracy: Blue horizontal line: patient isocenter estimated by the radiographer, green horizontal line: Algorithm isocenter estimated by the camera, green dotted line: Algorithm isocenter curve, red horizontal line: average patient isocenter (ideal table height), red dotted line: patient isocenter per axial cross-section, yellow line: depth measurements.

cases of infants placed in fixation aids, like a baby cradle (Fig. 1) or a vacuum cushion (Fig. 2), it was not possible to fit a patient Avatar due to the small body size and the large occlusions. Instead, the fallback described above was applied, where the isocenter is directly estimated as geometric mean between the depth measurements and the table. This approach introduces a deviation, because these fixation aids add a considerable layer between patient and table, which in the absence of the Avatar is wrongly attributed to the patient, leading to an overestimation of patient size. Nevertheless, positioning of patients in a fixation aid seems feasible with a 3D camera. Small performance differences between camera and radiographers could not be detected due to the limited number of patients included. However, post hoc power analysis showed that the performance difference was not larger than 8.2 mm; otherwise, this would have been noted given our sample size. Thus, the fallback routine facilitates automatic positioning of a pediatric patient while keeping possible differences with a well-trained radiographer below 10 mm on average.

However, the deviation from the ideal table height could be reduced by taking the positioning devices into account. Therefore, applying an intermediate step consisting of the detection of the presence of a fixation aid like a baby cradle and a vacuum cushion

(open and closed) might be of use and may be considered for further research. After detection of such aid, a correction for the thickness of such an aid can be applied to the geometric isocenter for these specific cases. The correction can be determined upfront by estimating the mean error for the vacuum cushion and by accounting for the fairly constant thickness of the baby cradle.

The two main challenges for the algorithm are the small size of the patients that are positioned with such aids and the large degree of occlusions introduced by the aids. Given a large amount of 3D camera training images, probably we could reliably fit the patient Avatar also under these circumstances. Then, as usual for cases without a baby cradle or a vacuum cushion, it would be possible to compute the center of the patient Avatar and naturally exclude additional layers such as blankets or fixation aids. The Avatar fitting was only possible in three out of nine cases when patients were positioned in a baby cradle and the fallback had to be applied in all cases when positioned in a vacuum cushion. Therefore, further work on the development with additional training data might improve the algorithm even further to reliably obtain a patient isocenter when patients are positioned in fixation aids like the baby cradle and vacuum cushion.

The 3D camera is able to assist the radiographer in positioning of pediatric patients, especially in cases without fixation aid. It should be emphasized that radiographers will continue to play an important role in patient positioning by patient guidance and verification of the table height suggested by the 3D camera, especially when fixation aids are used.

Studies demonstrated a significant impact on radiation dose and image quality when a pediatric patient is not properly positioned in the scanner isocenter [15; 16]. In those studies, an anthropomorphic head, thorax, and/or abdomen simulating on a 5-year-old child was used. Organ doses and noise differences with several vertical table height deviations were compared with organ dose and noise levels at the scanner isocenter/center position. A noise increase of up to 45% in chest scans relative to the center position was demonstrated for table positions in the highest (+54 mm) and lowest (-60 mm) vertical positions and a breast dose increase of up to 16% with 40 mm lower vertical position [16]. Although the absolute table height deviations in our study were not always that high, maximum deviation values were high, especially with radiographers (Tables 1 and 2). Relative breast dose increase was considered to be 7% lower with 20 mm vertical lower positioning compared with the 40 mm lower position. These vertical positions are comparable to the values of the largest deviations between the 3D camera and radiographers in our study. With the tendency to position pediatric patients more often lower than the ideal table height, the noise would increase. With less extreme deviations from the ideal table height that can be obtained with the 3D camera (Tables 1 and 2), both the radiation dose and the image quality will be more constant. The same applies for organ radiation doses and image noise in head and abdominal CT [15]. Large

vertical table height deviation was of substantial influence on radiation dose and image noise, where the impact of these deviations depends on the body region and location of individual organs within the body [15]. However, accurate and less deviations from the ideal table height are required to consolidate image quality and radiation dose. Our results were obtained in an academic facility with highly trained radiographers. It is conceivable that both the median and maximum values of deviation from the ideal positioning would be even larger when the study was obtained in a hospital without dedicated training in pediatric CT scanning.

There are limitations to this study that require considerations. For the purpose of the analysis, the algorithm used the actually scanned range to calculate the isocenter. This differs from routine operation of the camera system, whereby the algorithm uses the scan range that is defined on the planning image (=color photograph taken by the camera) prior to obtaining the localizer radiograph and scanning the patient. Consequently, the suggested ideal table height by the 3D camera based on the planned scan range may differ from the suggested table height based on the actual scan range. Nevertheless, our results demonstrate the accuracy when a 3D camera is used properly and the selected body region on the localizer radiograph and the actual scan range are the same.

In conclusion, a 3D camera for body contour detection allows for accurate pediatric patient positioning in CT. The 3D camera is able to assist the radiographer in positioning of pediatric patients, especially in cases without fixation aid. Positioning of patients in a fixation aid is feasible with a 3D camera, but evaluation of possible improvements in positioning accuracy was limited by the small sample size.

REFERENCES

1. Brenner DJ, Hall EJ. Computed tomography--an increasing source of radiation exposure. N Engl J Med. 2007;357(22):2277-84.
2. Miglioretti DL, Johnson E, Williams A, Greenlee RT, Weinmann S, Solberg LI, et al. The use of computed tomography in pediatrics and the associated radiation exposure and estimated cancer risk. JAMA Pediatr. 2013;167(8):700-7.
3. Strauss KJ, Somasundaram E, Sengupta D, Marin JR, Brady SL. Radiation Dose for Pediatric CT: Comparison of Pediatric versus Adult Imaging Facilities. Radiology. 2019;291(1):158-67.
4. Directorate-General for Energy. Radiation Protection N° 185: European Guidelines on Diagnostic Reference Levels for Pediatric Imaging. EU Publications. 2018; Available via: https://ec.europa.eu/energy/sites/ener/files/rp_185.pdf. Accessed 11-11-2020.
5. Yoon H, Kim MJ, Yoon CS, Choi J, Shin HJ, Kim HG, et al. Radiation dose and image quality in pediatric chest CT: effects of iterative reconstruction in normal weight and overweight children. Pediatr Radiol. 2015;45(3):337-44.
6. Siegel MJ, Ramirez-Giraldo JC, Hildebolt C, Bradley D, Schmidt B. Automated low-kilovoltage selection in pediatric computed tomography angiography : Phantom study evaluating effects on radiation dose and image quality. Invest Radiol. 2013;48(8):584-9.
7. Singh S, Kalra MK, Shenoy-Bhangle AS, Saini A, Gervais DA, Westra SJ, et al. Radiation dose reduction with hybrid iterative reconstruction for pediatric CT. Radiology. 2012;263(2):537-46.
8. Booij R, Dijkshoorn ML, van Straten M, du Plessis FA, Budde RP, Moelker A, et al. Cardiovascular imaging in pediatric patients using dual source CT. J Cardiovasc Comput Tomogr. 2016;10(1):13-21.
9. Almohiy H, Alasar EMM, Saade C. Correct Patient Centering Increases Image Quality without Concomitant Increase of Radiation Dose during Adult Intracranial Computed Tomography. J Med Imaging Radiat Sci. 2016. Radiat Sci. https://doi.org/10.1016/j.jmir.2016.05.002
10. Saltybaeva N, Schmidt B, Wimmer A, Flohr T, Alkadhi H. Precise and Automatic Patient Positioning in Computed Tomography: Avatar Modeling of the Patient Surface Using a 3-Dimensional Camera. Invest Radiol. 2018;53(11):641-6.
11. Booij R, Budde RPJ, Dijkshoorn ML, van Straten M. Accuracy of automated patient positioning in CT using a 3D camera for body contour detection. Eur Radiol. 2019;29(4):2079-88.
12. Singh V, Ma K, Tamersoy B, Chang Y-J, Wimmer A, O'Donnell T, et al. DARWIN: Deformable Patient Avatar Representation With Deep Image Network. In: Descoteaux M, Maier-Hein L, Franz A, Jannin P, Collins DL, Duchesne S, editors. Medical Image Computing and Computer-Assisted Intervention – MICCAI 2017: 20th International Conference, Quebec City, QC, Canada, September 11-13, 2017, Proceedings, Part II. Cham: Springer International Publishing; 2017: 497-504.
13. Cohen J. Statistical power analysis for the behavioral sciences, 2nd edn. ISBN 0-8058-0283-5. Lawrence Erlbaum Associates, United States of America1988.
14. Faul F, Erdfelder E, Lang AG, Buchner A. G*Power 3: a flexible statistical power analysis program for the social, behavioral, and biomedical sciences. Behavior research methods. 2007;39(2):175-91.
15. Euler A, Saltybaeva N, Alkadhi H. How patient off-centering impacts organ dose and image noise in pediatric head and thoracoabdominal CT. Eur Radiol. 2019;29(12):6790-3.
16. Kaasalainen T, Palmu K, Lampinen A, Kortesniemi M. Effect of vertical positioning on organ dose, image noise and contrast in pediatric chest CT - Phantom study. Pediatr Radiol. 2013;43(6):673-84.

CHAPTER 5

Influence of breathing state on the accuracy of automated patient positioning in thoracic CT using a 3D camera for body contour detection

Submitted

Ronald Booij, Marcel van Straten, Andreas Wimmer, Ricardo P. Budde

ABSTRACT

Objective

To assess the influence of breathing state on the accuracy of a 3D camera for body contour detection and patient positioning in thoracic CT.

Methods and materials

Sixty-four patients that underwent CT of the thorax with both an inspiratory and expiratory scan were prospectively included for analysis of differences in the ideal table height at different breathing states. For a subgroup of 43 patients, ideal table height suggestion based on 3D camera images at both breathing states was available to assess the influence of different breathing state on patient positioning accuracy. Ideal patient positioning was defined as the table height at which the scanner isocenter coincides with the patient's isocenter.

Results

The mean (SD) difference between the inspiratory and the expiratory breathing state of the ideal table height was 10.6 (4.5) mm ($p<0.05$). The mean (SD) positioning accuracy, i.e. absolute deviation from the ideal table height, within the subgroup was 4.6 (7.0) mm for inspiratory scans and 7.1 (7.7) mm for expiratory scans ($p<0.05$) when using corresponding 3D camera images. The mean (SD) accuracy was 14.7 (7.4) mm ($p<0.05$) when using inspiratory camera images on expiratory scans; vice versa, the accuracy was 3.1 (9.5) mm ($p<0.05$).

Conclusion

A 3D camera allows for the most accurate patient positioning when the camera image and the subsequent CT scan are acquired in the same breathing state. It is recommended to perform an expiratory planning image when acquiring a thoracic CT scan in both the inspiratory and expiratory breathing state.

INTRODUCTION

Two of the main technological developments in computed tomography (CT) automatic exposure control (AEC) have been automated tube current modulation (ATCM) and automatic tube voltage selection. These optimize radiation dose while maintaining image quality (IQ) [1]. AEC generally relies on the CT localizer radiograph to determine patient size. Positioning of a patient lower or higher than the scanner isocenter affects the patient's shape on the localizer radiograph, thereby affecting the AEC behavior [2-4]. Therefore, ideal patient positioning, defined as setting the table height such that the patient's isocenter coincides with the scanner isocenter, is important. Deviation from the ideal table height may result in relative organ dose differences and deviation of IQ from ideal settings. Besides that, the breathing state of the patient (inspiratory or expiratory) likely results in different anterior-posterior chest sizes and hence in different ideal table heights. Furthermore, clinical indications may call for image acquisition in both full inspiration and expiration to assess the lung parenchyma.

Recent studies described accurate patient positioning with the aid of a commercially available 3D camera [5; 6]. Ideal table height is suggested by the 3D camera with the aid of a single planning image triggered by the radiographer when the patient is lying on the scanner table in the target pose of the examination. The ideal table height for the individual patient and the scheduled examination is proposed such that the isocenter of the body region to be examined and scanner isocenter align. We hypothesize that obtaining the planning image in a breathing state that differs from the breathing state during the scan, will result in less accurate patient positioning by the 3D camera. The aims of this study were to: 1) determine the difference in ideal table height for a CT scan in inspiration versus expiration and 2) assess the influence of a mismatch in breathing state between the planning image and the actual CT scan on the accuracy of automated patient positioning using a 3D camera.

MATERIALS AND METHODS

Study design and patient selection

The study was conducted in accordance with the declaration of Helsinki and international standards of Good Clinical Practice. The medical ethics committee of our hospital waived the need for informed consent. All patients (>18-year-old), scanned during routine clinical care in our hospital on two CT scanners equipped with a commercially available 3D camera (Siemens Healthineers) for body contour detection: a dual-source CT scanner (SOMATOM Drive; software version VA62A, Siemens Healthineers) and a single-source CT scanner (SOMATOM Edge Plus, software version VB10, Siemens Health-

ineers), that underwent non-contrast enhanced CT of the thorax with both an inspiratory and expiratory scan over an eight-month period were prospectively included. For the first part of the study, the difference in ideal table height between an inspiratory and expiratory breathing state was determined by including all patients with an inspiratory and an expiratory CT scan. For the second part of the study, a subgroup with only patients with both the expiratory and inspiratory 3D camera images and accompanying CT scans were included. CT image reconstructions with 3.0 mm slice thickness and 3.0 mm reconstruction increment were used.

Patient positioning using a 3D camera for body contour detection

The 3D camera is part of the CT system and attached to the ceiling and in front of the CT scanner, facing down onto the patient table. The camera acquires a color and a depth image. Each pixel in the depth image describes the distance from the camera to the closest object surface. The image analysis starts after taking the planning image. The algorithm detects the patient and estimates the body contour of the patient using the depth measurements and the known table position and shape. The 3D camera proposes the ideal table height for the individual patient and the scheduled examination such that the isocenter of the selected scan range and the scanner isocenter align. Therefore, a virtual patient Avatar is fitted to the camera data. The Avatar is a statistical shape model, which in the fitting process assumes the pose, and body proportions of the patient found in the depth data. The isocenter curve of the Avatar is finally averaged across all slices of the body region selected. The used 3D camera algorithm is similar to the algorithm described in detail before [5; 7]. For this study, a depth image and color image were recorded in the inspiratory breathing state; for the subgroup, both the expiratory and inspiratory breathing state were recorded (Fig. 1).

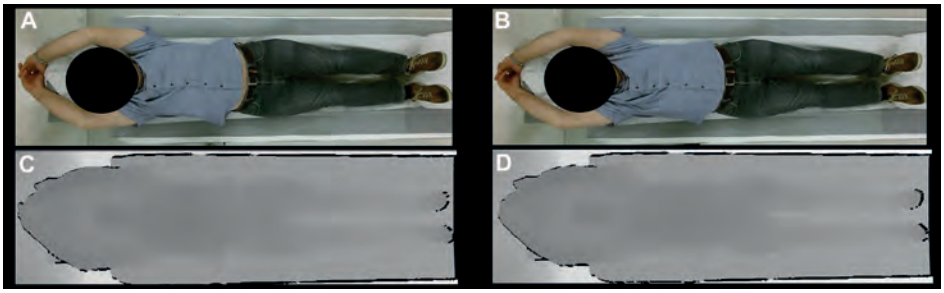

Figure 1 (a-d) (a and b) enzCase presentation of a male patient in the inspiratory **(a and c)** and an expiratory **(b and d)** breathing state. **(a and b)** Color image taken by the 3D camera system. **(c and d)** Gray scale image corresponding to measured depth values.

Calculation of patient positioning accuracy

Cases were excluded with obvious patient movement or repositioning after the body contour detection by the 3D camera, or when large items were blocking the camera sight. Cases where the field of view (FoV) of the CT scan did not cover the anterior-posterior extent of the patient were excluded as well. Skin surface was extracted from the CT data in each axial slice. The results of the skin extraction were used to calculate the middle of the patient in the anterior-posterior direction. These values were averaged over all slices along the z-axis, providing the patient isocenter, needed to determine the ideal table height as described in detail before [5].

In the clinical workflow, table height suggested by the camera is based on the latest planning image only. Therefore, analysis of proposed patient positioning based on the inspiratory and expiratory camera image was assessed off-line, without the need of additional data or user input. By doing so, off-line system performance reflect the real-world situation. In general, a radiographer may adjust the table height proposed by the 3D camera. However, the positioning accuracy by radiographers was beyond the scope of this study since it was assessed in our previous paper [5]. Accuracy in patient positioning is demonstrated as the deviation between the ideal table height and the table height proposed by the camera algorithm. The difference in ideal table height and the accuracy are expressed as a single and absolute value in mm.

Statistical analyses

Mean and standard deviation (SD) of the differences between the ideal table height for an inspiratory and expiratory scan were analyzed. For the subgroup, the mean and SD of the absolute table height deviation of the inspiratory and expiratory scans and accompanying camera images were assessed. SPSS (version 25, IBM Corp) was used for statistical analysis. Normality of data was tested with the Shapiro-Wilk test. Paired T-Test was performed to evaluate statistically significant difference of the ideal table height deviation between the inspiratory and expiratory breathing state. A p value <0.05 was considered statistically significant.

RESULTS

After exclusion of three cases from analysis due to the anterior-posterior extent of the patient not being fully included in the FoV, sixty-four CT studies (37 male and 27 female) with both an inspiratory and an expiratory CT scan were available for analysis of differences between the ideal table height for CT scans in inspiration and expiration. For the subgroup, 43 patients (27 male and 16 female) of the 64 patients, ideal table height suggestion by the 3D camera was collect by off-line analysis for both breathing states.

Ideal table height as a function of breathing state

Figure 2 illustrates an example of an inspiratory and expiratory breathing state. Within the 64 patients, the mean (SD) difference for the ideal table height between inspiration and expiration was 10.6 (4.5) mm ($p<0.05$) (Fig. 3). The maximum and minimum absolute difference of the ideal table height between the inspiratory and expiratory scan was 24.3 mm and 2.6 mm, respectively. In all cases, the ideal scanner table height position was lower for the CT scans in inspiration than for the scans in expiration.

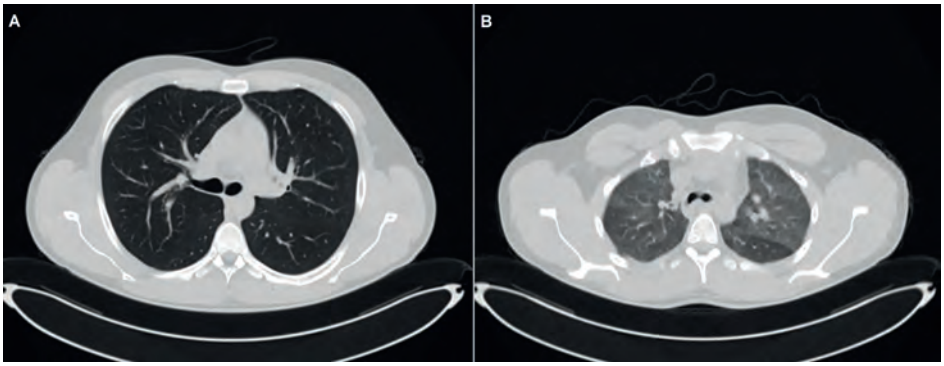

Figure 2 (a-b) Adult patient with an inspiratory **(a)** and expiratory **(b)** breathing state. **(a)** Axial image of the thorax in an inspiratory breathing state. **(b)** Axial image of the thorax in an expiratory breathing state.

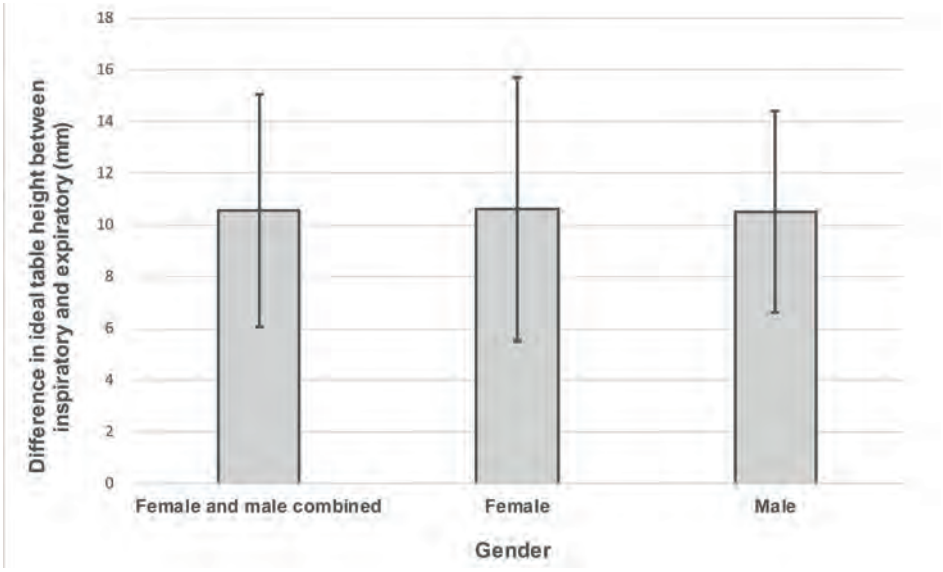

Figure 3 Differences between the ideal table height at the inspiratory breathing state and the expiratory breathing state for the "female and male combined", female, and male.

Patient positioning accuracy of a 3D camera for inspiratory and expiratory thoracic CT

Figure 4 demonstrates a difference in the inspiratory and expiratory breathing state and the depth measurements. When considering the same breathing state for both the CT scan and the planning image, the mean (SD) difference between the ideal table height and the table height proposed by the 3D camera was 4.6 (7.0) and 7.1 (7.7) mm for the

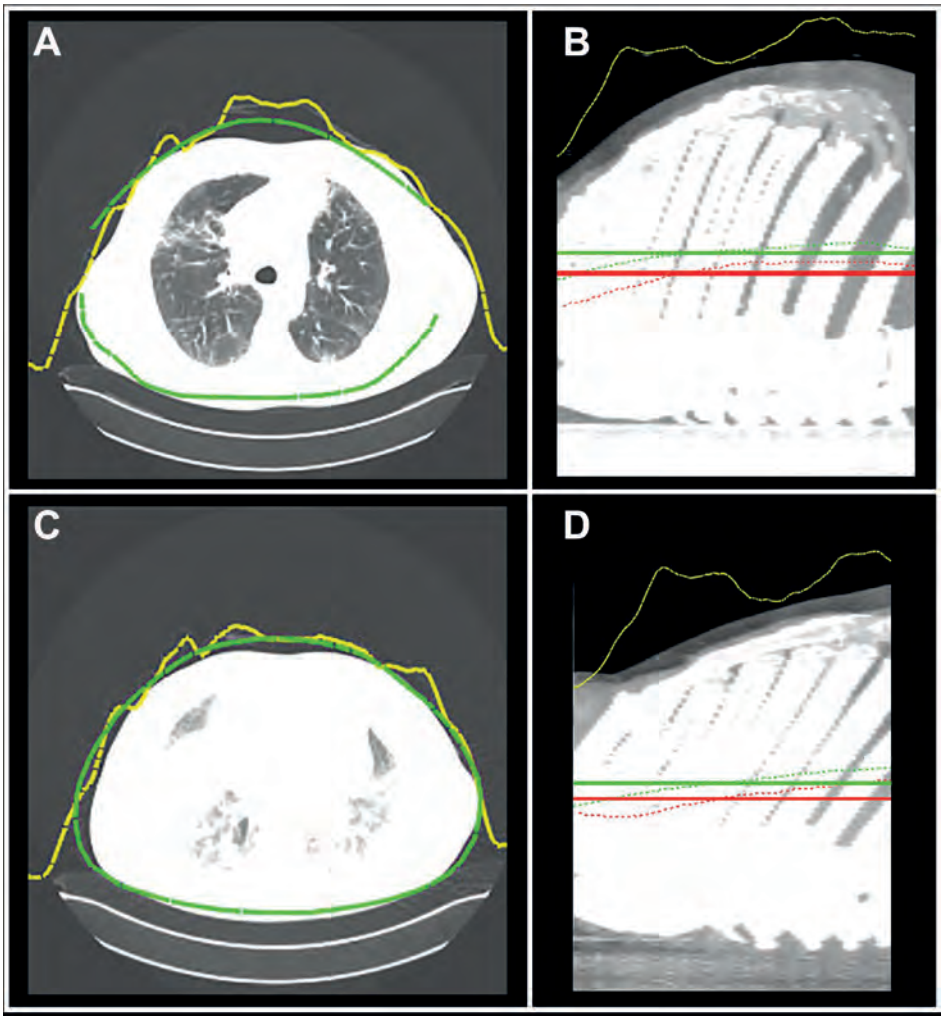

Figure 4 (a-d). Case presentation of a male patient with an inspiratory **(a and b)** and expiratory **(c and d)** breathing state with depth measurements. **(a and c)** Axial image of the thorax with depth measurements (yellow line) by the 3D camera and the body contour (green) estimated by the algorithm. **(b and d)** Sagittal image of the thorax with patient positioning accuracy: green horizontal line: average patient isocenter estimated by the camera, green dotted line: Avatar isocenter curve, red horizontal line: average patient isocenter (ideal table height), red dotted line: patient isocenter per axial cross-section, yellow line: depth measurements.

inspiration and expiration breathing state, respectively ($p<0.05$). The mean (SD) difference between the ideal table height and the table height proposed by the 3D camera for both the inspiratory and the expiratory CT scan was higher for males than females and considered statistically significant (Table 1). The differences between the ideal table height and the table height proposed by the 3D camera for both the inspiratory ($p=0.340$) and expiratory ($p=0.093$) breathing state scans were considered not statistically significant for females (Table 1).

The mean (SD) difference between the 3D camera proposed table height based on the inspiratory planning image compared to the ideal table height of the expiratory CT scan was statistically significant (Table 1). The mean (SD) difference between the table height proposed by the 3D camera based on the expiratory planning image compared to the ideal table height of the inspiratory scan was considered statistically significant for female/male combined and for females, but not for males (Table 1). The accuracy in patient positioning was less when an inspiratory 3D camera planning image was used for an expiratory CT scan with 14.7 (7.4) mm than when an expiratory 3D camera planning image was used for an inspiratory CT scan with an accuracy of 3.1 (9.5) mm.

Table 1 3D camera mean patient positioning accuracy and standard deviation (SD) for all combinations of breathing state while taking the camera image and performing the subsequent CT scan.

Table 1. Absolute table height deviation from ideal table height as a function of breathing state						
	Breathing state CT scan					
	Inspiratory			**Expiratory**		
Breathing state 3D planning image	Female & Male	Female	Male	Female & Male	Female	Male
Inspiratory						
	4.6 (7.0)	1.7 (7.1)	6.3 (6.6)	14.7 (7.4)	11.7 (6.8)	16.6 (7.2)
	<0.05	0.340	<0.05	<0.05	<0.05	<0.05
Expiratory						
	3.1 (9.5)	6.3 (10.1)	1.2 (8.7)	7.1 (7.7)	3.6 (8.1)	9.2 (6.8)
	<0.05	<0.05	0.502	<0.05	0.093	<0.05

Data are mean (SD) in mm with *p*-value per gender and for both genders combined

DISCUSSION

We assessed the influence of breathing state on the differences in ideal table height and on the accuracy of automated patient positioning using a 3D camera. In the first part of our study, different ideal table heights were observed between an inspiratory and an expiratory breathing state CT scan. Previously we reported on the accuracy of automated patient positioning, where we assumed that the camera image and the subsequent CT scan were acquired in the same breathing state [5]. The results in positioning accuracy

by the 3D camera of this study were comparable with the results of our previous study, which had a statistically significant median (interquartile range) deviation of 5.4 (6.4) mm. When taking a different breathing state used for the planning image and the subsequent CT scan into account, a less accurate patient positioning by the 3D camera was observed in most cases, as demonstrated in Table 1.

Accurate body contour detection by the 3D camera might be affected when ripples and folds in clothing are present, giving rise to false interpretations of body shape, as described before [5]. Consequently, both situations may lead to larger deviations from the ideal table height and might explain why no statistically significant differences were found. Interestingly, the difference in table height between the expiratory planning image and an inspiratory CT scan was smaller than the difference between the inspiratory planning image and expiratory CT scan, but the SD was larger when combining the expiratory planning image and the inspiratory CT scan (Table 1). Nevertheless, from a "practical work around" perspective, positioning of a patient for both an inspiratory and expiratory CT scan based on the expiratory planning image seems to be the best choice. Further research is needed to look into other solutions which do not demand a change in workflow e.g. possibilities to adapt the table height in between the CT scans for different breathing state.

Several studies demonstrated a significant impact on radiation dose or image quality (IQ) due to deviation from proper patient positioning [2; 8; 9]. For instance, an anthropomorphic phantom study demonstrated that off-centering above 40 mm was associated with 20% higher organ dose changes [3]. Vertical off-centering of a patient not only affects radiation dose, but also image noise. Even though subjective IQ is not necessarily significantly affected with small changes in the amount of image noise, organ dose can still be higher [3]. Additionally, another study demonstrated a variation in CT numbers of nodules near the center of the lungs or spine [10]. In our pursuit of optimization, it remains important to do everything possible to achieve optimal scanning procedures, even when individual optimization steps seem small. Therefore, it is of the essence to strive for proper patient positioning to retain optimal radiation dose and IQ by a correct operation of the bowtie filtering and ATCM applied [11].

One limitation of this study requires consideration. The calculation of the isocenter for both the expiratory and inspiratory 3D camera images and accompanying CT scans was based on the actually scanned range. In routine operation, the algorithm uses the scan range that is defined on the planning image (=color photograph taken by the camera) prior to obtaining the localizer radiograph and scanning the patient. Consequently, this suggested table height may differ from the suggested table height based on the scan range defined on the planning image.

In conclusion, a 3D camera allows for the most accurate patient positioning when the camera image and the subsequent CT scan are acquired in the same breathing state. It

is recommended to perform an expiratory planning image when acquiring a thoracic CT scan in both the inspiratory and expiratory breathing state.

REFERENCES

1. Kalender WA, Buchenau S, Deak P, Kellermeier M, Langner O, van Straten M, et al. Technical approaches to the optimisation of CT. Phys Med. 2008;24(2):71-9.
2. Matsubara K, Koshida K, Ichikawa K, Suzuki M, Takata T, Yamamoto T, et al. Misoperation of CT automatic tube current modulation systems with inappropriate patient centering: phantom studies. AJR Am J Roentgenol. 2009;192(4):862-5.
3. Saltybaeva N, Alkadhi H. Vertical off-centering affects organ dose in chest CT: Evidence from Monte Carlo simulations in anthropomorphic phantoms. Med Phys. 2017;44(11):5697-704.
4. Szczykutowicz T, Duplissis A, Miller D. How Patient Positioning in CT Affects More Than the AEC: Image Noise Uniformity and CT Number Changes as a Function of Positioning. Medical Physics. 2016;43(6).
5. Booij R, Budde RPJ, Dijkshoorn ML, van Straten M. Accuracy of automated patient positioning in CT using a 3D camera for body contour detection. Eur Radiol. 2019;29(4):2079-88.
6. Saltybaeva N, Schmidt B, Wimmer A, Flohr T, Alkadhi H. Precise and Automatic Patient Positioning in Computed Tomography: Avatar Modeling of the Patient Surface Using a 3-Dimensional Camera. Invest Radiol. 2018;53(11):641-6.
7. Singh V, Ma K, Tamersoy B, Chang Y-J, Wimmer A, O'Donnell T, et al. DARWIN: Deformable Patient Avatar Representation With Deep Image Network. In: Descoteaux M, Maier-Hein L, Franz A, Jannin P, Collins DL, Duchesne S, (eds) Medical Image Computing and Computer-Assisted Intervention – MICCAI 2017: 20th International Conference, Quebec City, QC, Canada, September 11-13, 2017, Proceedings, Part II, Springer International Publishing, Cham. 2017: 497-504.
8. Kaasalainen T, Palmu K, Reijonen V, Kortesniemi M. Effect of patient centering on patient dose and image noise in chest CT. Am J Roentgenol. 2014;203(1):123-30.
9. Szczykutowicz TP, DuPlissis A, Pickhardt PJ. Variation in CT number and image noise uniformity according to patient positioning in MDCT. Am J Roentgenol. 2017;208(5):1064-72.
10. Goodsitt MM, Chan HP, Way TW, Larson SC, Christodoulou EG, Kim J. Accuracy of the CT numbers of simulated lung nodules imaged with multi-detector CT scanners. Med Phys. 2006;33(8):3006-17.
11. Habibzadeh MA, Ay MR, Asl ARK, Ghadiri H, Zaidi H. Impact of miscentering on patient dose and image noise in x-ray CT imaging: Phantom and clinical studies. Phys Med. 2012;28(3):191-9.

PART III

Improvement of acquisition and reconstruction techniques

CHAPTER 6

Cardiovascular imaging in pediatric patients using dual source CT

This chapter is based on the publication in J Cardiovasc Comput Tomogr. 2016;10(1):13-21

Ronald Booij, Marcel L. Dijkshoorn, Marcel van Straten, Frederik A. du Plessis, Ricardo P. Budde, Adriaan Moelker, Mohamed Ouhlous

ABSTRACT

Cardiovascular CT acquisition protocol optimization in pediatric patients, including newborns is often challenging. This might be due to non-cooperative patients, the complexity and variety of diseases and the need for stringent dose minimization. Motion artifacts caused by voluntary and involuntary motion are most frequently seen in cardiac imaging with high heart and respiratory rates. Dual source scanners of the second and third-generation are particularly well suited to respond to these challenges. This can be accomplished with advanced scan options, such as high pitch scanning, short rotation times, automated tube voltage selection, tube current modulation and iterative reconstruction.

INTRODUCTION

Ultrasound is the procedure of choice in the identification of congenital heart disease. Good and informative ultrasound images of extra-cardiac structures and of right ventricular morphologic features are difficult to obtain. MRI demonstrates superior soft tissue contrast in comparison to ultrasound or CT; however, the limitation of this imaging technique is the long scan time and the frequent need for sedation. Despite its inherent advantages in visualizing complex anatomy, CT is generally not the modality of choice for cardiovascular imaging in pediatric patients. The use of ionizing radiation, the presence of a high heart rate (HR) and the inability to instruct patients are well-documented drawbacks and limiting factors [1]. State-of-the-art dual source CT (DSCT) scanners are equipped with modern technology including low tube voltage acquisition, high-pitch scanning, and iterative reconstruction that may mitigate these obstacles.

This paper will provide practical guidelines for cardiovascular CT imaging with regard to the use of above mentioned technological features, patient positioning and intravenous contrast material injection, tips to avoid artifacts of contrast agent and ECG electrodes and at an optimized radiation dose.

PATIENT POSITIONING

Patient positioning is an essential part in imaging pediatric patients, especially in newborns. Artifacts can arise from poor positioning of the arms or ECG electrodes in the thoracic region (Fig. 1). The use of a vacuum cushion for pediatric patients (aged 0-4 years) is highly recommended for comfort and safety, movement prevention and to secure the position of the arms above the head (Fig. 2).

The radiation dose might increase or image quality could be affected when the CT localizer radiograph is made with the patient positioned off-center, therefore, a visual check that the child is centrally positioned in the axial plane using the laser beams on the scanner is mandatory (Fig. 3). Furthermore, in pediatric cardiac CT imaging, an additional bowtie-shaped filter is automatically positioned between the X-ray tube and patient to reduce the radiation dose in the patient's periphery, which makes central positioning vital (Fig. 4). Scanning of pediatric patients is a challenging procedure, which requires a collaboration between a radiographer and radiologist to set-up scan and injection protocol to be certain to obtain all clinically useful information.

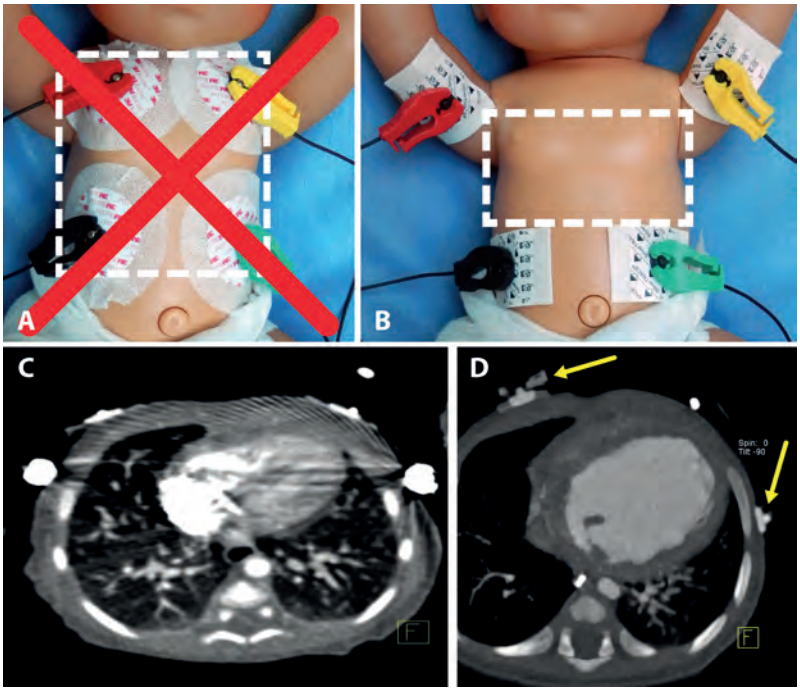

Figure 1 (a-d). ECG electrodes and cables can cause serious beam hardening and streak artifacts by positioning them in the scan range **(a+c)**. Placement of the ECG electrodes on the arms and upper abdomen **(b)** will avoid artifacts. MRI compatible carbon ECG patches (yellow arrows in **d**) are preferred and generate far less artifacts than normal ECG patches.

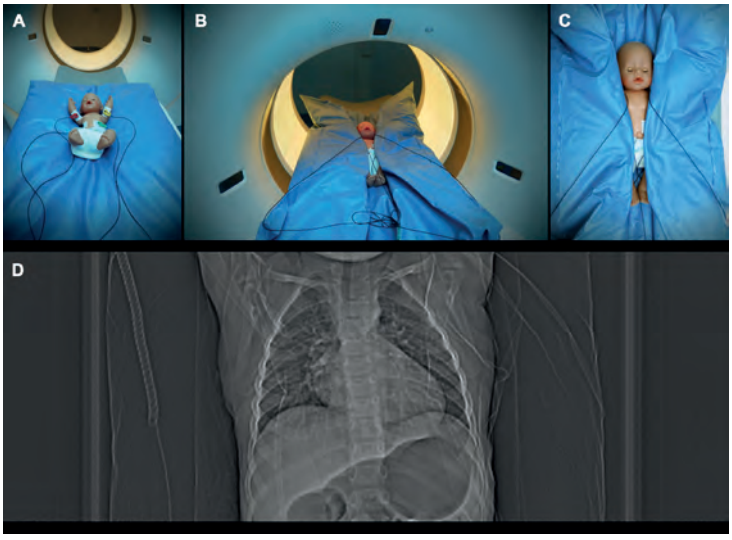

Figure 2 (a-d). Vacuum cushion with a doll representing a pediatric patient **(a, b, c**) and CT localizer radiograph of a pediatric patient positioned in vacuum cushion **(d)**. Special care should be taken to conduct the ECGelectrodes and arms away from the thorax **(b, c)**.

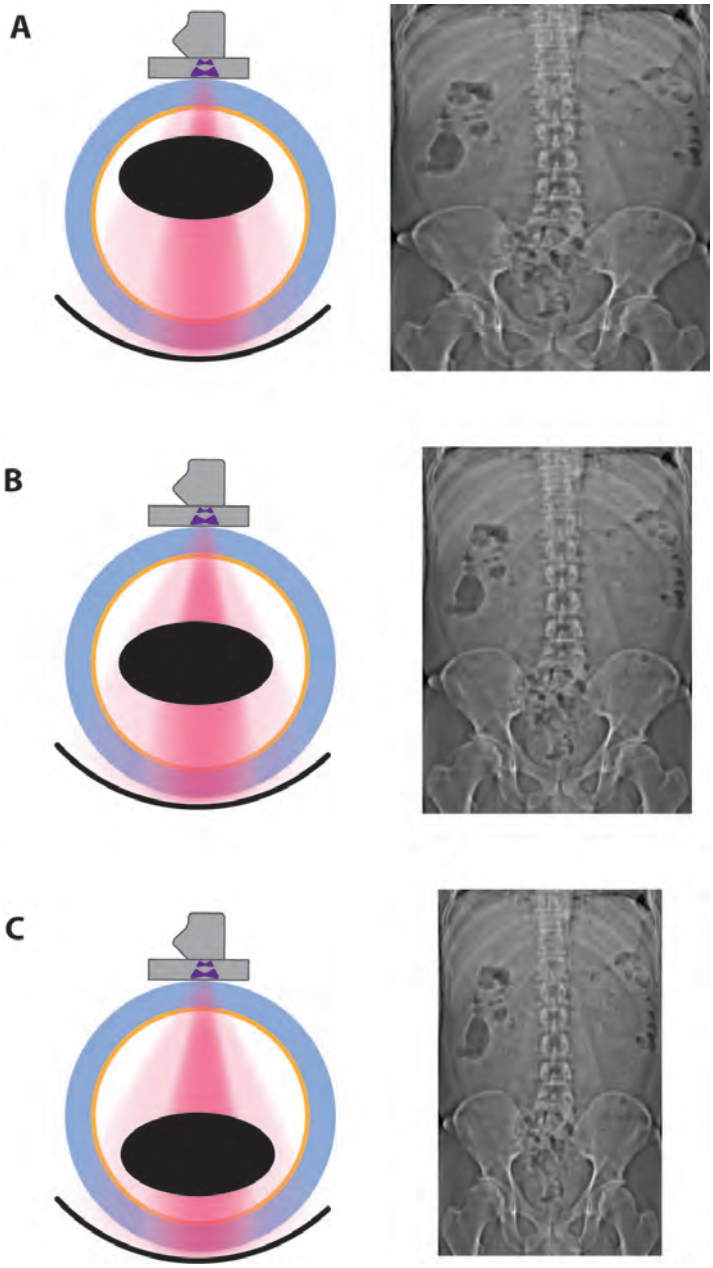

Figure 3 (a-c). Positioning the patient off-center will cause different scaling of the CT localizer radiograph compared to a centralized position. This changes the projected body size and influences the automated exposure control algorithm. Compared to a properly positioned patient in the isocenter **(b)** higher positioning **(a)** makes body habitus appear bigger on an AP survey and dose will increase in comparison to the optimal situation **(b)**.
Positioning the patient lower than the isocenter (**c**) will in turn make body habitus seem smaller and underexpose the exam in comparison to the optimal situation. This may lead to unacceptably high noise levels.

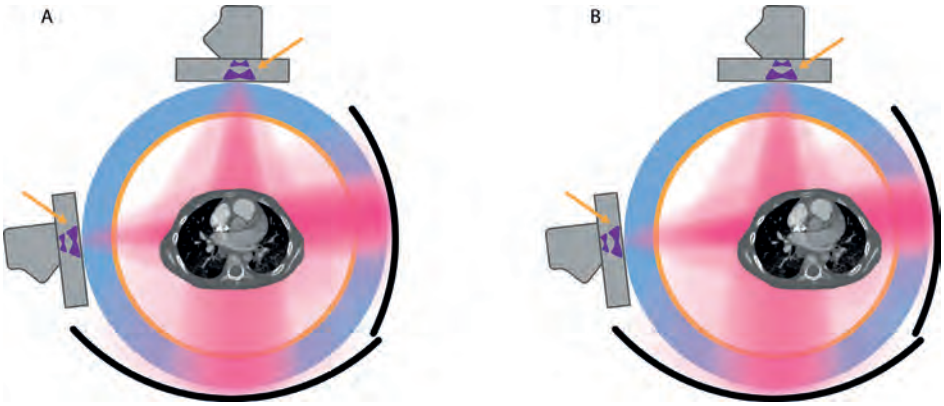

Figure 4 (a-b). The (additional) bowtie filters (orange arrows) reduce radiation dose at the lateral sides of the patient **(a)**. Positioning the patient off-center **(b)** may cause an uneven noise distribution in the image.

CONTRAST INJECTION AND TIMING

Contrast injection in pediatric cardiothoracic imaging is difficult to standardize. In children, especially neonates it is more difficult to get venous access and is often located more peripherally like in the hand, foot or forehead. Suggested flow rates adapted to body weight can be found in Table 1.

Table 1. Suggested flow rates for contrast and saline push injection in pediatric CTA.

Body Weight (kg)	Minimum Flow (ml/s)	Maximum Flow (ml/s)
0.5–5 kg	0.3	0.8
5-15	0.7	1.2
15–24	1.2	2.0
25–34	2.0	3.0
35-44	3.0	4.0

Congenital cardiovascular anomalies might alter the normal order of vascular enhancement. This has implications for contrast timing and therefore the contrast phases should be tailored to anatomy, diseases, congenital anomalies or variants to make your diagnosis. Therefore, it is of the essence to decide which contrast phases are needed and deliberation between radiologist and technologist might be needed. In adults often, multiple scan phases are planned. In pediatrics, this leads to an unacceptable increase of radiation dose. For children it is beneficial to combine several contrast phases in a single scan to keep radiation dose to a minimum. Split-bolus and contrast mixing techniques are helpful to achieve this goal. Either reducing the flowrate or applying a mixing technique of contrast agent and saline can reduce the iodine delivery rate (IDR). The

mixing technique however is not always available on injectors. With injection from an antecubital vein, the start of the scan can occur at a fixed delay, but is age range related and depends on the clinical situation. It is often sufficient for the more adolescent aged, but can be too long in neonates and in imaging of a Fontan pathway. With a more distal location of the intravenous access and/or in neonates, the aortic enhancement timing is more uncertain. In these cases, the use of a bolus tracking technique is recommended. However, several issues of automatic bolus tracking in children have to be considered. The most important ones being the movements of the patient during the bolus measurement, which can cause the scan to start too early or too late and second, high bolus tracking frequencies, which result in higher radiation dose. (Fig. 5). These issues can be solved by a visual tracking approach and with manual kV and mA values adapted to the size and weight of the patient for the automatic bolus tracking. A real-time measurement of the bolus arrival may be used. It is recommended to switch off the automatic tracking and manually start the scan when sufficient enhancement has been reached. Instead of measuring at the level of the aortic root, a mid-cardiac level is advised as this enables the visualization of the cardiac chambers and descending aorta in the same plane. The real-time visualization of the order and strength of enhancement of different structures can help to adapt the scan start accordingly. Basically, the scan can be started when sufficient contrast is present in all four hear chambers and the descending aorta. If the scan triggers to start while the bolus is still being injected, the injection can be manually stopped at this point.

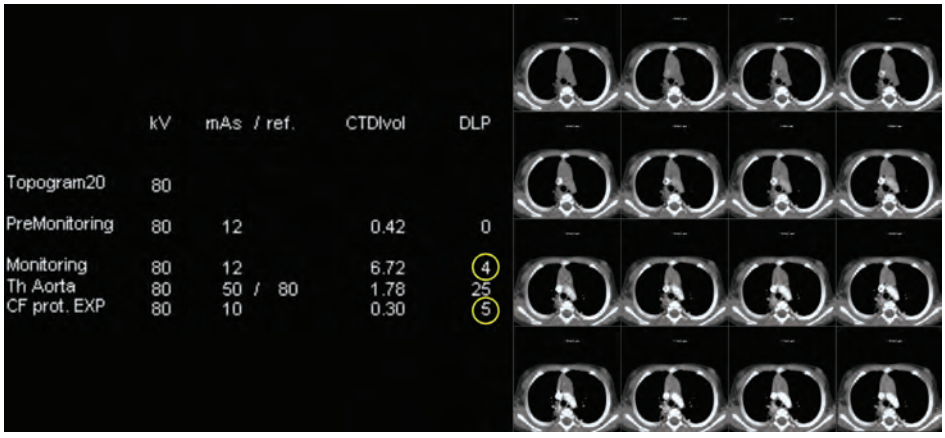

Figure 5. Dose report and bolus tracking images in a 6-month old patient. Bolus tracking was started to early (delay 4 seconds, IV was positioned on head) and 16 static images were acquired. Note that the bolus tracking dose (yellow circles) was almost as high as the spiral CT of chest ("CF prot. EXP").

FAST SCAN OPTIONS AND SLICE THICKNESS IN DUAL SOURCE CT SCANNER

The advent of second-generation DSCT scanners has made it possible to scan non-cooperative (especially pediatric) patients without anaesthesia because of the high scan speed and improved temporal resolution [2]. Imaging speed has further increased with third-generation DSCT scanner due to the wider detectors and even faster rotation time, thereby reducing possible breathing/motion artifacts even more Breathing artifacts can be quite tricky and are often seen in single-source CT, but hardly in DSCT.

In spite of higher heart rates in pediatric patients, the scan speed of the high pitch mode will provide sufficient diagnostic image quality in most scans [3]. The high pitch mode provides the shortest acquisition time while the individual slices maintain the highest temporal resolution (66 ms for the third-generation DSCT and 75 ms for the second-generation DSCT). There is a craniocaudal gradient, if scanned craniocaudally, of the phase of the cardiac cycle within the scanned volume (Fig. 6). Meaning the whole scan is made during a large part of the cardiac cycle and has different time phases from top to bottom of the heart.

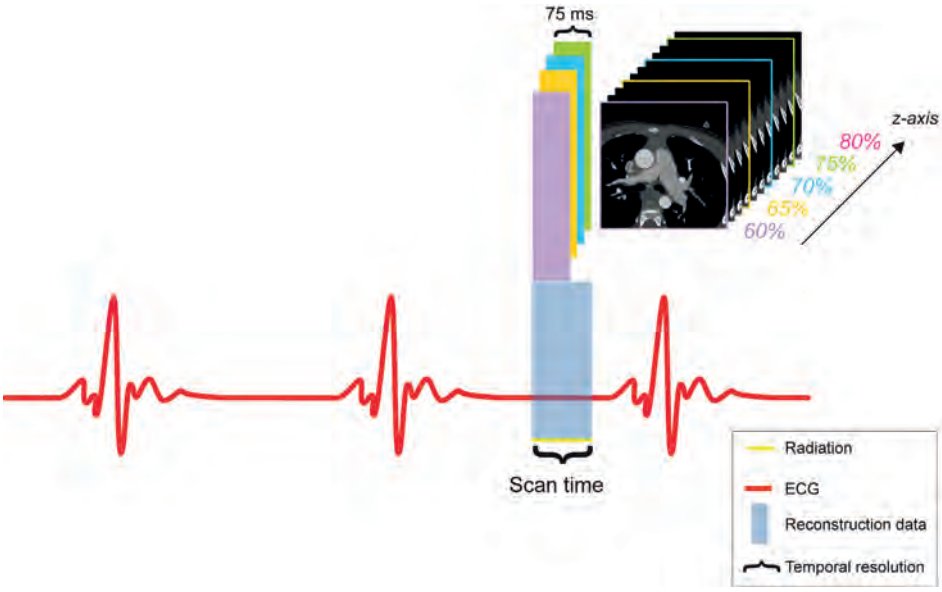

Figure 6. Illustration of high pitch mode regarding scan time and maintained highest temporal resolution for individual slices with the craniocaudal transition of the phase of the cardiac cycle within the scanned volume.

The length of the RR-interval in pediatric patients is around 500 ms at a heart rate of around 120 beats per minute. An ECG-triggered high pitch scan with a 11 cm scan length takes up to 150 ms. With increasing heart rate, the mean velocity of all coronary arteries

significantly increases [4]. ECG-triggered high pitch scanning in the end systolic and motion free phase is possible but due to the high heart rate and relative short motion free acquisition time, motion artifacts at the end of the scan may still occur, despite the highest available temporal resolution and fast pitch. In contrast to adults, the length of the heart is shorter in children. Consequently, scan time will be shorter. Mostly only information on the anatomy is required and not the rule out of atherosclerotic stenosis as in adults. Therefore, slight motion can often be tolerated and as a result, higher heartrates are eligible for the high pitch mode than used in adults. When imaging larger structures such as the ventricles in children, the use of thin slices is less important. Normally imaging the heart of a child, will be done with 0.5-0.75 mm thick slices and a 0.25-0.4 mm increment. When imaging larger structures or for quantification of ventricular function (in case of unclear ultrasound results or contraindicated MRI) the use of 1.5 mm slice thickness and low kilovoltage is recommended to reduce radiation dose. An increase in slice thickness allows the use of decreased mA. For some scanner types and other vendors, the use of thicker collimation in combination with decreased mA is an option, because the z-coverage of the thicker and thinner collimation is different. However, this is not the case in the second- and third-generation DSCT, where the 0.6 and 1.2 mm collimation have identical z-coverage.

SCAN PHASE AND ECG MODULATION

A sequential prospective triggered protocol in the systolic phase will provide the proper ECG phase selection to optimize images from the motion free perspective with lower dose in comparison to retrospectively triggered acquisition [2]. An inconvenience of the sequential prospective technique in comparison to the high pitch mode is the possibility of a stack artifact when scanning a larger length in the z-axis than the collimation width. Nevertheless, it has advantages in comparison to the retrospective mode because prospective requires less stacks than retrospective due to the absence of oversampling from low pitch. The high temporal resolution of dual source scanners eliminates the need for dose intensive multi-segment retrospective protocols, which are required for single source scanners at high heart rates.

In children, the focus is mainly on assessment of anatomy, the stack artifacts can be less problematic, yet can still affect the diagnosis or interpretation of images. A retrospectively triggered acquisition is an option, but should only be considered in very challenging irregular heart rates where the need for ECG editing is expected at the cost of a higher radiation dose. In retrospective mode the pulsing technique, especially the Mindose technique, will still keep the dose at a low level but the pulsing will lose efficiency because of less efficient slope-up time and slope-down time of the

ECG-based tube current modulation [5]. The sequential prospective mode is preferred with a systolic padding range in ms to achieve comparable diagnostic performance with lower dose [6].

Especially in children, the heart rate may change considerably during the scan because of contrast injection, stress or a Valsalva manoeuvre. Modern scanners are equipped with online ECG modulation to correct for ECG variation. In case of heart rate variability, the scanner will widen the ECG radiation window to ensure data acquisition in the requested percentages of the R-R interval (Fig. 7a). This wider acquisition (and radiation) window provides more possibilities to select the proper heart phase for motion free reconstruction. However, increasing the radiation window results in an increase of radiation dose. To prevent a radiation dose increase because of automatic ECG radiation adaptation, the use of a protocol with absolute scan time in milliseconds (ms) instead of a relative R-R interval in percentages (%) is recommended (Fig. 7b) and can be done within prospective and retrospective mode (Mindose). Choosing the absolute value prevents the radiation window to open up and ensures shorter exposure times with consistent imaging in end systole. Although this technique is less robust, it prevents large increase in radiation dose with irregular heart rate. It is recommended to keep a wider acquisition and radiation margin, allowing flexibility in reconstruction window to minimize motion. To set up such a protocol in ms, a recalculation of the percentage settings to ms is needed, for instance to have a safe margin with 35% to 55% of the R-R interval, but can be set smaller based on user preference. The recalculation has to be done for the lowest and highest relative phase preferred and for different heart rate groups. Creating these groups can be done by combining the highest and lowest ms of the heart rate group preferred. Table 2 shows an example how to recalculate percentage to ms. If coronaries are not the aim of the scan but just the cardiac chambers and/or

Table 2. Suggested scan windows in absolute ms for prospective coronary CTA based on a recalculation of a 35% to 55% systolic percentage scan phase. Recalculation is recommended to prevent the increase of radiation window with heart rate variability.

HR group	HR	RR in ms	35%	55%	Scan Range 35% - 55% converted to ms
60 to 75	60	1000	350	550	280 - 550
75 to 100	75	800	280	440	210 - 440
100 to 125	100	600	210	330	168 - 330
125 to 150	125	480	168	264	140 - 264
150 to 175	150	400	140	220	120 - 220
175 to 200	175	343	120	189	105 - 189
	200	300	105	165	0 - 165
Variable HR					Prospective in ms; choose ms of highest and lowest HR
Irregular HR					Prospective in ms; 120 - 500 ms

great vessels, a high pitch scan or prospective acquisition without padding is sufficient. One can also use a low dose ECG-triggered high pitch scan for anatomy and/or for a delayed scan in addition to an arterially timed scan.

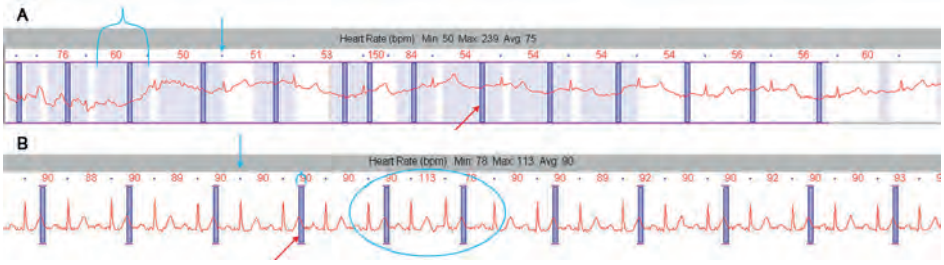

Figure 7 (a-b). ECG as presented on the scanner console of a third-generation dual source ct. Blue dots indicates the R-peak to set the scan range (straight blue arrow). The dark blue area (red arrow) represents the temporal resolution (66ms) and image reconstruction position. The red numbers indicate the heartrate. **(a)** Radiation pulsing range was initially set to only 68% of the R-R interval. Due to RR-variability and the use of a relative delay, the radiation window was widened (light blue parts indicated with }) to ensure data acquisition in the requested range and the possibility to reconstruct the suitable phase(s) with the least possible motion artifacts. As a result, dose there is a severe dose increase. **(b)** The predefined scan range in absolute time (ms) and systolic phase prevented the opening of the radiation window with variable heart-rate (indicated with the blue circle).

AUTOMATED TUBE CURRENT MODULATION, AUTOMATIC TUBE VOLTAGE SELECTION AND DOSE CURVES

The CT acquisition starts with obtaining a CT localizer radiograph. The dose of the localizer should be adapted according to body size as instructed in the manufacturers' manuals. This is normally done by adjusting the 100 kV (which is used in adults) to 80kV and keeping the mA the same. Although often only regarded as a means to determine the scan range, the CT localizer radiograph is used to assess the patient's size and shape. Based on this information, the system will automatically select the optimal tube voltage and determine the required exposure given a predefined image quality (milliampere second per rotation=mAs/rot).

Tube voltage and mA settings to be applied are often selected based on patient weight or age. Novel auto exposure control systems can select the optimal tube voltage and adapt the tube current to body size by using automatic tube current modulation (ATCM) [7, 8]. Especially in contrast enhanced examinations the use of a low tube voltage (70-80 kV) is recommended because of higher contrast to noise ratio of iodine at low kV and reduced radiation dose [9].

Despite being an automated feature, advanced settings of the ATCM can be customized. Most importantly different dose curve strengths can be selected. The dose curve

strength determines the slope of the increase and decrease of the tube current in patients deviating from the reference patient (70-80 kg). This adaptation can be set for 3 different body types and for each organ characteristic with 5 different strengths (Fig. 8) of the mA adaptation curve.

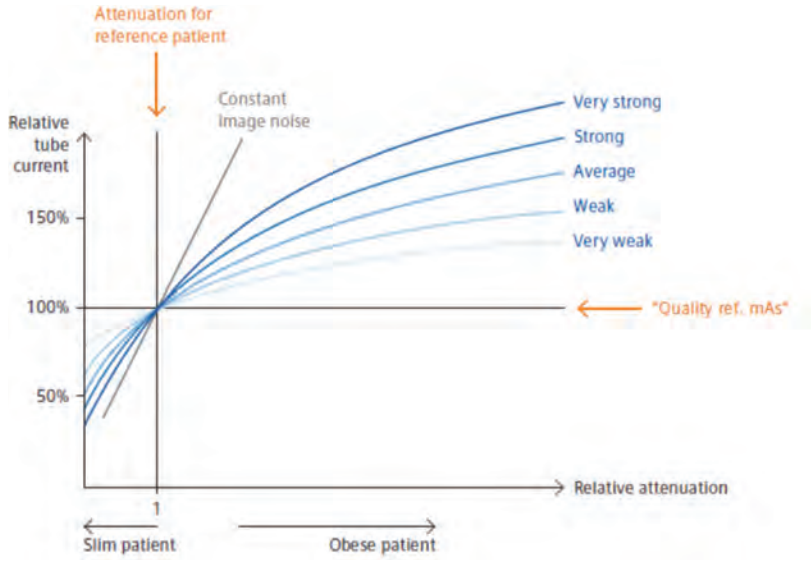

Figure 8. Different tube current adaptation curves for the automated tube current modulation (image courtesey of Siemens Healthineers.

When changing the curve strength and protocols, monitoring of image quality is recommended. This should be done by collaboration between radiographers, a medical physicist and/or radiologist, to ensure that the image quality of the different CT exam types is still sufficient.

It is not recommended to use estimations of the effective dose in pediatric CT because the International Commission on Radiation Protection (ICRP) clearly states that effective dose cannot provide a patient specific radiation dose or detriment [10, 11]. It is therefore recommended to use the Dose Length Product (DLP) and $CTDI_{vol}$ instead to compare doses between scanners and protocols. In order to estimate corresponding radiation risks another approach is required because $CTDI_{vol}$ is based on standardized 16 or 32 cm PMMA phantoms and the body size of pediatric patients differs significantly from these phantoms and as a consequence, direct use of these dose values might lead to dose and radiation risk underestimations (factor 5-10). Therefore, recently developed approach should be used instead, i.e. the Size-specific Dose Estimates and age-specific risk factors are more of use in this case [12].

Iterative reconstruction techniques (IR) can increase image quality with equal dose or potentially get similar image quality as in filtered back-projection (FBP) with less dose. [3, 13]. The baseline of in setting up pediatric protocols could be the same as in adults However, one should avoid lowering the dose too far, because noise might increase which has a negative impact on image quality. Dose reduction potential depends on the current dose level, the anatomy of interest, body size and weight. Each factor has to be taken into account when creating protocols.

CASE EXAMPLES

Two case examples are provided. Case 1 (Fig. 9 and Table 3) and case 2 (Fig. 10 and Table 4).

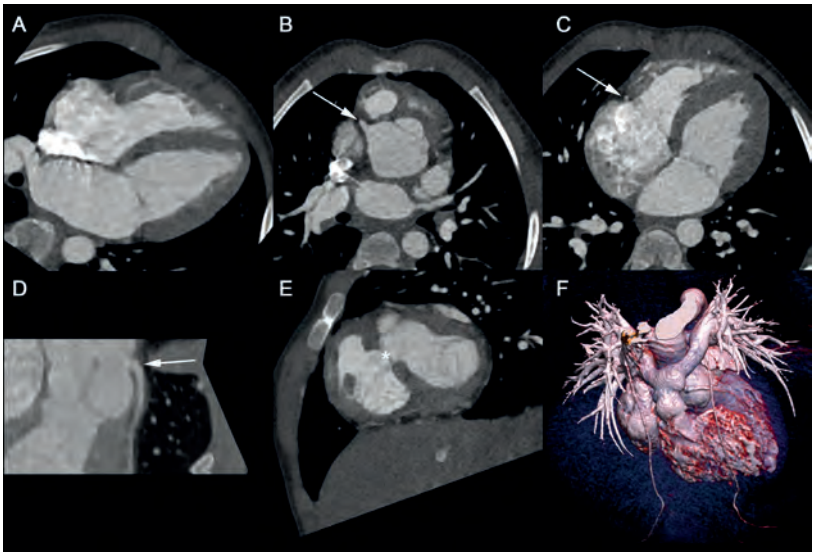

Figure 9 (a-f). Case 1: A 3 year old boy with a history of TGA, hypoplastic aortic arch and double outlet right ventricle (DORV), which was surgically corrected **(a)** with an arterial switch operation, closing of the ventricular septal defect (VSD, marked with * in **(e)** and aortic arch correction using a homograft. CTA demonstrated normal anatomy of RCA (**b, c and d;** marked with a white arrow) and LAD. **(f)** 3D volume rendering (VRT) of the heart.

Table 3. Scan, reconstruction and dose parameters of case 1.

Scan parameters	Case 1
Reference tube voltage	120 kV
Reference mAs/rot	230 mAs/rot
Dose saving slider position	11 (vascular)
Child dose adaptation curve strength	Very strong
ECG scan range	210 to 440 ms
Collimation	2 x 96 x 0.6 mm *
Rotation time	0.25 seconds
Patient instruction	None **
Reconstruction parameters	
Slice width	Recon 1: 0.75 mm & recon 2: 0.5 mm
Slice increment	Recon 1: 0.4 mm & recon 2: 0.25 mm
Kernel	Bv40
ADMIRE strength	Recon 1: 3 & recon 2: 4
Cardiac phase	Best Systolic phase (ms)
Window width (FAST)	900/200
Dose parameters:	
$CTDI_{vol}$ (32 cm)	3.27 mGy
DLP	33.4 mGy*cm

* Collimation and feed/rotation were automatically adapted by scanner to fit scan range
** Instruction of patient was not possible, therefore no patient breath hold command was given

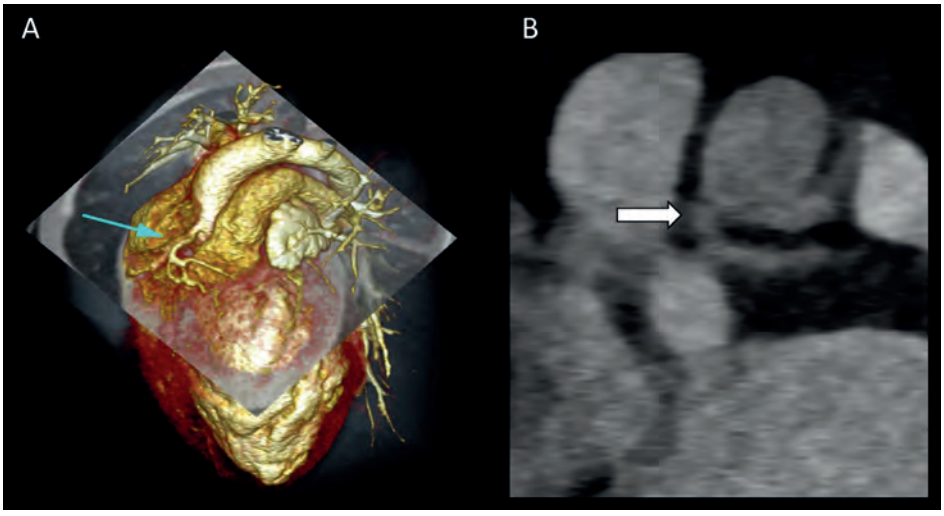

Figure 10 (a-b). Case 2: CTA of the heart of a 3-month-old-boy. The ALCAPA is indicated with the green **(a)** and with a white arrow **(b)**.

Table 4. Scan, reconstruction and dose parameters of case 2.

Scan parameters	**Case 2**
Reference tube voltage	120 kV
Reference mAs/rot	160 mAs/rot
Dose saving slider position	11 (vascular)
Child dose adaptation curve strength	very strong
ECG scan range	130 to 280 ms
Collimation	2 x 64 x 0.6 mm
Rotation time	0.285 seconds
Patient instruction	None *
Reconstruction parameters	
Slice width	Recon 1: 3.0 mm & Recon 2: 1.0 mm
Slice increment	Recon 1: 3.0 mm & Recon 2: 0.5 mm
Kernel	Recon 1: I26 & Recon 2: I70
SAFIRE strength	3
Cardiac fase	Best Systolic fase (ms)
Window width (FAST)	900/200
Dose parameters:	
$CTDI_{vol}$ (32 cm)	1.03 mGy
DLP	11 mGy*cm

* Instruction of patient was not possible, therefore no patient breath hold command was given

SUMMARY

Despite its excellent spatial and temporal resolution CT is often not the modality of choice for thoracic cardiovascular evaluation in pediatric patients. This article shows how thorough knowledge on recent improvements in DSCT image acquisition time, temporal resolution and dose reduction as low as reasonable achievable have reduced some of the major drawbacks of CT and allows one to visualize the complex anatomy which helps to determine treatment policy. 'Just copying' the adult parameters is not ideal, and special attention is needed to optimization in the pediatric population. A pediatric specific protocol should be used because of the extra bowtie filter, algorithms and several background parameters.

REFERENCES

1. Johnson JN, Hornik CP, Li JS, Benjamin DK, Jr., Yoshizumi TT, Reiman RE, et al. Cumulative radiation exposure and cancer risk estimation in children with heart disease. Circulation. 2014;130(2):161-7.
2. Paul JF, Rohnean A, Elfassy E, Sigal-Cinqualbre A. Radiation dose for thoracic and coronary step-and-shoot CT using a 128-slice dual-source machine in infants and small children with congenital heart disease. Pediatric radiology. 2011;41(2):244-9.
3. Zheng M, Zhao H, Xu J, Wu Y, Li J. Image quality of ultra-low-dose dual-source CT angiography using high-pitch spiral acquisition and iterative reconstruction in young children with congenital heart disease. J Cardiovasc Comput Tomogr. 2013;7(6):376-82.
4. Husmann L, Leschka S, Desbiolles L, Schepis T, Gaemperli O, Seifert B, et al. Coronary artery motion and cardiac phases: dependency on heart rate -- implications for CT image reconstruction. Radiology. 2007;245(2):567-76.
5. Martini C, Palumbo A, Maffei E, Rossi A, Rengo M, Malago R, et al. Dose reduction in spiral CT coronary angiography with dual source equipment. Part II. Dose surplus due to slope-up and slope-down of prospective tube current modulation in a phantom model. Radiol Med. 2010;115(1):36-50.
6. Neefjes LA, Rossi A, Genders TS, Nieman K, Papadopoulou SL, Dharampal AS, et al. Diagnostic accuracy of 128-slice dual-source CT coronary angiography: a randomized comparison of different acquisition protocols. European radiology. 2013;23(3):614-22.
7. Siegel MJ, Hildebolt C, Bradley D. Effects of automated kilovoltage selection technology on contrast-enhanced pediatric CT and CT angiography. Radiology. 2013;268(2):538-47.
8. Siegel MJ, Ramirez-Giraldo JC, Hildebolt C, Bradley D, Schmidt B. Automated low-kilovoltage selection in pediatric computed tomography angiography: phantom study evaluating effects on radiation dose and image quality. Investigative radiology. 2013;48(8):584-9.
9. Durand S, Paul JF. Comparison of image quality between 70 kVp and 80 kVp: application to paediatric cardiac CT. European radiology. 2014;24(12):3003-9.
10. Wrixon AD. New ICRP recommendations. Journal of radiological protection : official journal of the Society for Radiological Protection. 2008;28(2):161-8.
11. ICRP. ICRP Publication 103. 2007. Available from: ICRP_Publication_103-Annals_of_the_ICRP_37(2-4)-free_extract.pdf. Accessed on 11-11-2020.
12. AAPM. AAPM Report No. 204. 2011. Available from: Size-Specific Dose Estimates (SSDE) in Pediatric and Adult Body CT Examinations_AAPM_rpt_204. Accessed on 11-11-2020.
13. Han BK, Grant KL, Garberich R, Sedlmair M, Lindberg J, Lesser JR. Assessment of an iterative reconstruction algorithm (SAFIRE) on image quality in pediatric cardiac CT datasets. Journal of cardiovascular computed tomography. 2012;6(3):200-4.

CHAPTER 7

Dose reduction for CT coronary calcium scoring with a calcium-aware image reconstruction technique: a phantom study

This chapter is based on the publication in Eur Radiol. 2020;30(6):3346-55

Ronald Booij, Niels van der Werf, Ricardo Budde, Daniel Bos, Marcel van Straten

ABSTRACT

Objective

To assess the dose reduction potential of a calcium-aware reconstruction technique, which aims at tube voltage independent computed tomography (CT) numbers for calcium.

Methods and materials

A cardiothoracic phantom, mimicking different patient sizes, was scanned with two calcium inserts (named D100 and CCI), containing calcifications varying in size and density. Tube voltage was varied both manually (range 70– 150 and Sn100 kVp) and automatically. Tube current was automatically adapted to maintain reference image quality defined at 120 kVp. Data was reconstructed with the standard reconstruction technique (kernel Qr36) and the calcium-aware reconstruction technique (kernel Sa36). We assessed the radiation dose reduction potential (volumetric CT dose index values ($CTDI_{vol}$)), noise (standard deviation (SD)), mean CT number (HU) of each calcification, and Agatston scores for varying kVp. Results were compared with the reference acquired at 120 kVp and reconstructed with Qr36.

Results

Automatic selection of the optimal tube voltage resulted in a $CTDI_{vol}$ reduction of 22%, 15%, and 12% compared with the reference for the small, medium, and large phantom, respectively. CT numbers differed up to 64% for the standard reconstruction and 11% for the calcium-aware reconstruction. Similarly, Agatston scores deviated up to 40% and 8% for the standard and calcium-aware reconstruction technique, respectively.

Conclusion

CT numbers remained consistent with comparable calcium scores when the calcium-aware image reconstruction technique was applied with varying tube voltage. Less consistency was observed in small calcifications with low density. Automatic reduction of tube voltage resulted in a dose reduction of up to 22%.

INTRODUCTION

Ischemic heart diseases remain one of the leading causes of death worldwide [1, 2]. Within the framework of individual risk prediction for these diseases, the assessment of coronary artery calcium has become increasingly important. Currently, the most common strategy for quantification of the coronary artery calcium score (CACS) is on computed tomography (CT) examinations using the Agatston method [3]. Despite the excellent prognostic value of this CT-based strategy, the Agatston scoring method has some limitations [4, 5]. Recent guidelines demand a fixed tube voltage of 120 peak kilo voltage (kVp) in combination with filtered back projection (FBP) or iterative reconstruction with 100 kVp acquisition after site- and literature-based validation [5, 6]. However, there is a main argument for the use of lower, or even patient-specific, tube voltages: the need to reduce radiation dose given the increase in the number of CT examinations [7].

Lowering tube voltage potentially reduces radiation dose in CACS at the cost of inconsistent scores because CT numbers, expressed in Hounsfield units (HU), are energy dependent. In this case, the standard calcium scoring threshold should be made tube voltage or patient-specific.

Recently, a calcium-aware reconstruction technique was introduced via the application of a new reconstruction kernel (Sa36f). The technique is also known by the name "Agatston score equivalent calcium scoring," "artificial 120 kV equivalent CT images," or "artificial 120." Please refer to the vendor's whitepaper for a detailed explanation [8]. With this technique, CT numbers of calcium are scaled to match the CT numbers that would have been measured at 120 kVp, enabling the use of the standard 130 HU threshold [9]. The technique might enable acquiring images at reduced radiation dose, while preserving the Agatston score and its risk assessment potential. In contrast to tube voltage–dependent threshold adjustments, the calcium-aware reconstruction technique seems an easy tool to implement clinically.

The purpose of our phantom study was to evaluate the calcium-aware reconstruction technique with regard to coronary calcium quantification for a wide range of tube voltages and calcifications varying in size and density and for different chest sizes. Moreover, the radiation dose reduction by automatic tube voltage selection was assessed for these cases.

MATERIALS AND METHODS

Phantom

An anthropomorphic (cardio) thoracic CT phantom (QRM Thorax, QRM GmbH) in combination with two different inserts was used for quantitative assessment of CACS for both the standard and the calcium-aware reconstruction technique (Fig. 1).

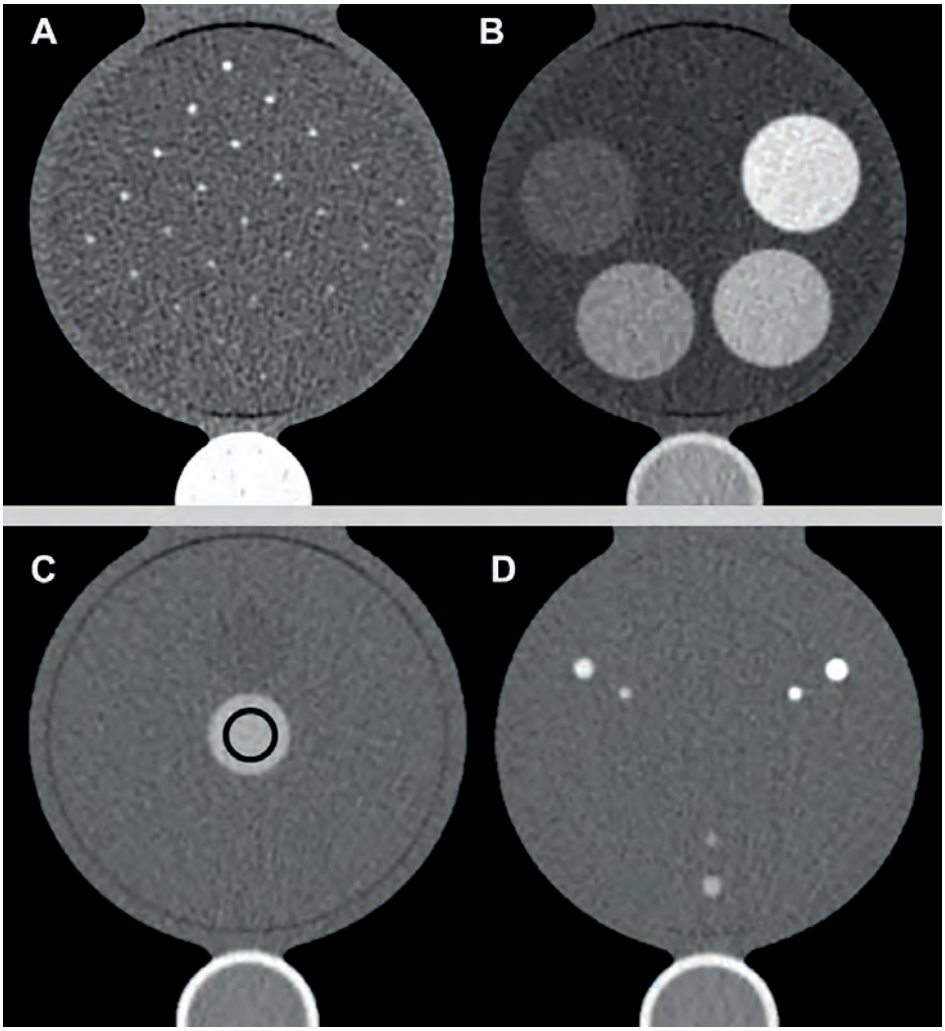

Figure 1 (a-d). Phantom inserts: **(a)** Calcium cylinders of the D100 insert (0.5 mm – 2.0 mm). **(b)** Calibration rods of the D100 insert (30 mm), nominal hydroxyapatite (HA) 90 – 540 mgHA/cm^3. **(c)** HU measurement of the central calcium insert in the CCI insert. **(d)** Cylindrical calcification inserts of three different HA densities: 800 mgHA/cm^3 at 2 o'clock position, 200 mgHA/cm^3 at 6 o'clock position, and 400 mgHA/cm^3 at 10 o'clock position of the CCI insert.

One insert (D100, QRM GmbH) contained 100 calcifications of different diameters (0.5 to 2.0 mm) and hydroxyapatite (HA) densities (90 to 540 mg HA/cm^3) [10]. The other insert was a cylindrical cardiac calcification insert (CCI, QRM GmbH) with nine calcifications varying in size (1.0 to 5.0 mm) and density (200 to 800 mg HA/cm3). To simulate different chest sizes, the thorax phantom was scanned with and without fat-equivalent extension rings (QRM GmbH), resulting in three different chest sizes: small (300 × 200 mm), medium (350 × 250 mm), and large (400 × 300 mm). To ensure a realistic translation of the results from different phantom sizes to human chest sizes, the water equivalent diameter (Dw) was used. Dw reflects the x-ray attenuation of the patient and is therefore a preferred patient size metric [11]. Retrospective analysis of Dw's in 41 patient scans for CACS performed in our hospital showed that these diameters mostly matched with the Dw of the medium and large extension rings.

Acquisition and reconstruction parameters

Scans were performed on a dual source CT (DSCT) system (SOMATOM Force, Siemens Healthineers, Syngo CT VB10). A reference tube voltage of 120 kVp in combination with automated tube current modulation (ATCM) CARE Dose4D was used for both inserts (Table 1). The calcium-aware reconstruction technique was assessed by acquiring data with varying tube voltages of 70–150 kVp, in steps of 10 kVp. Additionally, automatic tube voltage selection ("kVon") was set to keep the contrast to noise ratio for calcium constant when selecting the optimal tube voltage for radiation dose optimization. Finally, a scan was performed using a dedicated CACS Tin filtration protocol with an adaptation of the reference tube voltage to Sn100 in combination with ATCM CARE Dose4D (Table 1). All scans were repeated five times after manual repositioning (approximately 2 mm translation and 2 degrees rotation) of the phantom to assess positioning influence and interscan variation.

Images were reconstructed with the conventional calcium scoring reconstruction technique (kernel Qr36) and the dedicated calcium-aware reconstruction technique (kernel Sa36), both based on FBP. For the latter technique, calcium is identified in preliminary reconstructed images and a lookup table is used to correct the CT numbers of calcium in the finally reconstructed images [8]. The exact working of the algorithm is proprietary information of the vendor. The algorithm is fully integrated within the standard image reconstruction interface and can be activated by selecting the corresponding reconstruction kernel (Sa36). It does not need an additional workstation or increased reconstruction times.

Table 1. Acquisition and reconstruction parameters.

Scanner*	SOMATOM Force	SOMATOM Force-tin filtration
Acquisition mode	Sequential	Sequential
Scan length (mm)	100.5	100.5
Reference tube voltage	120	Sn100
Reference tube current product	80	534
Manual tube voltage settings	70–150	Sn100
CARE kV dose optimization slider**	5 (bone/calcium)	5 (bone/calcium)
Collimation (mm)	32 × 1.2	32 × 1.2
Rotation time (sec)	0.25	0.25
Image reconstruction (FBP)	Qr36 and Sa36	Qr36 and Sa36
Slice thickness (mm)	3.0	3.0
Increment (mm)***	1.5	1.5
FoV (mm)	180	180
Reconstruction matrix	512 × 512	512 × 512

*Siemens Healthineers, Syngo CT VB10
**The dose optimization slider from the default calcium scoring protocol was retained
***Increment of 1.5 mm is the standard for calcium scoring with Siemens equipment

Image and dose analysis

The volumetric CT dose index values ($CTDI_{vol}$) in mGy were noted to assess potential radiation dose reduction. Consistency of CT numbers (mean and standard deviation (SD)) was determined in the central calcium insert (200HA) of the CCI insert. Noise SD was determined within a homogeneous region of the CCI insert. Agatston score, together with different image quality metrics, was computed using an in-house developed Python script (Python version 3.7) for the D100 and CCI insert. Resulting Agatston scores of the Python script were validated against the standard vendor-specific scoring software (Syngo.via, Siemens Healthineers) with the aid of CCI data and proven equal (maximum deviation 0.1%).

This study addresses directly the CT number or CT value in HU of calcifications. CT numbers are related to the linear x-ray attenuation coefficients and depend on the density, the effective atomic number, and x-ray tube voltage [12]. The attenuation coefficient of the phantom base material does not resemble the attenuation coefficient of human soft tissue equally well at all tube voltages. Allmendinger et al previously described a base material-specific correction, necessary for correct Agatston scores at varying tube voltages by adjustment of the standard 130 HU threshold [8]. This correction was applied automatically in our study as well as for all reconstructions.

Image noise was compared with recommended noise targets (in HU) for calcium scoring CT scans defined for different chest sizes (small, medium, large chest width): 20 HU for the small and medium chest width, and 23 HU for the large chest width [13].

Additionally, an Agatston score was determined in a non-calcium region (55 × 55 mm), therefore depending purely on noise. This score was called the background Agatston score (BAS). For acquisitions with a non-zero BAS, the Agatston scores of calcifications could be less reliable, as it was uncertain if a calcification was seen at a specific location, or just noise. These scores were noted.

Reference values for both inserts were the Agatston scores acquired with a tube voltage of 120 kVp and reconstructed with the standard technique (Qr36). Each deviation in acquisition or reconstruction was compared against this reference.

Statistical analyses

SPSS (version 25, IBM Corp) was used for statistical analysis. Normality of data was tested with the Shapiro-Wilk test. Wilcoxon signed-rank test was performed to evaluate statistically significant difference of the median Agatston scores. Intraclass correlation coefficients (ICC) with a 95% confidence interval (CI) and Bland-Altman plots of the Agatston scores between two different techniques were assessed. A p value of < 0.05 was considered statistically significant. Agatston scores are given as median values of the five measurements.

RESULTS

Radiation dose and noise values

Reference dose levels at 120 kVp for the small, medium, and large phantom size were 1.57, 2.59, and 3.84 mGy respectively. For the scans with automatic tube voltage selection, tube voltage was reduced to 90 kVp for the small and medium phantom size, while 100 kVp was selected for the large phantom. In comparison with the corresponding reference, radiation dose levels decreased by 22%, 15%, and 12% for the small, medium, and large phantom size, respectively.

Within the dedicated Tin CACS protocol, dose values were 55% lower for both small and medium phantom size and 60% for the large phantom size compared with the reference dose levels at 120 kVp.

Median noise values for the 120 kVp and the images obtained with automatic tube voltage selection increased with increasing phantom diameter for both reconstruction techniques (Fig. 2). The noise level in all three phantom sizes was highest when using Tin filtration. Moreover, the recommended noise target for calcium scoring CT scans was exceeded for some tube voltages in the medium phantom and for all tube voltages in the large phantom size (Fig. 2). Despite the high number of noise limit exceeding scans, BAS values were zero for most reconstructions. A BAS > 0 was found only for the large phantom in combination with a tube voltage of 70 kVp or Sn100.

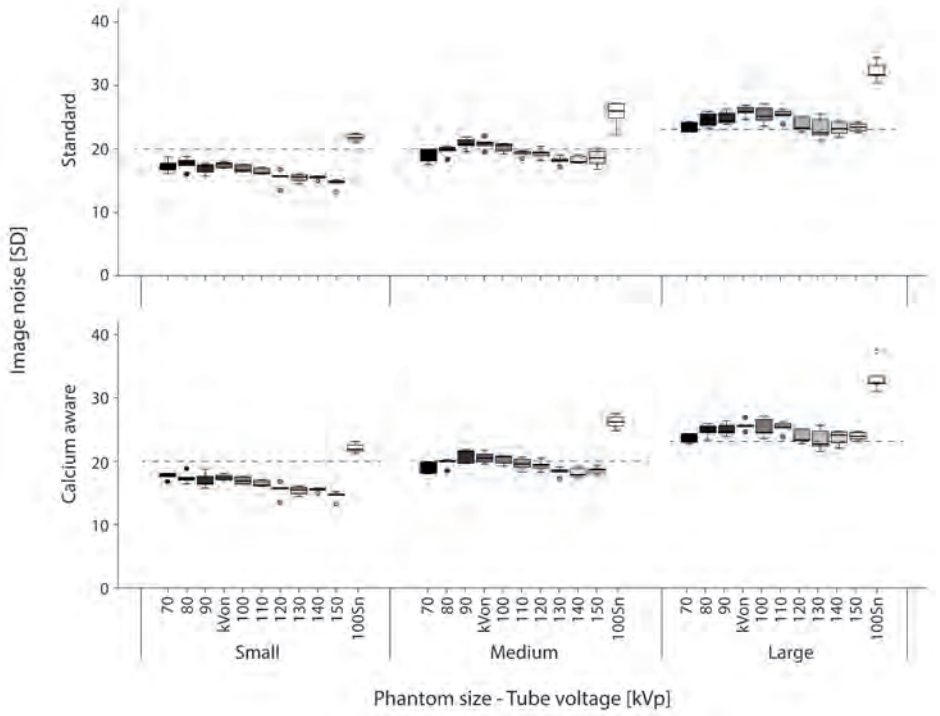

Figure 2. Box-and-whisker plots of the noise measurements of the homogeneous central slice of the CCI insert. Recommended noise targets (in HU) for calcium scoring CT scans defined for different chest sizes were applied to the images as dotted lines: 20 HU for the small and medium chest width, and 23 HU for the large chest width. The automatic tube voltage selection is illustrated by "kVon".

CT number constancy

Considering the large calcification with 200 mg HA/cm^3 in the CCI insert for all phantom sizes, CT numbers increased with decreasing tube voltage for the standard reconstruction technique, while these numbers remained virtually constant for the calcium-aware reconstruction technique (Table 2). Median HU (min HU–max HU) of the reference (120 kVp + Qr36) was 266 HU (265HU—268HU), 257 HU (257HU—258HU), and 247 HU (246HU—248HU) for the small, medium, and large phantom size, respectively. Compared with the reference, the deviation was up to 64% with the standard reconstruction technique and up to 11% with the calcium-aware reconstruction technique when varying the tube voltage (Table 2).

Table 2. Deviation of the CT number of calcium at varying tube voltage and phantom size compared with the reference with a tube voltage of 120 kV and the standard reconstruction technique (Qr36)

	Deviation of the CT number of calcium					
	Calcium-aware reconstruction technique			Standard reconstruction technique		
Tube voltage	**Small phantom**	**Medium phantom**	**Large phantom**	**Small phantom**	**Medium phantom**	**Large phantom**
70	-11.0% (-9.9% to-11.1%)	-4.3% (-4.0% to -5.0%)	2.2% (1.8% to 3.5%)	60.5% (59.6% to 61.6%)	61.0% (60.4% to 62.0%)	63.6% (62.0% to 65.6%)
80	-7.0% (-6.7% to -7.6%)	-2.7% (-2.3% to -2.8%)	3.2% (2.6% to 3.8%)	40.1% (39.4% to 40.4%)	39.1% (39.0% to 40.1%)	40.8% (40.3% to 41.6%)
90	-3.6% (-3.4% to -4.6%)	-0.5% (-0.9% to 0.7%)	3.7% (3.6% to 5.4%)	25.4% (25.3% to 26.3%)	24.4% (24.1% to 25.9%)	25.3% (24.2% to 26.5%)
100	-2.4% (-2.0% to -2.9%)	0.6% (0.3% to 1.7%)	4.7% (3.3% to 5.6%)	14.9% (14.6% to 15.3%)	13.6% (13.3% to 15.0%)	14.0% (12.5% to 15.9%)
110	-2.2% (-1.7% to -2.7%)	1.1% (0.8% to 1.3%)	5.2% (4.2% to 5.6%)	6.3% (5.7% to 6.9%)	5.8% (5.6% to 6.2%)	6.4% (5.4% to 6.7%)
120	-1.5% (-0.7% to -2.0%)	2.1% (1.9% to 2.3%)	5.4% (5.1% to 6.0%)	0.0% (-0.5% to 0.8%)	0.0% (-0.2% to 0.2%)	0.0% (-0.3% to 0.6%)
130	-1.4% (-0.6% to -2.3%)	1.9% (0.9% to 2.1%)	5.8% (5.5% to 6.5%)	-5.3% (-4.5% to -6.2%)	-5.6% (-5.4% to -6.3%)	-4.6% (-4.0% to -4.7%)
140	-0.9% (-0.8% to -1.7%)	2.0% (0.8% to 2.9%)	4.7% (4.4% to 6.1%)	-9.4% (-9.3% to 10.1%)	-9.6% (-8.8% to 10.7%)	-9.6% (-8.6% to 10.0%)
150	-1.1% (-0.6% to -1.8%)	1.9% (1.2% to 3.0%)	5.7% (5.2% to 6.5%)	-13.0% (-12.6% to -13.6%)	-13.2% (-12.4% to -13.8%)	-12.3% (-11.3% to -12.5%)
Sn100	-5.3% (-4.3% to -7.0%)	-2.5% (-1.4% to -3.8%)	1.5% (0.2% to 3.7%)	-16.5% (-16.2% to -17.9%)	-13.9% (-13.0% to -14.8%)	-11.1% (-9.0% to -11.8%)

Values given in median% (min% to max%]

Table 3. Agatston score deviation at varying tube voltage and phantom size compared with the reference with a tube voltage of 120 kV and the standard reconstruction kernel (Qr36).

	Agatston score deviation					
	Calcium-aware reconstruction technique			Standard reconstruction technique		
Tube voltage	**Small phantom**	**Medium phantom**	**Large phantom**	**Small phantom**	**Medium phantom**	**Large phantom**
70	-7.5% (-1.9% to -10.4%)	-2.5% (2.6% to -7.1%)	1.8% (-3.1% to 5.6%)	39.7% (33.6% to 44.0%)	38.1% (33.0% to 44.3%)	36.7% (31.6% to 43.3%)
80	-7.0% (-3.0% to -11.7%)	-3.8% (1.7% to -8.0%)	-1.6% (5.2% to -7.0%)	26.3% (21.9% to 28.8%)	24.6% (20.9% to 28.4%)	24.4% (19.1% to 27.7%)
90	-5.2% (-1.2% to -8.8%)	-2.0% (2.5% to -7.4%)	-2.2% (4.3% to -6.1%)	18.1% (14.2% to 22.3%)	16.8% (11.6% to 20.0%)	14.5% (9.9% to 20.4%)
100	-3.4% (-1.2% to -7.2%)	-2.8% (1.9% to -6.8%)	-1.5% (4.4% to -5.7%)	13.1% (5.8% to 16.5%)	7.0% (2.7% to 15.8%)	7.7% (1.1% to 13.1%)
110	-5.6% (-0.5% to -8.5%)	-0.8% (3.2% to -6.2%)	2.5% (-3.4% to 6.8%)	1.7% (-1.3% to 7.4%)	2.2% (-0.6% to 7.2%)	3.7% (-2.5% to 8.4%)
120	-1.1% (3.8% to -5.6%)	0.7% (-2.8% to 4.6%)	2.2% (-2.3% to 10.3%)	0.0% (-4.4% to 5.3%)	0.0% (-4.6% to 3.9%)	0.0% (-4.7% to 5.6%)
130	-3.5% (1.1% to -5.7%)	-0.9% (4.9% to -5.5%)	2.4% (-5.2% to 10.7%)	-6.2% (-2.5% to -7.5%)	-6.2% (-2.0% to -11.1%)	-7.5% (-0.6% to -11.3%)
140	-2.6% (2.4% to -5.8%)	-0.1% (-4.1% to 6.8%)	0.6% (-3.5% to 7.9%)	-10.2% (-5.3% to 12.2%)	-10.5% (-6.6% to -14.4%)	-11.3% (-6.8% to -16.5%)
150	-3.1% (3.1% to -5.5%)	0.1% (-2.9% to 6.7%)	1.7% (-3.4% to 10.1%)	-12.7% (-10.0% to -14.1%)	-11.3% (-8.8% to -16.8%)	-14.5% (-7.2% to -17.1%)
Sn100	-4.4% (0.1% to -8.7%)	-2.5% (5.6% to -7.8%)	-0.4% (9.3% to -17.4%)	-13.7% (-9.7% to -17.2%)	-15.7% (10.5% to -41.0%)	-12.2% (-3.0% to -28.3%)

Values given in median% [min% to max%]

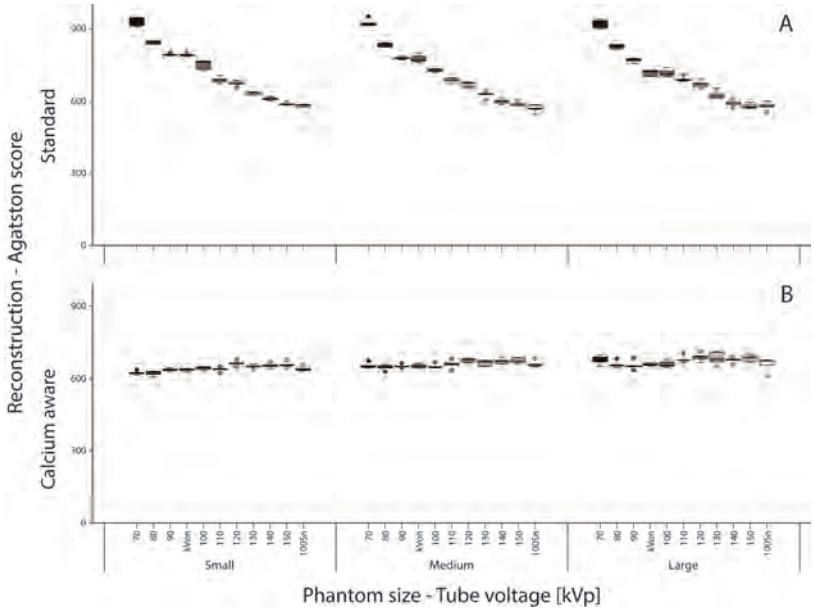

Figure 3 (a-b). (a) Box-and whisker plots of the Agatston score within the CCI insert with the standard reconstruction technique. **(b)** Box-and- whisker plots of the Agatston score within the CCI insert with the calcium-aware reconstruction technique. Scores are given per phantom size-tube voltage combination. The automatic tube voltage selection is illustrated by "kVon".

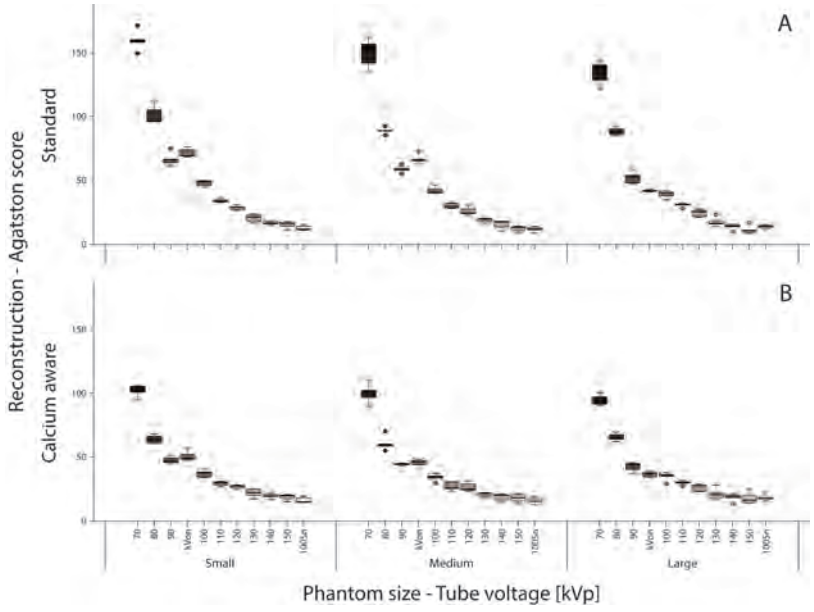

Figure 4 (a-b). (a) Box-and-whisker plots of the Agatston score within the D100 insert with the standard reconstruction technique. **(b)** Box- and whisker-plots of the Agatston score within the D100 insert with the calcium-aware reconstruction technique. Scores are given per phantom size-tube voltage combination. The automatic tube voltage selection is illustrated by "kVon".

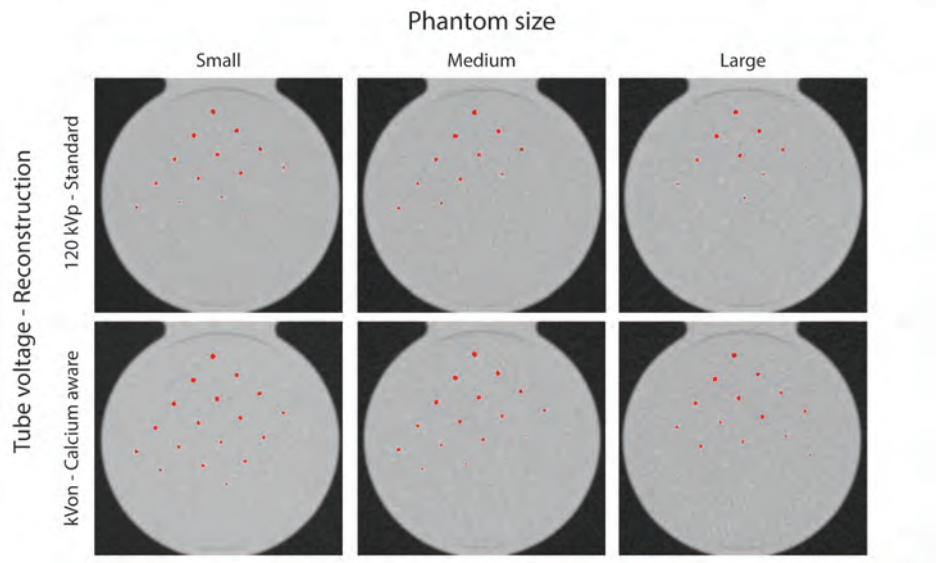

Figure 5. Visualization of calcifications in the D100 insert with all voxels with a CT number above the threshold colored red. From left to right, the phantom size increases. The upper row images were reconstructed with the standard reconstruction technique with a tube voltage of 120 kVp. Lower row images were reconstructed with the calcium-aware reconstruction technique and automated tube voltage selection (90 kVp for the small and medium size phantom and 100 kVp for the large size phantom).

Agatston score

When varying the tube voltage, Agatston scores deviated up to 40% and 8% from the reference for the standard and calcium-aware reconstruction technique, respectively (Table 3). The overall spread in median Agatston scores for varying tube voltages decreased for the calcium-aware reconstruction technique for both the CCI and D100 insert (Fig. 3 and Fig. 4). Considering all phantom sizes, the Agatston scores in the CCI insert increased with 14% for the automated tube voltage selection and decreased with 14% within the tin-filtrated scans for the standard reconstruction technique (Fig. 3a). For the calcium-aware reconstruction technique, Agatston score deviations from the reference were much less: 3.6% at automated tube voltage selection and 2.4% with the tin-filtrated scans (Fig. 3b). For the D100 insert, we observed similar results; however, the deviations from the reference were larger than in the CCI insert, especially for the varying tube voltage in combination with the standard reconstruction technique (Fig. 4). Representative images of the D100 insert for the standard reconstruction technique with 120 kVp and the calcium-aware reconstruction technique at reduced tube voltage for all three phantom sizes are shown in Figure 5. This Figure shows calcifications with an Agatston score of zero for the reference, while the calcium-aware reconstruction technique Agatston scores are non-zero.

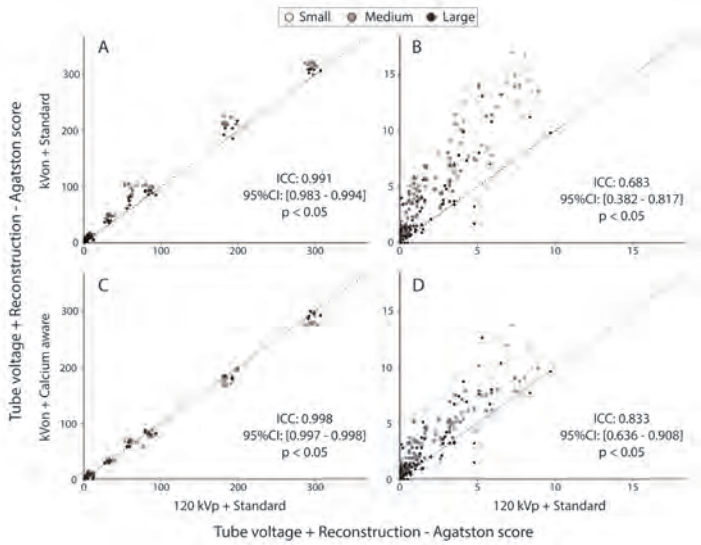

Figure 6 (a-d). The ICC of the Agatston score for the small, medium, and large phantom for. **(a)** The standard reconstruction technique with automatic tube voltage selection compared with the standard reconstruction with 120 kVp. **(b)** Detail of the graph in a representing the low density and small calcifications. **(c)** The calcium-aware reconstruction technique with automatic tube voltage selection and the standard reconstruction with 120 kVp. **(d)** Detail of the graph in **(c)** representing the low density and small calcifications.

There was a very high ICC (0.991) and 95% CI for the automated tube voltage selection with the standard reconstruction technique compared with the reference when considering all calcifications (Fig. 6a). When considering only the low Agatston scores, both the ICC and 95% CI decreased (Fig. 6b). There was a very high ICC (0.998) and 95% CI for the automated tube voltage selection and the calcium-aware reconstruction technique compared with the reference (Fig. 6c). When considering only the low Agatston scores, both the ICC and 95% CI decreased (Fig. 6d). However, this decrease was less than observed within the standard reconstruction technique. A Bland-Altman analysis of the data is shown in Figure 7. The Bland-Altman plots demonstrate the agreement between the two reconstruction kernels. The negative mean difference within Figure 7 a, b, and d demonstrates that, regardless of reconstruction technique, Agatston scores are higher for automatic tube voltage selection in comparison with 120 kVp. The opposite applies for the calcium-aware reconstruction technique and automatic tube voltage selection (Fig. 7c).

For the CCI insert, increasing the phantom diameter from small to large demonstrated no statistically significant decrease (p = 0.5) of the median (range) Agatston scores from 671 (656.2—686.5) to 669.9 (651.1—689.4) for the reference (120 kVp and Qr36). A statistically significant increase (p < 0.05) in Agatston score from 639 (626.9—642.4) to 657.4 (652to 664.5) was observed for the calcium-aware technique with automated

tube voltage selection. For the D100 insert and increasing phantom size from small to large, there was a statistically significant decrease ($p < 0.05$) in Agatston score from 29.3 (26.5—31.2) to 25.6 (21.4—27.8) for the reference ($p < 0.05$). A statistically significant ($p < 0.05$) decrease was observed for the Agatston score from 49.0 (47.4—56.7) to 37.1 (34.0—39.4) for the calcium-aware reconstruction technique with automatic tube voltage selection.

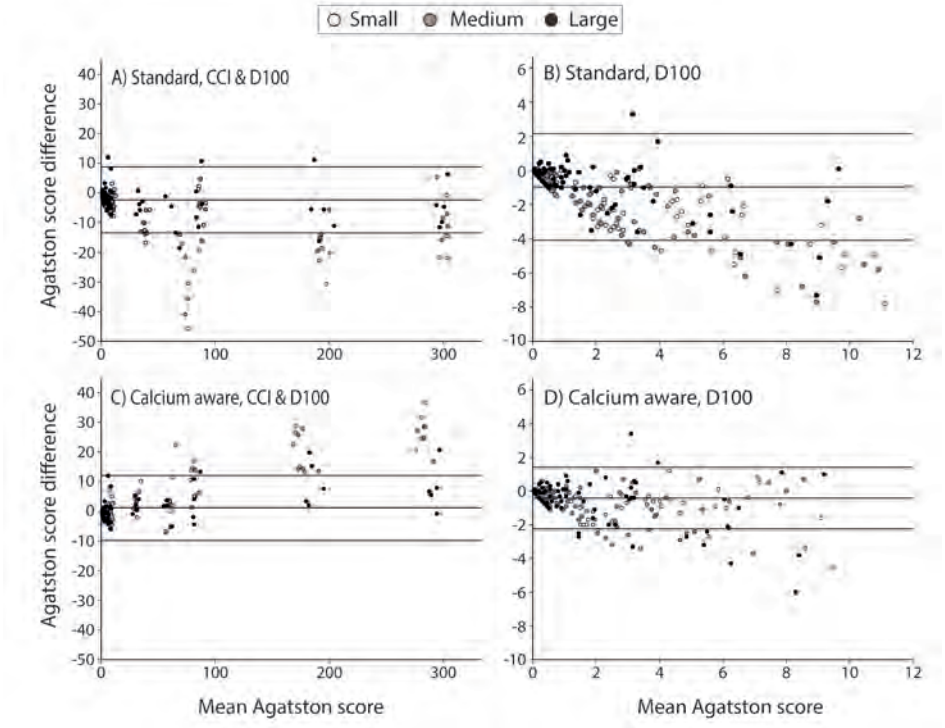

Figure 7 (a-d). Bland-Altman Plots with mean difference and 95% limits of agreement for the small, medium, and large phantom with the CCI and/or D100 insert. All plots show an Agatston score comparison between the reference at 120 kVp (with standard reconstruction technique) and scans with automatic tube voltage selection (with standard reconstruction technique **(a, b)** and with calcium-aware reconstruction technique **(c, d)**.

DISCUSSION

Our results demonstrate that CACS with a calcium-aware image reconstruction technique allows for consistent CT numbers when varying the tube voltage and allows for reduced radiation exposure with automatic reduction of tube voltage. The Agatston scores with the calcium-aware reconstruction technique deviated up to 8% for the calcifications of the CCI insert across 70 to 150 kVp and Sn100, whereas the Agatston

score with the standard reconstruction deviated much more with up to 40%. The latter might be explained by the increase of the photoelectric effect for calcium when scanning with low tube voltage settings. In contrast to the CCI insert, Agatston scores were not stable for the calcifications of the D100 insert when varying the tube voltage. For the calcium-aware reconstruction technique, this might be explained by a sub-optimal identification of the voxels containing calcifications of small diameter and low density and subsequently a sub-optimal correction of the CT numbers.

As seen in Figure 5, there were additional calcifications detected when lowering tube voltage. Thus, it might be possible that a patient with a zero Agatston score at 120 kVp might have a non-zero Agatston score at a lower tube voltage, despite the application of the calcium-aware reconstruction technique. This might influence the work-up of patients suspected for coronary artery disease. However, the increase of Agatston score in the D100 insert, as demonstrated in Figure 5, is due to true calcified lesions. Instead of improving the calcium-aware reconstruction technique presented in this study to better resemble the Agatston scores at 120 kV, we prefer to reinvent calcium imaging and think it is time to let go the conventional scoring method (14, 15]. For example, Groen et al described a correction applied to the 130 HU calcium scoring threshold for the increased CT numbers of calcium when varying tube voltage and applying the standard reconstruction technique (16].

Our study demonstrated a decrease in Agatston score with increasing phantom size, as previously described for the standard reconstruction technique and the D100 insert (17]. However, our study used both the CCI and the D100 insert and in addition the calcium-aware reconstruction technique. We observed an increase of the Agatston score for the CCI insert when using the calcium-aware reconstruction technique. The increase in Agatston score might be explained by the suboptimal identification of the voxels containing small and low-density calcifications, while noise increased.

Calcium CT numbers were constant for the calcium-aware reconstruction technique with automated tube voltage selection, irrespective of phantom size. However, Agatston scores varied more than the reference for different patient sizes. The reason for this is twofold. First, the constancy of CT numbers is calculated as the mean of a large ROI enclosing the calibration rod of the CCI phantom, while Agatston scores are calculated for the smaller nine calcifications. Second, despite the use of clinical scan protocols, higher noise levels were shown especially for the lower tube voltages and the automated tube voltage selection (Fig. 2). Our computation of the Agatston score was validated to the standard vendor-specific software, calculating every single voxel above a threshold of 130 HU for CACS. With higher noise levels, Agatston scores also increase.

Technological developments like tin filtration and automated tube voltage selection allow for a substantial dose reduction. For example, a 100 kVp with tin filtration CACS protocol demonstrated similar Agatston scores as the reference protocol with 120 kVp

despite using the standard reconstruction technique (18]. Larger deviations are expected for tube voltages like 70 and 80 kVp (Table 2). A great advantage of the currently considered calcium-aware reconstruction technique is that CACS can be obtained more accurately from any acquisition, regardless of applied tube voltage and filtration. This allows CACS to be considered within cancer screening protocols. The use of a CACS with the aid of tin filtration combined with an early prototype of a calcium-aware reconstruction technique was described in a patient study and considered potentially feasible for calcium scoring (19]. However, in this study and our study, an increased image noise for the tin-filtrated scans was observed. The noise levels were above the recommended noise levels by the SCCT in all three phantom sizes, especially for the large phantom size. Possible solutions for sub-optimal identification of calcification when applying tin filtration with increased noise levels are proposed, e.g., a HU threshold correction for CACS (20] or investigation to apply iterative reconstructions. Within our study, we observed BAS of > 0 for the tin-filtrated vendor-recommended scans in the large phantom size. Therefore, caution must be taken when applying the tin-filtrated scans in clinical routine, especially when CACS is obtained for calcification of small diameter and low density, as the calcium-aware reconstruction technique is also not able to correct these.

The recommended noise levels were not only exceeded for the tin-filtrated scanning protocols but also for all tube voltage settings within the large phantom diameter, despite the use of the vendor-recommended scanning protocols. This warrants further investigation for adjusting the reference tube current value or the adaptation strength of the CARE Dose4D dose curve to achieve the recommended noise target level (13]. However, it seems that the recommended noise target limit comes with a very safe margin. After all, the BAS was zero for all reconstructions in the small- and medium-sized phantoms and for the calcium-aware reconstruction technique with automated tube voltage selection in all phantoms.

There are limitations in this study that need to be considered. This study was phantom-based and despite the effort to represent clinical routine, patient studies are necessary to validate our findings. $CTDI_{vol}$ is an indicator of the CT scanner radiation output. The dose received by a patient depends on this $CTDI_{vol}$ and the individual patient size. It is recommended to use the size-specific dose estimates (SSDE) to reflect estimated doses for the individual patient (21]. Furthermore, it might be of interest to use a non-stationary phantom model instead of a stationary one. This makes it feasible to assess whether or not heart rate variability will influence Agatston scores when using the calcium-aware reconstruction technique.

CONCLUSION

In general, CT numbers remained consistent with comparable calcium scores when the calcium-aware image reconstruction technique was applied with varying tube voltage. Less consistency was observed in small calcifications with low density. Automatic reduction of tube voltage resulted in a dose reduction of up to 22%.

ACKNOWLEDGMENTS

We would like to thank Maarten Kremer and Marcel Dijkshoorn (Erasmus MC, Rotterdam) for their support during scanning and Marcel Greuter, PhD (University medical center Groningen, Groningen), for lending the D100 insert.

REFERENCES

1. Eurostat. Statistics Causes of Death in the European Union (EU) 2005 – 2015. 2018. Available from: https://ec.europa.eu/eurostat/statistics-explained/index.php/Causes_of_death_statistics. Accessed 11-11-2020.
2. Greenland P, Alpert JS, Beller GA, Benjamin EJ, Budoff MJ, Fayad ZA, et al. 2010 ACCF/AHA guideline for assessment of cardiovascular risk in asymptomatic adults: a report of the American College of Cardiology Foundation/American Heart Association Task Force on Practice Guidelines. J Am Coll Cardiol. 2010;56(25):e50-103.
3. Elias-Smale SE, Proenca RV, Koller MT, Kavousi M, van Rooij FJ, Hunink MG, et al. Coronary calcium score improves classification of coronary heart disease risk in the elderly: the Rotterdam study. J Am Coll Cardiol. 2010;56(17):1407-14.
4. Willemink MJ, van der Werf NR, Nieman K, Greuter MJW, Koweek LM, Fleischmann D. Coronary artery calcium: A technical argument for a new scoring method. J Cardiovasc Comput Tomogr. 2018.
5. Hecht HS, Cronin P, Blaha MJ, Budoff MJ, Kazerooni EA, Narula J, et al. 2016 SCCT/STR guidelines for coronary artery calcium scoring of noncontrast noncardiac chest CT scans: A report of the Society of Cardiovascular Computed Tomography and Society of Thoracic Radiology. J Cardiovasc Comput Tomogr. 2017;11(1):74-84.
6. Hecht H, Blaha MJ, Berman DS, Nasir K, Budoff M, Leipsic J, et al. Clinical indications for coronary artery calcium scoring in asymptomatic patients: Expert consensus statement from the Society of Cardiovascular Computed Tomography. J Cardiovasc Comput Tomogr. 2017;11(2):157-68.
7. Bijwaard H, Pruppers M, de Waard-Schalkx I. The influence of population aging and size on the number of CT examinations in The Netherlands. Health Phys. 2014;107(1):80-2.
8. Allmendinger T, Hamann A. Agatston calcium quantification with arbitrary tube voltage - White paper. 2018. Available via https://www.siemens-healthineers.com/computed-tomography/clinical-imaging-solutions/cardiovascular-imaging#CLINICAL_USE. Accessed 11-11-2020.
9. Agatston AS, Janowitz WR, Hildner FJ, Zusmer NR, Viamonte M, Jr., Detrano R. Quantification of coronary artery calcium using ultrafast computed tomography. J Am Coll Cardiol. 1990;15(4):827-32.
10. Groen JM, Kofoed KF, Zacho M, Vliegenthart R, Willems TP, Greuter MJ. Calcium score of small coronary calcifications on multidetector computed tomography: results from a static phantom study. Eur J Radiol. 2013;82(2):e58-63.
11. McCollough C, Bakalyar DM, Bostani M, Brady S, Boedeker K, Boone JM, et al. Use of Water Equivalent Diameter for Calculating Patient Size and Size-Specific Dose Estimates (SSDE) in CT: The Report of AAPM Task Group 220. AAPM report. 2014;2014:6-23.
12. Lamba R, McGahan JP, Corwin MT, Li CS, Tran T, Seibert JA, et al. CT Hounsfield numbers of soft tissues on unenhanced abdominal CT scans: variability between two different manufacturers' MDCT scanners. AJR Am J Roentgenol. 2014;203(5):1013-20.
13. Voros S, Rivera JJ, Berman DS, Blankstein R, Budoff MJ, Cury RC, et al. Guideline for minimizing radiation exposure during acquisition of coronary artery calcium scans with the use of multidetector computed tomography: a report by the Society for Atherosclerosis Imaging and Prevention Tomographic Imaging and Prevention Councils in collaboration with the Society of Cardiovascular Computed Tomography. J Cardiovasc Comput Tomogr. 2011;5(2):75-83.

14. Blaha MJ, Mortensen MB, Kianoush S, Tota-Maharaj R, Cainzos-Achirica M. Coronary Artery Calcium Scoring: Is It Time for a Change in Methodology? JACC: Cardiovascular Imaging. 2017;10(8):923-37.
15. Nieman K. Evolve or perish for coronary calcium imaging. Eur Heart J Cardiovasc Imaging. 2015;16(4):354-5.
16. Groen JM, Dijkstra H, Greuter MJ, Oudkerk M. Threshold adjusted calcium scoring using CT is less susceptible to cardiac motion and more accurate. Med Phys. 2009;36(2):438-46.
17. Willemink MJ, Abramiuc B, den Harder AM, van der Werf NR, de Jong PA, Budde RP, et al. Coronary calcium scores are systematically underestimated at a large chest size: A multivendor phantom study. J Cardiovasc Comput Tomogr. 2015;9(5):415-21.
18. Apfaltrer G, Albrecht MH, Schoepf UJ, Duguay TM, De Cecco CN, Nance JW, et al. High-pitch low-voltage CT coronary artery calcium scoring with tin filtration: accuracy and radiation dose reduction. Eur Radiol. 2018;28(7):3097-104.
19. Tesche C, De Cecco CN, Schoepf UJ, Duguay TM, Albrecht MH, De Santis D, et al. CT coronary calcium scoring with tin filtration using iterative beam-hardening calcium correction reconstruction. Eur J Radiol. 2017;91:29-34.
20. Vonder M, Pelgrim GJ, Huijsse SE, Meyer M, Greuter MJ, Henzler T, et al. Feasibility of spectral shaping for detection and quantification of coronary calcifications in ultra-low dose CT. Eur Radiol. 2017;27(5):2047-54.
21. Brink JA, Morin RL. Size-specific dose estimation for CT: how should it be used and what does it mean? Radiology. 2012;265(3):666-8.

CHAPTER 8

Efficacy of a dynamic collimator for overranging dose reduction in a second- and third-generation dual source CT

This chapter is based on the publication in Eur Radiol. 2017;27(9):3618-24

Ronald Booij, Marcel L. Dijkshoorn, Marcel van Straten

ABSTRACT

Objectives

The purpose of this study was to assess the efficacy of the renewed dynamic collimator in a third-generation dual source CT (DSCT) scanner and to determine the improvements over the second-generation scanner.

Methods

Collimator efficacy is defined as the percentage overranging dose in terms of dose-length product (DLP) that is blocked by the dynamic collimator relative to the total overranging dose in case of a static collimator. Efficacy was assessed at various pitch values and different scan lengths. The number of additional rotations due to overranging and effective scan length were calculated based on reported scanning parameters. Based on these values, the efficacy of the collimator was calculated.

Results

The second-generation scanner showed decreased performance of the dynamic collimator at increasing pitch. Efficacy dropped to 10% at the highest pitch. For the third-generation scanner the efficacy remained above 50% at higher pitch. Noise was for some pitch values slightly higher at the edge of the imaged volume, indicating a reduced scan range to reduce the overranging dose.

Conclusions

The improved dynamic collimator in the third-generation scanner blocks the overranging dose for more than 50% and is more capable of shielding radiation dose, especially in high pitch scan modes.

INTRODUCTION

Spiral Computed Tomography (CT) has proven its superiority over sequential CT in routine clinical practice. A downside of spiral CT, particularly at an increased detector width and higher pitch values, is the increase of the overranging effect, resulting in a higher dose to the patient [1-4]. Overranging dose is defined as primary radiation that is given to the patient outside the imaged volume [5-7]. The dose penalty due to overranging relative to the total patient dose increases with shorter scan lengths as in paediatrics, the coronary arteries or head and neck imaging [8-10].

In order to reduce the overranging dose, manufacturers introduced dynamic or adaptive collimators to block the dose, which is irrelevant for image reconstruction [11-13]. Dynamic collimators are mechanical blades, which move in and out of the radiation area to block the irrelevant radiation. With the introduction of a third-generation dual source CT (DSCT) scanner, the speed of the blade movement of the dynamic collimator was improved compared to the second-generation DSCT scanner. To our knowledge, no literature is available on the performance of dynamic collimators in state-of-the-art DSCT scanners. Since DSCT is often used at high scan speeds, it is important to be aware of the impact of overranging dose especially in protocols with short scan ranges in (high) radiation-sensitive organs, where overranging can contribute to a larger dose.

The purpose of this study was to assess the efficacy of the renewed dynamic collimator of the third-generation DSCT scanner and compare it to the second-generation DSCT scanner. This was examined by determining the amount and nature of the overranging dose as a function of pitch and scan length.

MATERIALS AND METHODS

Scanners, phantom and scanning protocols

Overranging dose was assessed for a second- and third-generation DSCT scanner. The software version of the second-generation DSCT scanner (SOMATOM Definition Flash; Siemens Healthcare, Forchheim, Germany) was Syngo CT 2012B and that of the third-generation DSCT scanner (SOMATOM Force; Siemens Healthcare, Forchheim, Germany) was Syngo CT VA50A.

A 32-cm-diameter CTDI phantom of 15 cm length was positioned at the isocenter of the scanner. Scans started at the center of the phantom in order to assess the image quality at the edge of the imaged volume in a homogenous object.

Scans were made at various pitch values with a thorax protocol. The pitch values used in single source mode were 0.35, 0.7, and 1.4. Using the dual source mode, the pitch values were 1.55 and 3.2. In addition to the thorax protocol, scans were made with a

dedicated dual source mode cardiac ECG-gated protocol at pitch 3.4 and pitch 3.2 on the second- and third-generation scanner, respectively.

The other scanning parameters were 120 kVp tube voltage for both tubes, and a combined fixed tube load for both tubes of 100 effective milliampere second (eff. mAs). For the second-generation DSCT scanner the rotation time was 0.285 seconds and the beam collimation was 64 x 0.6 mm. For the third-generation DSCT scanner a rotation time of 0.25 seconds was used and a beam collimation of 96 x 0.6 mm. All scans were made at three distances between the first and last reconstructable slice position: 100, 200 and 300 mm. For each scan, the DICOM radiation dose structured report (RDSR) was stored.

Collimator efficacy

The collimator efficacy is defined as the percentage of overranging dose in terms of the dose-length product (DLP) that is blocked by the dynamic collimator relative to the total overranging dose in case of a static open collimator. The efficacy is derived from information available in the DICOM RDSR.

The overranging scan length $L_{o,\,scan}$ is defined as the length of the actual scan range outside the range of the reconstructable volume [14]:

$$L_{o,scan} = L_{scan} - L_r$$

Where L_{scan} is the reported scan range and L_r is the length of the reconstructable volume [15], i.e. the distance between the first and last reconstructed slice position plus the nominal value of the largest possible slice thickness. The nominal slice thickness is used instead of a value based on measurements of the slice sensitivity profile (SSP) because unambiguous measurements are complicated in the context of this study. The SSP might depend on the position in the axial plane and on the position of the axial slice in the imaged volume. The latter possible dependency was investigated by noise measurements (see "Image reconstruction and noise measurements").
The number of additional scan rotations $N_{o,\,scan}$ due to overranging is calculated by

$$N_{o,scan} = \frac{L_{o,scan}}{M \cdot S \cdot p}$$

Where M is the single detector row width, S is the number of detector rows and p is the pitch. Thanks to the dynamic collimator, the additional dose due to overranging is smaller than one would expect from the additional scan length. The effective overranging length $L_{o,dose}$ associated with the increase of the DLP due to overranging is derived from the reported DLP and $CTDI_{vol}$ values for a given reconstructable volume length L_r:

$$L_{o,dose} = \frac{DLP}{CTDI_{vol}} - L_r$$

Finally, the efficacy E of the dynamic collimator is calculated as follows:

$$E = \frac{L_{o,scan} - L_{o,dose}}{L_{o,scan}} \cdot 100\%.$$

The uncertainties in the calculated values for $N_{o,\ scan}$, $L_{o,dose}$ and E depend on both the accuracy and precision of the underlying variables $CTDI_{vol}$, DLP, L_{scan} and L_r. Repeated scans proved that these variables are very precisely reported in the DICOM RDSR. The precision is limited only by the number of significant figures of the data representation in the RDSR. The imprecision in E is therefore estimated by propagation of the imprecisions in the underlying variables $CTDI_{vol}$, DLP, L_{scan} and L_r. The inaccuracy of the underlying variables and its influence on the uncertainties in the calculated values were negligible as determined below.

The length L_r of the reconstructable volume was assumed highly accurate. The accuracy of the reported scan range L_{scan} was checked by comparing the corresponding scan time with scan time measurements made with an ionization chamber. Preliminary experiments confirmed that the reported scan times are equal to the total time the x-ray tube is on and thus that the reported scan range is equal to the actual scan range.

It is known that the reported $CTDI_{vol}$ value might deviate as much as 30% from the true dose value. The scanner software calculates the DLP value via multiplication of the reported $CTDI_{vol}$ value by the effective scan length. It is safe to assume that the error in the $CTDI_{vol}$ value is independent of the error in the effective scan length. Therefore, the errors in the $CTDI_{vol}$ value and DLP value correlate, and the error in the $CTDI_{vol}$ cancels out in the calculation of $L_{o,\ dose}$ because the $CTDI_{vol}$ value and DLP value appear in the denominator and numerator of the same fraction, respectively. Consequently, any deviation of the reported $CTDI_{vol}$ value from the true dose value does not affect the calculation of the efficacy E.

An inaccurate estimation of the effective scan length by the scanner software results in an inaccurately reported DLP value. Therefore, the accuracy of this effective scan length was checked by comparison of reported DLP values with measured DLP values for various pitch values and scan lengths. Preliminary experiments showed a coefficient of determination $R2$ of 1.00. Therefore, it was assumed that the reported DLP values accurately reflect any change in effective scan length and no additional DLP measurements were performed.

Image reconstruction and noise measurements

All axial images were reconstructed with a slice thickness of 0.6 mm, 3.0 mm and 10 mm (minimum, mid and maximum slice width reconstruction) using a standard kernel (second-generation scanner: B30, third-generation scanner, Br40). In addition, images with an iterative reconstruction algorithm were reconstructed, with a level 3 iterative strength. Sinogram Affirmed Iterative Reconstruction (SAFIRE, Siemens Healthcare,

Forchheim, Germany) was used in the second-generation scanner. Adaptive Model-based Iterative Reconstruction (ADMIRE, Siemens Healthcare, Forchheim, Germany) was used in the third-generation scanner [16-18]. The iterative reconstructions were made to verify whether iterative reconstruction methods influenced the image noise assessment. All images were reconstructed at the maximum field of view available for all pitch values, i.e. 332 mm for the second-generation scanner and 354 mm for the third-generation scanner.

Noise measurements were performed for each reconstructed image throughout the phantom. Measurements of the standard deviation of the CT numbers in a homogeneous region of interest were performed with mathematical computing software (MATLAB R2008a, The MathWorks Inc., Natick, Massachusetts, U.S.A.). It was assumed that a constant image noise level as a function of the longitudinal position of the image corresponds to a constant slice thickness equal to the nominal thickness throughout the reconstructed volume.

RESULTS

Collimator efficacy

Figure 1 shows the number $N_{o,scan}$ as a function of pitch for both generations of DSCT scanner. This number is slightly higher than 1 for pitches less than 1.55. For pitches of 1.55 or more, this number drops to approximately 0.4. No large differences between the second- and third-generation DSCT scanner were observed, with the exception of the considerably lower number of extra rotations at pitch 1.55 for the third-generation scanner.

Figure 2 shows the effective overranging length $L_{o,dose}$ as a function of pitch for both generations of DSCT scanner. The length is comparable for the second- and third-generation DSCT scanner for pitches less than 1.55 (differences less than 0.8 cm). In these cases, the overranging length is virtually absent at pitch 0.35 and increases with increasing pitch. For pitches of 1.55 or more, the length is 2 – 4 cm lower for the third-generation DSCT scanner than for the second-generation DSCT scanner.

Figure 3 shows the efficacy E as a function of pitch for both generations of DSCT scanner. For the second-generation scanner, efficacy is high at low pitch and rapidly decreases to approximately 10% at the maximum pitch. For the third-generation scanner, efficacy is high at low pitch as well and remains above 50% for higher pitch values.

The results in Figure 1-3 are for a scan length of 300 mm. For scan lengths of 100 mm and 200 mm, the efficacy values did not change more than 1 percentage point compared to the corresponding values at a length of 300 mm, except for the third-generation scan-

ner at pitches of at least 1.55 and a scan length of 100 mm. In these cases the efficacy was 46% - 65% instead of 61% - 76%.

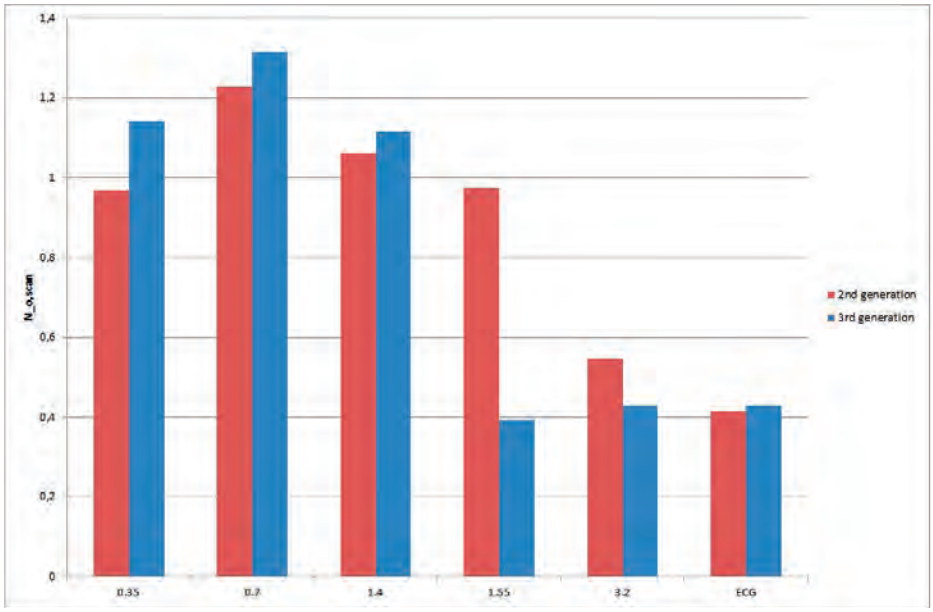

Figure 1. Number $N_{o,scan}$ of additional rotations as a function of pitch for both generations DSCT scanners. Values labeled with "ECG" correspond with a pitch of 3.4 and 3.2 for the second- and third-generation scanner, respectively. A substantial difference between scanner generations is present at pitch 1.55 only.

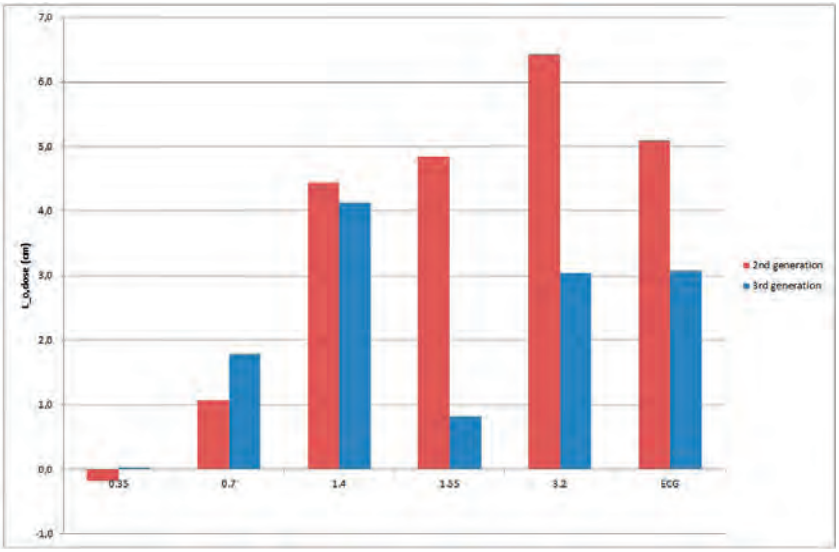

Figure 2. Effective overranging length $L_{o,dose}$ as a function of pitch for both generations DSCT scanners. Values labeled with "ECG" correspond with a pitch of 3.4 and 3.2 for the second- and third-generation scanner, respectively. $L_{o,dose}$ is up to 4 cm shorter for the third-generation DSCT scanner than for the second-generation DSCT scanner.

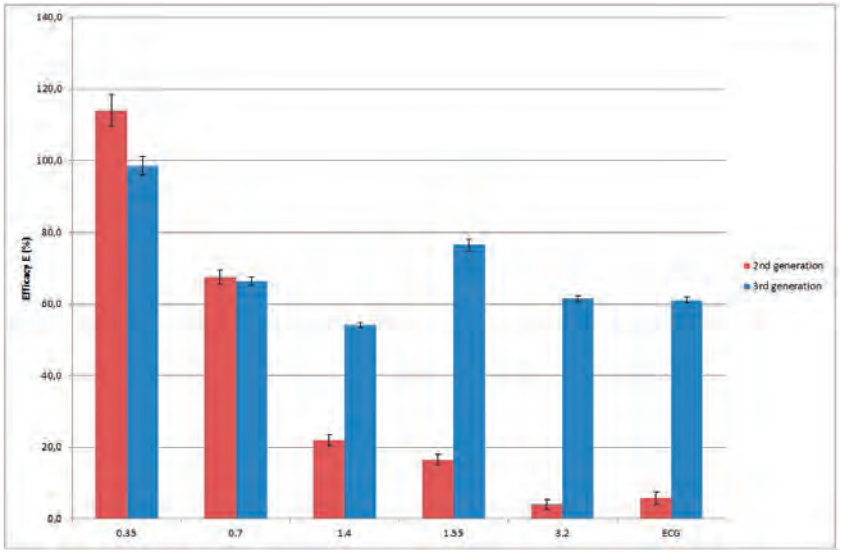

Figure 3. Efficacy E as a function of pitch for both generations DSCT scanners. Values labeled with "ECG" correspond with a pitch of 3.4 and 3.2 for the second- and third-generation scanner, respectively. For the second-generation scanner, efficacy can be as low as 10%. For the third-generation scanner, efficacy lies above 50% for all pitch values. The error bars illustrate the uncertainty in E as estimated by propagation of the uncertainties in the underlying variables.

Image noise measurements

In general, measured image noise varied less than 1 HU as a function of the z-position of the reconstructed slice. In Figure 4 a typical example of constant image noise is shown for the second-generation scanner at pitch 1.55 (dashed red line), scan length of 300 mm and a reconstructed slice thickness of 10 mm. There were three exceptions to this flat noise profile: a slight noise increase was present at the edge of the imaged volume for the third-generation scanner at pitch 1.55 (solid blue line in Fig. 4). Such an increase was present at pitch 0.35 for both scanners as well (not shown).

The noise increase at the edge of the imaged volume is assumed to be the result of the smaller amount of data and thus dose used for image reconstruction of the corresponding slices, compared to the amount of data used for reconstruction of the more centrally located slices in the volume. Consequently, the effective slice thickness at the edges of the imaged volume might be smaller than the nominal thickness of 10 mm.

In cases in which iterative reconstruction techniques were used, the image noise level decreased, as expected. The reconstruction technique and the reconstructed slice thickness did not affect the shape of the image noise profiles as a function of slice position.

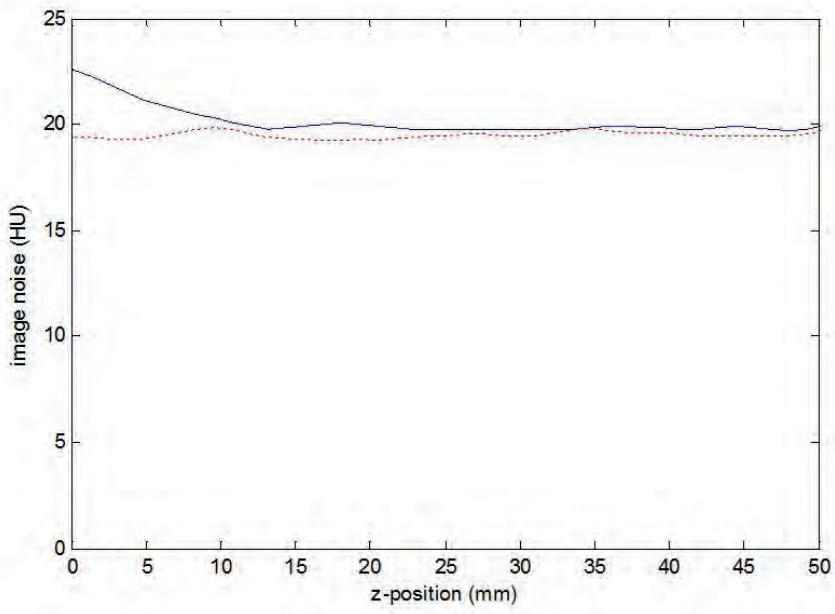

Figure 4. Standard deviation of image noise as a function of z-position for the second-generation scanner (dashed red line) and third-generation scanner (solid blue line). Position z=0 mm corresponds with the first position that can be reconstructed. Scan and reconstruction parameters: pitch 1.55; kernel B30f (second-generation) and Br40 (third-generation); slice thickness 10 mm.

DISCUSSION

The improved performance of the third-generation DSCT scanner over the second-generation DSCT scanner with respect to the reduction of overranging dose in spiral CT for the full range of pitch values was investigated and quantified.

At least two overranging dose reduction strategies exist. One can reduce the number of rotations required for image reconstruction of the very first and last slice of the imaged volume or one can block the radiation that is not used for image reconstruction with the aid of a dynamic collimator. Both strategies are applied in the DSCT scanners investigated.

For a given pitch value, the number of overranging rotations was approximately equal for the second- and third-generation scanner (see Fig. 1), except at pitch 1.55 where the third-generation scanner used approximately half the number of overranging rotations compared to the second-generation scanner. Consequently, the overranging dose showed the largest relative change at this pitch value (see Fig. 2). In general, however, overranging dose was reduced by improved performance of the dynamic collimator. Note that a relatively low efficacy can be due to the particular reconstruction algorithm used and not technical limitations of the dynamic collimator. Overranging might therefore be even further reduced by dedicated reconstruction techniques that are able to reconstruct images beyond the boundaries of the currently imaged volume [19]. Connected to this issue, it would be impossible to gain an efficacy of 100% for high pitch scan mode because of incomplete sampling and arising artifacts, which would deteriorate image quality.

As a results of the inclusion of the nominal slice width (10 mm) in the definition of the length of the reconstructable volume and thus in the definition of the effective overranging length and efficacy, some paradoxical results were present at pitch 0.35: the effective overranging length had a negative value and the efficacy was higher than 100% for the second-generation scanner. Given the exceptional noise behaviour at pitch 0.35, an explanation can be found in the fact that the effective slice thickness of the first and last slice most likely was smaller than the nominal value. This leads to an overestimation of the length L_r and an underestimation of the overranging dose. Similarly, the efficacy for the third-generation scanner at pitch 0.35 and at pitch 0.7 might be lower than reported because of the possibly reduced effective slice thickness and overestimated volume length L_r.

For high pitch values and a short scan length of 100 mm, the efficacy was less than at long scan lengths of 200 mm and 300 mm. This can be explained by the additional slot plate with a fixed opening taking over in dynamic collimation in dual source mode. The slot plate is designed to fully perform the opening phase, even if the trigger for the closing phase is received during the opening phase. For short scans, the time needed

for fully opening and fully closing may be longer than the total scan time. Hence, at the end of a short scan, the collimator may not be fully closed. However, these conditions are very rarely met clinically.

Even with a perfectly working dynamic collimator, the dose penalty will increase with increasing pitch. This is because the scanner keeps the effective mAs constant when increasing the pitch by increasing the tube current [11]. Consequently, the overranging dose will increase although the number of additional rotations does not change. This effect can nicely be seen in Figure 1 where the number of additional rotations does not change when changing the pitch from 1.55 to 3.2 in a third-generation scanner while in Figure 2 the effective overranging length does increase in this case.

Nevertheless, this study showed an improved performance of the dynamic collimator in the third-generation DSCT scanner at high pitch mode. This is clinically relevant information to determine optimal scan protocols. When high scan speeds are preferred as a result of non-cooperative patients (e.g. newborns), it is useful to know that with the dual-source, high pitch, scan modes the dose penalty can be less than the penalty in single-source, low pitch, mode thanks to the combination of an effectively working dynamic collimator at high scan speeds and the smaller number of additional rotations made in dual source mode.

CONCLUSION

Thanks to dynamic collimation, approximately 50% or more of the overranging dose is blocked in the latest generation DSCT scanner. In comparison to the second-generation scanner, the improved dynamic collimator is better capable of shielding the overranging dose, especially in the high pitch, high-speed scan modes.

ACKNOWLEDGEMENTS

We would like to thank Martin Petersilka and Christianne Leidecker (Siemens Healthineers, Forchheim, Germany) for providing useful information on the technical details of the dynamic collimator and reconstruction algorithms.

REFERENCES

1. Irwan R, de Vries HB, Sijens PE. The impact of scan length on the exposure levels in 16- and 64-row multidetector computed tomography: a phantom study. Academic radiology. 2008;15(9):1142-7.
2. Schilham A, van der Molen AJ, Prokop M, de Jong HW. Overranging at multisection CT: an underestimated source of excess radiation exposure. Radiographics : a review publication of the Radiological Society of North America, Inc. 2010;30(4):1057-67.
3. Theocharopoulos N, Damilakis J, Perisinakis K, Gourtsoyiannis N. Energy imparted-based estimates of the effect of z overscanning on adult and pediatric patient effective doses from multislice computed tomography. Med Phys. 2007;34(4):1139-52.
4. Kroft LJ, Roelofs JJ, Geleijns J. Scan time and patient dose for thoracic imaging in neonates and small children using axial volumetric 320-detector row CT compared to helical 64-, 32-, and 16-detector row CT acquisitions. Pediatr Radiol. 2010;40(3):294-300.
5. Tzedakis A, Damilakis J, Perisinakis K, Stratakis J, Gourtsoyiannis N. The effect of z overscanning on patient effective dose from multidetector helical computed tomography examinations. Medical Physics. 2005;32(6):1621.
6. Trevisan D, Bonutti F, Ravanelli D, Valentini A. Real time evaluation of overranging in helical computed tomography. Phys Med. 2014;30(8):968-72.
7. van der Molen AJ, Geleijns J. Overranging in multisection CT: quantification and relative contribution to dose--comparison of four 16-section CT scanners. Radiology. 2007;242(1):208-16.
8. Tzedakis A, Damilakis J, Perisinakis K, Karantanas A, Karabekios S, Gourtsoyiannis N. Influence of z overscanning on normalized effective doses calculated for pediatric patients undergoing multidetector CT examinations. Med Phys. 2007;34(4):1163-75.
9. Tzedakis A, Perisinakis K, Raissaki M, Damilakis J. The effect of z overscanning on radiation burden of pediatric patients undergoing head CT with multidetector scanners: a Monte Carlo study. Med Phys. 2006;33(7):2472-8.
10. Tsalafoutas IA. The impact of overscan on patient dose with first generation multislice CT scanners. Physica medica : PM : an international journal devoted to the applications of physics to medicine and biology : official journal of the Italian Association of Biomedical Physics. 2011;27(2):69-74.
11. Christner JA, Zavaletta VA, Eusemann CD, Walz-Flannigan AI, McCollough CH. Dose reduction in helical CT: dynamically adjustable z-axis X-ray beam collimation. AJR Am J Roentgenol. 2010;194(1):W49-55.
12. Deak PD, Langner O, Lell M, Kalender WA. Effects of adaptive section collimation on patient radiation dose in multisection spiral CT. Radiology. 2009;252(1):140-7.
13. Shirasaka T, Funama Y, Hayashi M, Awamoto S, Kondo M, Nakamura Y, et al. Reduction of the unnecessary dose from the over-range area with a spiral dynamic z-collimator: comparison of beam pitch and detector coverage with 128-detector row CT. Radiol Phys Technol. 2012;5(1):53-8.
14. National Electrical Manufacturers Association. Digital Imaging and Communications in Medicine (DICOM) Part 16: Content Mapping Resource [Internet]. Rosslyn, Virginia 22209 USA. 2011.
15. Commision iE. European standard IEC 60601-2-44 Amendment1. 2012.
16. Gordic S, Morsbach F, Schmidt B, Allmendinger T, Flohr T, Husarik D, et al. Ultralow-dose chest computed tomography for pulmonary nodule detection: first performance evaluation of single energy scanning with spectral shaping. Investigative radiology. 2014;49(7):465-73.
17. Wang R, Schoepf UJ, Wu R, Reddy RP, Zhang C, Yu W, et al. Image quality and radiation dose of low dose coronary CT angiography in obese patients: Sinogram affirmed iterative reconstruction versus filtered back projection. Eur J Radiol. 2012;81(11):3141-5.

18. Winklehner A, Karlo C, Puippe G, Schmidt B, Flohr T, Goetti R, et al. Raw data-based iterative reconstruction in body CTA: Evaluation of radiation dose saving potential. Eur Radiol. 2011;21(12):2521-6.
19. Tang X, Hsieh J, Dong F, Fan J, Toth TL. Minimization of over-ranging in helical volumetric CT via hybrid cone beam image reconstruction--benefits in dose efficiency. Med Phys. 2008;35(7):3232-8.

PART IV

General discussion and summary

CHAPTER 9

General discussion

In general, technological developments have always driven users to investigate their added value and to implement them in order to optimize processes. The process of CT imaging is no exception. Currently, most of the steps within the chain of CT imaging are still driven by humans, rather than by smart technologies. At the same time, technologies for automation, optimization and standardization within the whole imaging chain are being developed by vendors and introduced into clinical practice. These technological advancements may help to exploit all options available within a CT scanner and to optimize the CT procedure. Merging of knowledge obtained by man and machine may assist in making a CT scan procedure more accurate, standardized and automated; in other words: making the CT scanner more "knowledgeable".

In this thesis, the performance, advantages and weaknesses of several technological advancements in the "data acquisition" and the "data (post-)processing" parts of the imaging chain were investigated (Fig. 1). As there is a wide variety in patient characteristics, the "knowledgeable" CT scanner may overcome the challenge to optimize a CT scanning procedure for every individual patient. Additionally, it may assist in optimizing the exam for different referral questions, as this may demand different imaging strategies.

It must be noted that the developments demonstrated and investigated in this thesis were restricted to one CT vendor. Vendors often restrict the disclosure of proprietary information on the working and validation of algorithms, for example in automatic exposure control (AEC). Vendors developed AEC strategies with different relationships between image noise, radiation dose and patient size. The same restrictions apply to several aspects within the parts of the imaging chain discussed in this thesis, as some specifications are unknown to the users. Therefore, knowledge on technological developments is often also vendor specific.

In this chapter, first the subject of patient positioning with a 3D camera is discussed; including the importance of proper positioning, the possible influence of off-center positioning on image quality (IQ) and radiation dose, and other potential applications of this camera. Next, the performance and possibilities of several technological developments in data acquisition and image reconstruction are discussed; including insights of dynamic collimator efficacy, contrast injection and scan parameters tailoring in pediatric patients and a new reconstruction method in Agatston scoring. Finally, future perspectives for a "knowledgeable" CT scanner are given.

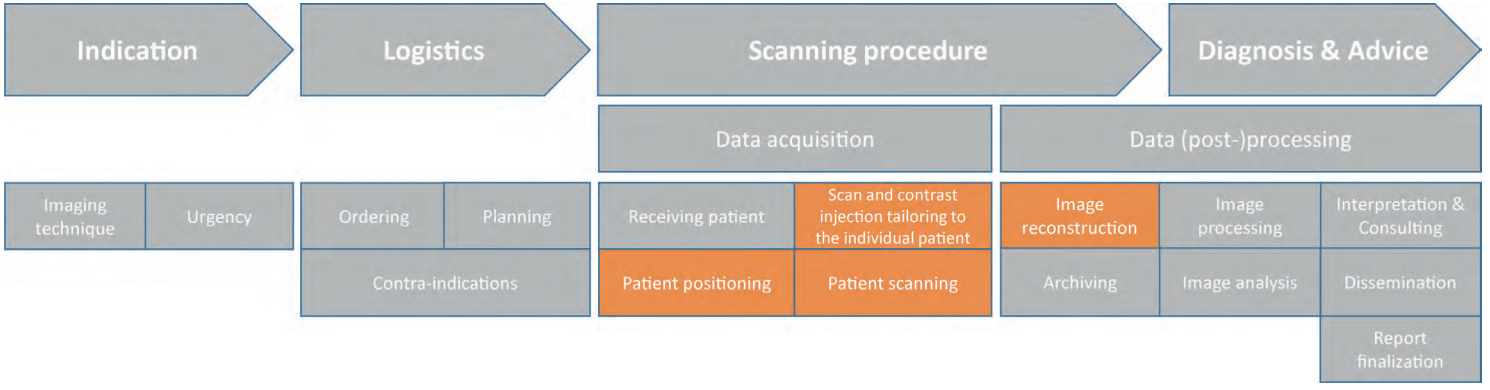

Figure 1. Graphical illustration of the steps in the diagnostic imaging chain for a CT exam. This thesis highlighted the use of technological developments within the "data acquisition" and "data (post-)processing": "patient positioning", "scan and contrast injection tailoring to the individual patient", "patient scanning" and "image reconstruction" (in orange).

PATIENT POSITIONING IN CT

Proper patient positioning

In this thesis, proper patient positioning for a CT examination is defined as using the (ideal) table height at which the average isocenter of all slices of the body region to be scanned, coincides with the scanner isocenter. Proper positioning is essential for an optimal working of AEC and bowtie filters. Unfortunately, improper patient positioning is a common problem in clinical routine and is user-dependent [1-3]. Several studies assessed off-center positioning (manual positioning only) and found a mean off-center positioning of 1 cm [4] – 2.5 cm [5]. A study with 20.316 patients reported off-centering with more than 2 cm in almost 20% of the cases [6]. Extremes with more than 4 cm off-center positioning were observed in all studies as well.

Software for proper patient positioning was proposed earlier [5], but was not widely adopted by users of CT scanners since the positioning software was not integrated into the CT scanner. We demonstrated that a 3D camera, fully integrated into the scanner system workflow, allows for accurate patient positioning and even outperformed radiographers (**Chapter 3**). Therefore, a 3D camera may be a good step to be included in the process of making a CT scanner more "knowledgeable". Even though the mean deviations of the ideal table height for different body parts within the 3D camera studies were not large at our institute, we still reported deviations larger than 2 cm from the scanner isocenter like others did as well [1, 2, 4-7].

Significant improvements in patient positioning accuracy were also demonstrated by another group applying a similar 3D camera as the one described within this thesis [7]. They described patient off-centering of approximately 1.9 (± 1.0) cm for both CT scans of the chest and abdomen when positioning manually, which was comparable to the results found in our study with 1.3 (± 1.7) cm. Automatic patient positioning reduced the average off-center positioning to less than 1 cm. This is in agreement with the results found in our study as well.

Until now, very little is known about the influence of the breathing state on proper patient positioning. We demonstrated differences of the ideal table height for CT scans of the thorax between inspiration and expiration of on average 1.1 cm, but differences of up to 2.4 cm were observed too. Additionally, we analyzed the influence of different breathing states on the accuracy of automated (adult) patient positioning in thoracic CT with a 3D camera. When both an inspiratory and expiratory CT scan are made, we recommend the use of an expiratory planning image for the most accurate result. The 3D camera planning images in **Chapter 3** were obtained while the patient was free breathing, which is similar to the current clinical routine workflow. So theoretically, more accurate positioning can be achieved when an expiratory planning image is obtained. It must be noted, however, that the mean difference was very small (0.2 cm) between the results

obtained in **Chapter 3 and 5.** Therefore, for the sake of simplicity, the free-breathing workflow seems more appropriate in clinical practice. Further research on accuracy of patient positioning in abdominal CT is not recommended, as it is not likely that the difference in anterior-posterior abdomen size would be larger than for chest sizes.

Accurate positioning of pediatric patients can be even more challenging than positioning adults. As the median absolute table height deviation for all body parts combined was approximately 1 cm (radiographers) and 0.4 cm (3D camera), we found deviations up to 8 cm from the scanner isocenter as well when positioning manually. Median values for off-centering of 2.5 to 3.5 cm below the scanner isocenter and deviations up to 5 cm were reported by another study [8]. We demonstrated that extremes in deviation from the isocenter were smaller for pediatric patients positioned with a 3D camera than for positioning by radiographers (**Chapter 3**). Therefore, automated patient positioning is recommended. The knowledge obtained from these studies (**Chapter 3-5**) may help in the further development and improvement of the 3D camera system.

Off-center positioning: Image quality and radiation dose

We did not evaluate the effect of improper patient positioning on radiation dose and image quality. We know from previous studies that off-centering patients in a CT scanner may influence IQ and radiation dose. Monte Carlo simulations in a phantom study already showed relative organ dose differences above 7% when a patient was more than 2 cm off-center [9]. Off-centering more than 4 cm resulted in organ dose differences around 20%. A change in CT number, expressed in Hounsfield units (HU), is expected in patients and may be more pronounced in obese patients, especially with improper positioning; possibly affecting the diagnostic accuracy. Interestingly, an absolute CT number change for the anterior versus the posterior part of an anthropomorphic thorax-abdomen phantom was observed in a study when off-centering with 10 cm and applying AEC [6]. Another study demonstrated that more than 4 cm off-center positioning may result in up to 15 HU decrease for the mid thorax [6]. Additionally, a 20 HU change when off-centering 6 cm was reported. A wide variation and inconsistency in off-centering may influence diagnostic confidence due to less effective working of AEC and bowtie filters. Nevertheless, it is hard to draw conclusions based on reported average off-centering values only, as the impact of reduced IQ depends on the referral question(s), the body part examined and the general acceptance by radiologists.

Most protocols have a certain bandwidth of acceptable noise levels, since there is a certain level of image noise variation when imaging different body types, like slim and obese patients [10-12]. Consequently, this allows for small deviations from the ideal table height as well. A recent article by Ria et al. addressed a certain bandwidth in noise change [13]. They demonstrated a noise variation of approximately 5 HU for patients with the same size. The variation was observed for different scan protocols, scanner

systems and for different patient diameters. Additionally, they demonstrated different trends in terms of noise magnitude across patient diameter when applying different implementations of AEC.

The current table height position suggested by the 3D camera is such that the patient and scanner isocenter coincide, aiming for an optimal working of the AEC. During the study presented in **Chapter 3**, a cardiac subset (n=63) was also assessed for the table height for optimal temporal resolution, i.e. when the heart isocenter coincides with the scanner isocenter. The results were included in the Appendix of **Chapter 3**. We found that the ideal cardiac table height was a median of 37.8 (interquartile range: 8.2) mm lower than the height for optimal AEC performance. Therefore, cardiac CT may benefit from more "knowledgeable" scanners with the aid of the body contour detection system and taking the isocenter of the organ of interest into account. After all, for optimal temporal resolution, the heart isocenter should coincide with the scanner isocenter.

As the 3D camera positions patients better than radiographers, more consistent image quality and diagnostic accuracy is expected. Altogether, the large deviations found when positioning patients manually and the overall preferred consistency of diagnostic confidence in the population, argue for the use of a 3D camera.

Potential of a 3D camera in CT

In a medical world with continuously emerging technologies, it can be difficult to keep up with the latest developments. Added to this is an increase in workload and a demand for high quality images and reports. As the recent outbreak of the coronavirus disease COVID-19 (SARS-CoV-2) [14] also demonstrated, there is a need for automation and, like in this pandemic, minimal contact with patients during the scanning procedure for protection of the radiographers. A study demonstrated that artificial intelligence (AI) empowered image acquisition, with a 3D camera identical to the one discussed in this thesis, can significantly help to automate the scanning procedure and reshape the workflow, minimizing physical contact to patients [15]. This may also lighten the workload for radiographers.

As nowadays the individual profile of the patient geometry derived from a 3D camera is primarily used for accurate patient positioning, patient height and weight are important clinical parameters that could be derived from the camera images as well. Tailoring contrast injection protocols to an individual patient can be difficult in clinical routine, especially when contrast media administration has to be manually adapted to a wide variety of patient characteristics [16, 17]. In addition, injection protocols have to be adapted to CT scanner type and type of exam. This might be challenging. A logical next step in deploying a 3D camera would be the determination of a patient and CT study specific contrast injection protocol.

PATIENT SCANNING IN CT

One of the major developments in CT was the introduction of spiral CT that enabled faster scan times. Especially developments like multi-detector, dual source CT (DSCT) and the dynamic collimator opened up possibilities in challenging pediatric imaging cases, as described in C**hapter 6 and 8**. The dual source mode is preferred in imaging of (very young) children because of the improved temporal resolution and the ability to scan with a high pitch (3.0) to reduce scan time and decrease motion artifacts. However, with increasing pitch, the overranging dose increases too. Previous studies described the impact of the overranging dose, but only assessed it in single source CT scanners. Consequently, the used pitch values were lower than in our study (**Chapter 8**) [18, 19]. Nevertheless, the results of these studies corresponded well with the results of the 2nd generation DSCT described in our study: the efficacy is higher with low pitch values. In addition, less overranging dose is blocked when applying a high pitch: only 10% efficacy remains at a pitch of 3.2. Fortunately, a reduced radiation dose was observed thanks to improved dynamic collimator efficacy (**Chapter 8**). Even at high pitch mode, the dynamic collimator of the 3rd generation DSCT blocked approximately 60% of the overranging dose. Nevertheless, we demonstrated that still a higher efficacy was achieved in dual source mode (76%) when lowering the pitch to 1.55. As most of the dose reduction tools available have to be selected and set by the users and saved in scan protocol settings, some are available or applied automatically in the background, like the dynamic collimator. Given the above facts and with this new insight of the dynamic collimator efficacy, a knowledge base could support the user in using the most appropriate protocol: One with the fastest scan option for non-cooperative patients by using the fastest rotation time, widest longitudinal collimation, and the highest pitch. Secondly a protocol with a lower pitch and the highest dynamic collimator efficacy when motion is not of concern.

By applying several technological improvements, a DSCT is able to acquire motion free images of pediatric patients (**Chapter 6**). A DSCT high pitch mode allows for low radiation dose without impairing IQ for diagnosis in congenital heart disease [20]. However, ECG-triggered high pitch scanning may lead to unsatisfactory IQ in coronary arteries due to a relatively short time window available with high heart rate to cover the entire heart motion free within one R-R interval [20]. The use of an ECG-triggered prospective mode may be a robust alternative. A prospective ECG-triggered scan protocol with an absolute scan time in milliseconds (ms), instead of the relative scan method in percentage (%), prevents an increase in radiation dose (**Chapter 6**) and the technique was previously described as suitable for coronary artery imaging [21]. Despite our results being based on clinical practice only, rather than a controlled clinical study, the scan method described within this thesis seems from a technical perspective more robust compared to their approach, as we provided scan windows for six heart

rate groups (**Chapter 6**). Either way, the prospective scan mode has no overranging, as this is a static image acquisition technique. The wider acquisition window as discussed in **Chapter 6** seems from a technical perspective more appropriate in achieving an optimal visualization of the coronary arteries. Hereby, contrast injection tailoring to the individual patient is challenging, especially with congenital anomalies in pediatric patients. A study described the same injection flow rates as we suggested in **Chapter 6** [22]. Additionally, they provided information about the injection site having a slight impact on IQ and radiation dose. The latter was in accordance with our results were we highlighted an increase in radiation dose due to a longer bolus tracking time when a long route from injection site to the heart was used.

As highlighted in this chapter, technological developments may come with challenges to implement them properly in clinical practice. Thereby, not all the possibilities of a CT scanner are always known to all users. In order to use the full potential of a CT scanner, optimization is achieved by human interaction and by incorporating and implementing newly provided technological developments. By doing so, a "knowledgeable" CT scanner may be of support in optimization of a CT exam.

IMAGE RECONSTRUCTION IN CT

Changing an acquisition or reconstruction technique (**Chapter 7**) requires understanding of its influence on IQ, radiation dose and, in case of quantified data like the Agatston score method, the impact on the prognostic value. Quantification of coronary artery calcifications (CAC) to predict cardiovascular risk is often performed by using the Agatston score method [23]. The Agatston score is validated on CT scans acquired with 120 kV, 3mm thick slices reconstructed with filtered backprojection and 130 HU as the threshold for calcifications. Several strategies in data acquisition and image reconstruction to reduce the radiation dose, while preserving the Agatston score and its risk assessment potential, have been introduced over the years [24-28]. However, adaptations made in the CAC scoring protocol often have an influence on detectability of small coronary calcifications. This has been demonstrated before in e.g. applying a different patient scanning technique, like spectral shaping by a tin filter [26]. Improvements by adapting the HU threshold for increased CT numbers of calcium when varying tube voltage have been demonstrated as well [24]. In this thesis, it was shown that a new reconstruction method, fully integrated within the standard image reconstruction interface, in combination with automatic selection of tube voltage allowed for a dose reduction. However, less consistency was observed with small, low-density calcifications. Other studies described possible affected quantification of CAC as well when applying a new reconstruction technique, like iterative reconstruction [29, 30]. With this knowledge,

it remains important to validate technological developments, as improvement is not guaranteed without additional adaptations.

FUTURE PERSPECTIVES FOR A "KNOWLEDGEABLE" CT SCANNER

In this thesis, it was shown that first steps have been taken to make a CT scanner more "knowledgeable". With new technologies on the horizon, the number of adjustable acquisition and reconstruction parameters continues to increase and many of these parameters are interrelated. This makes optimization even more difficult. Nevertheless, every step forward is one-step closer to the optimal scan protocol and personalized CT scan.

Incorporation of "smart" technologies or AI is not limited to performing a CT scan. For instance, relevant (patient) information provided by referring physicians for CT examinations, the patient scheduling, or information to prepare patients for a CT exam could possibly be integrated in the patient management system. Especially in the area of medical image analysis, there is a profound role for these "smart" technologies, supporting the use of "big data" to achieve personalized medicine. An example of upcoming challenges in optimization a CT exam is photon counting CT (PCCT). PCCT is likely able to extract quantitative imaging biomarkers from biological tissues and improve visualization of anatomy and pathology. This requires a large storage capacity to reconstruct and analyse the (raw) data. Consequently, this may require additional algorithms in processing the high amount of data and the deployment of PCCT and other new technologies in clinical practice.

AI driven workflow may support the optimization process of a CT exam by assisting the users with automation, efficiency and accuracy. Additionally, it may contribute to the development of a "knowledgeable" CT scanner. Therefore, applications of AI need to have a prominent role within the data acquisition, data (post-)processing, material decomposition and the image analysis domain. Prominent does not mean dominant. AI causes changes and changes are often received with fear. In general, AI is still seen as a "new frontier" and futuristic, but scenarios with computers taking over like "HAL9000" in "2001: A Space Odyssey" [31] or "The Matrix" [32] are, most likely, unfounded. Nevertheless, it is without a doubt that AI will change our life and work, most likely with great benefits, but also pitfalls. However, it cannot and should not replace properly educated operators. The user's knowledge remains essential in successful optimization of a scanning protocol. In addition, humans can easily adapt to (exceptional) situations that deviate from common cases or circumstances, where AI may perform less in such a situation. For example, in patients with physical constraints or (non-cooperative) pediatric patients. Users should therefore not rely completely on the technologies, nor

should they mistrust their capabilities. As a professor in AI (Toby Walsh) already stated: "I think the things we should be fearful of are actually not the intelligent machines, but the stupidity of machines. And that we'll be giving responsibility to machines that don't have the appropriate intelligence." [33]. Knowledgeable solutions like AI should be embraced, as they can be an important factor in assisting medical healthcare workers. In addition, a high knowledge base among the users of intelligent machines is essential for the (future) development and correct application of AI. Human interference and interaction by data normalization and (neural network) training on clinical datasets will further optimize machine analysis and accuracy. Along these lines, accuracy, efficiency and most of all, optimization can be achieved. An example in radiology and nuclear medicine is machine learning for automatic analysis, image-based diagnosis, disease prognosis, and tissue segmentation. Perhaps the biggest strength and profit lies in the opportunity of man-computer symbiosis, in which man and machine interact [34]. The man-machine symbiosis was first described by Licklider [35]. He argued for cooperation between a human user and a machine in fast decision making and controlling complex situations. Most likely, we are on the eve of such symbiosis as AI is integrated more and more in the daily practice of medical imaging [36]. The merge of knowledge obtained by man and machine will create ample opportunities for a "knowledgeable" CT scanner.

REFERENCES

1. Habibzadeh MA, Ay MR, Asl ARK, Ghadiri H, Zaidi H. Impact of miscentering on patient dose and image noise in x-ray CT imaging: Phantom and clinical studies. Phys Med. 2012;28(3):191-9.
2. Akin-Akintayo OO, Alexander LF, Neill R, Krupinksi EA, Tang X, Mittal PK, et al. Prevalence and Severity of Off-Centering During Diagnostic CT: Observations From 57,621 CT scans of the Chest, Abdomen, and/or Pelvis. Curr Probl Diagn Radiol. 2019;48(3):229-34.
3. Barreto I, Lamoureux R, Olguin C, Quails N, Correa N, Rill L, et al. Impact of patient centering in CT on organ dose and the effect of using a positioning compensation system: Evidence from OSLD measurements in postmortem subjects. J Appl Clin Med Phys. 2019;20(6):141-51.
4. Eberhard M, Bluthgen C, Barth BK, Frauenfelder T, Saltybaeva N, Martini K. Vertical Off-Centering in Reduced Dose Chest-CT: Impact on Effective Dose and Image Noise Values. Acad Radiol. 2019.
5. Li J, Udayasankar UK, Toth TL, Seamans J, Small WC, Kalra MK. Automatic patient centering for MDCT: effect on radiation dose. AJR Am J Roentgenol. 2007;188(2):547-52.
6. Szczykutowicz TP, DuPlissis A, Pickhardt PJ. Variation in CT number and image noise uniformity according to patient positioning in MDCT. Am J Roentgenol. 2017;208(5):1064-72.
7. Saltybaeva N, Schmidt B, Wimmer A, Flohr T, Alkadhi H. Precise and Automatic Patient Positioning in Computed Tomography: Avatar Modeling of the Patient Surface Using a 3-Dimensional Camera. Invest Radiol. 2018;53(11):641-6.
8. Kaasalainen T, Palmu K, Reijonen V, Kortesniemi M. Effect of patient centering on patient dose and image noise in chest CT. Am J Roentgenol. 2014;203(1):123-30.
9. Saltybaeva N, Alkadhi H. Vertical off-centering affects organ dose in chest CT: Evidence from Monte Carlo simulations in anthropomorphic phantoms. Med Phys. 2017;44(11):5697-704.
10. MacDougall RD, Kleinman PL, Callahan MJ. Size-based protocol optimization using automatic tube current modulation and automatic kV selection in computed tomography. J Appl Clin Med Phys. 2016;17(1):328-41.
11. Söderberg M, Gunnarsson M. The effect of different adaptation strengths on image quality and radiation dose using Siemens Care Dose 4D. Radiation Protection Dosimetry. 2010;139(1-3):173-9.
12. Söderberg M, La S. Evaluation of adaptation strengths of CARE Dose 4D in pediatric CT: SPIE; 2013.
13. Ria F, Solomon JB, Wilson JM, Samei E. Technical Note: Validation of TG 233 phantom methodology to characterize noise and dose in patient CT data. Med Phys. 2020;47(4):1633-9.
14. Zhu N, Zhang D, Wang W, Li X, Yang B, Song J, et al. A Novel Coronavirus from Patients with Pneumonia in China, 2019. New England Journal of Medicine. 2020;382(8):727-33.
15. Shi F, Wang J, Shi J, Wu Z, Wang Q, Tang Z, et al. Review of Artificial Intelligence Techniques in Imaging Data Acquisition, Segmentation and Diagnosis for COVID-19. IEEE Rev Biomed Eng. 2020.
16. Bae KT. Intravenous Contrast Medium Administration and Scan Timing at CT: Considerations and Approaches. 2010;256(1):32-61.
17. Perrin E, Jackson M, Grant R, Lloyd C, Chinaka F, Goh V. Weight-adapted iodinated contrast media administration in abdomino-pelvic CT: Can image quality be maintained? Radiography. 2018;24(1):22-7.
18. Schilham A, van der Molen AJ, Prokop M, de Jong HW. Overranging at multisection CT: an underestimated source of excess radiation exposure. Radiographics. 2010;30(4):1057-67.
19. Shirasaka T, Funama Y, Hayashi M, Awamoto S, Kondo M, Nakamura Y, et al. Reduction of the unnecessary dose from the over-range area with a spiral dynamic z-collimator: comparison of beam pitch and detector coverage with 128-detector row CT. Radiol Phys Technol. 2012;5(1):53-8.

20. Zheng M, Zhao H, Xu J, Wu Y, Li J. Image quality of ultra-low-dose dual-source CT angiography using high-pitch spiral acquisition and iterative reconstruction in young children with congenital heart disease. J Cardiovasc Comput Tomogr. 2013;7(6):376-82.
21. Paul JF, Rohnean A, Elfassy E, Sigal-Cinqualbre A. Radiation dose for thoracic and coronary step-and-shoot CT using a 128-slice dual-source machine in infants and small children with congenital heart disease. Pediatr Radiol. 2011;41(2):244-9.
22. Yang M, Mo XM, Jin JY, Zhang J, Liu B, Wu M, et al. Image quality and radiation exposure in pediatric cardiovascular CT angiography from different injection sites. Am J Roentgenol. 2011;196(2):W117-W22.
23. Agatston AS, Janowitz WR, Hildner FJ, Zusmer NR, Viamonte M, Jr., Detrano R. Quantification of coronary artery calcium using ultrafast computed tomography. J Am Coll Cardiol. 1990;15(4):827-32.
24. Groen JM, Dijkstra H, Greuter MJ, Oudkerk M. Threshold adjusted calcium scoring using CT is less susceptible to cardiac motion and more accurate. Med Phys. 2009;36(2):438-46.
25. Van Osch JAC, Mouden M, Van Dalen JA, Timmer JR, Reiffers S, Knollema S, et al. Influence of iterative image reconstruction on CT-based calcium score measurements. Int J Card Imaging. 2014;30(5):961-7.
26. Vonder M, Pelgrim GJ, Huijsse SE, Meyer M, Greuter MJ, Henzler T, et al. Feasibility of spectral shaping for detection and quantification of coronary calcifications in ultra-low dose CT. Eur Radiol. 2017;27(5):2047-54.
27. Vonder M, Pelgrim GJ, Meyer M, Henzler T, Oudkerk M, Vliegenthart R. Dose reduction techniques in coronary calcium scoring: The effect of iterative reconstruction combined with low tube voltage on calcium scores in a thoracic phantom. Eur J Radiol. 2017;93:229-35.
28. Willemink MJ, Takx RAP, De Jong PA, Budde RPJ, Bleys RLAW, Das M, et al. The impact of CT radiation dose reduction and iterative reconstruction algorithms from four different vendors on coronary calcium scoring. Eur Radiol. 2014;24(9):2201-12.
29. den Harder AM, Wolterink JM, Willemink MJ, Schilham AMR, de Jong PA, Budde RPJ, et al. Submillisievert coronary calcium quantification using model-based iterative reconstruction: A within-patient analysis. Eur J Radiol. 2016;85(11):2152-9.
30. Szilveszter B, Elzomor H, Károlyi M, Kolossváry M, Raaijmakers R, Benke K, et al. The effect of iterative model reconstruction on coronary artery calcium quantification. The International Journal of Cardiovascular Imaging. 2016;32(1):153-60.
31. Kubrick S. 2001: A Space Odyssey. United States: Metro-Goldwyn-Mayer; 1968.
32. Wachowskis. The Matrix. United States: Warner Bros. (United States); 1999.
33. Dege S. Artificial intelligence: Are machines taking over? Interview with Toby Walsh, professor of artificial intelligence at the university of New South Wales, Australia. Deutsche Welle 10 July 2019. https://www.dw.com/en/artificial-intelligence-are-machines-taking-over/a-49512596. Retrieved 6 June 2020.
34. Lesh N, Marks J, Rich C, Sidner C. "Man-Computer Symbiosis" Revisited: Achieving Natural Communication and Collaboration with Computers. IEICE Transactions. 2004;87-D:1290-8.
35. Licklider JCR. "Man-Computer Symbiosis" in transactions on Human Factors in Electronics, 1960. Volume HFE-1, pages 4-11. MIT Computer Science and Artificial Intelligence Laboratory. Retrieved 6 June 2020.
36. Ranschaert ER, Morozov S, Algra PR. Artificial intelligence in medical imaging : opportunities, applications and risks. 2019.

CHAPTER 10

Summary

The aim of this thesis was to evaluate the performance and accuracy of several technological advancements within the CT acquisition chain. Hereby, the influence of "patient positioning", "scan and contrast injection tailoring to the individual patient", "patient scanning" and "image reconstruction" on scanning protocol optimization was highlighted. An overview of technological developments over the past five decades was presented and considerations in optimization within the imaging chain, whether or not based on artificial intelligence (AI) software, were discussed. The accuracy of an automated patient positioning system was explored and further protocol optimization by technological developments in data acquisition and data (post-)processing was assessed. While the optimization process executed by humans can be time consuming and prone to errors, the process can be automated, standardized and reproducible with the aid of technological developments. Thereby, a knowledge base can be used to make the best use of the latest innovations for a given diagnostic question and could support the user in using the most appropriate protocol. Overall, these technological developments provide increasingly accurate and optimized CT exams. From these findings the development of a "knowledgeable" CT scanner are presented.

Part I (**Chapter 2**) focused on the technological developments in CT over the past 50 years and their influence on radiation dose and image quality. In the early years of CT scanning, technological developments were mainly introduced to reduce scan times, while later the focus was more on optimization of the scanning protocol. At first, a CT scan was performed with a stationary scanner table while the x-ray tube translated-rotated around the patient. Exam times could be several minutes, and the slice thickness was around 5–10 mm. The introduction of spiral CT in the late 1980s opened up new clinical imaging possibilities, like imaging of complete sub volumes of the lungs in a single breath hold. Another breakthrough came in the late nineties with multi-detector CT. From then on, scanning protocols evolved to imaging large volumes with isotropic image resolution, ECG-correlated image reconstruction, decreased scan times, and radiation dose optimization with the aid of automatic exposure control (AEC). The introduction of dual source CT (DSCT) and wider area detectors not only decreased scan times, but also made dual energy or spectral imaging and dynamic scanning possible. Within the optimization process, the user's influence has increased, while automated tools were integrated to assist in the optimization process. There is an interrelation between radiation dose and image quality for many acquisition and reconstruction parameters, making them more complicated to adjust individually and more difficult to comprehend. Especially when they are part of automated algorithms and, likely, in the near future controlled by AI. In the end, technological improvements and automated tools, combined with attention to the human side by the radiographer, will lead to the optimal scanning procedure.

Part II focused on the assessment of accuracy in automated patient positioning in CT with the aid of a 3D camera for body contour detection. The importance of proper patient positioning has not changed over the years. The image quality with respect to spatial, contrast and temporal resolution are best at the center of the CT scanner, due to the increased influence of the fan angle and bowtie filter at off-center positions. Moreover, positioning of a patient away from the isocenter directly affects the patient's size and shape on a CT localizer radiograph. A magnified patient width on the localizer subsequently increases the applied radiation dose when automatic exposure control is applied. Vice versa, a reduced patient width on the localizer will decrease the applied radiation dose and might result in suboptimal image quality. In **Chapter 3**, the accuracy of automated adult patient positioning with a 3D camera for body contour detection was assessed and compared to manual positioning by radiographers. Median (IQR) table height deviation, for all body parts combined, was 13.2 (17.0) mm for patients (n=423) positioned by radiographers and 6.1 (7.0) mm for patients (n=254) positioned by a 3D camera ($p<0.05$). Therefore, a 3D camera for body contour detection allows for accurate patient positioning and outperformed radiographers. The 3D camera demonstrated less extreme deviations from the ideal table position for all body parts than was seen in the group of patients positioned by radiographers. As the algorithm was not yet applicable to pediatric patients, due to their different body proportions compared to adults, an algorithm training was performed to improve this. With the adaptations made, automatic positioning of pediatric patients was evaluated (**Chapter 4**). Optimal positioning of pediatric patients can be quite challenging, partly because of the wide variation in body proportions. In addition, it is more difficult to estimate the patient's center when they need to be placed in fixation aids such as a baby cradle or a vacuum cushion due to lack of cooperation. It was concluded that a 3D body contour detection camera allows for accurate positioning of pediatric patients in CT. The 3D camera can assist the radiographer in positioning pediatric patients, especially in cases where no fixation aids are used. Positioning patients in a fixation aid is feasible with a 3D camera, but evaluation of possible improvements in positioning accuracy was limited by the small sample size. Radiographers will continue to play an important role and remain indispensable for optimization of radiation dose and image quality through optimized adult and pediatric patient positioning. Especially in (exceptional) situations that deviate from common cases, like in patients with physical constraints or non-cooperative patients.

In **Chapter 5,** the results of the influence of the kind of breath hold (inspiratory or expiratory) on the positioning accuracy are presented. The results of this study demonstrated a difference for the ideal table height between the inspiratory and expiratory breathing state ($p<0.05$). The 3D camera allows for more accurate patient positioning when the camera image and the subsequent CT scan are acquired in the same breath-

ing state ($p<0.05$). It is recommended to perform an expiratory planning image when acquiring a CT exam where both an inspiratory and expiratory thoracic scan is required.

Part III focused on improvement of CT acquisition and reconstruction techniques by using several technological developments.

Cardiovascular CT acquisition protocol development and optimization in pediatric patients, including newborns, is often challenging. This is due to non-cooperative patients, the complexity and variety of diseases, small patient sizes and the relatively large attention for dose minimization. Motion artifacts caused by voluntary and involuntary motion are most frequently seen in cardiac imaging with high heart and respiratory rates. In **Chapter 6**, the optimization of performing cardiovascular CT in pediatric patients with a DSCT is described. Options for acquisition and reconstruction optimization, contrast agent injection and timing in children, and the possible effects of the optimizations on the radiation dose and image quality are highlighted. Despite excellent spatial and temporal resolution, CT is generally not the modality of first choice for thoracic cardiovascular evaluation in pediatric patients due to the use of ionizing radiation. Technological developments, like DSCT, have reduced radiation dose substantially. DSCT also makes it possible to visualize the complex anatomy that helps determine the treatment policy. For optimization of pediatric scan and injection protocols, it is not recommended to "just copy" the parameters of adult protocols. Rather, optimization in pediatric CT protocols requires the knowledge and skills of a whole team, consisting of the radiographer, radiologist and medical physicist, to optimize CT scans in pediatric patients.

Quantified image data is often used in the analysis of CT scans. If adjustments are made in the scanning and reconstruction domain, other than required for the quantified data, the quantification might be affected. In **Chapter 7**, a new reconstruction method used in the quantification of calcium in the coronary arteries was assessed. The most common strategy of quantifying coronary artery calcifications is using the coronary calcium score (CACS) with the Agatston method. Recent guidelines still adhere to the fixed tube voltage of 120 kVp in combination with an imaging method using filtered back projection (FBP), or iterative reconstruction with 100 kVp acquisition (after site and literature validation). However, there is an important argument for the use of lower, or even patient specific, tube voltages: the need to reduce the radiation dose. Lowering the tube voltage may decrease the radiation dose in CACS at the expense of inconsistent scores because CT numbers, expressed in Hounsfield units (HU), are energy dependent. In this case, the standard calcium score threshold should be made tube voltage specific. By introducing a new reconstruction technique, the so-called "calcium-aware image reconstruction", it should be possible to scale calcium CT numbers according to the CT numbers that would have been measured at 120 kVp. This should make it possible to obtain images with a reduced radiation dose while maintaining the Agatston score and risk assessment potential. The conclusion of the study is that the calcium-aware recon-

struction technique allows for consistent CT numbers with comparable calcium scores when varying the tube voltage. Less consistency was observed with small, low-density calcifications. Automatic reduction of the tube voltage resulted in a dose reduction of up to 22%.

With the introduction of spiral CT and the continuously increasing detector, the overranging effect increased too. Hereby, the radiation dose to the patient increased. In **Chapter 8**, the efficacy of a renewed dynamic collimator in a third-generation dual source CT (DSCT) scanner was assessed and the improvements compared to the second-generation scanner were determined. The results of the study demonstrated that overranging dose is to a large extent blocked by the dynamic collimator and the efficacy is strongly improved within the third-generation DSCT scanner. Especially when using fast scan speed, i.e. a high pitch value, often used in imaging of pediatric patients, optimization in radiation dose is obtained with the use of the renewed dynamic collimator.

CONCLUSIONS

In conclusion, technological advancements, like a 3D camera for body contour detection, allows for a patient specific CT examination and assist users with the deployment of new technologies. Advantages and disadvantages of several insights in the CT scan protocol optimization were highlighted. Accurate positioning with the aid of the 3D camera has potential advantages in optimization of radiation dose and IQ. Therefore, consistent diagnostic accuracy is to be expected, as deviations were smaller within the groups of patients positioned with the aid of a 3D camera. Optimization was achieved by incorporating and implementation of newly provided technological developments and building of a knowledge base. Knowledgeable solutions like AI should be embraced, as they can be an important factor in assisting medical healthcare workers. For instance, AI empowered image acquisition may help to automate the acquisition procedure and reshape the workflow. This may also lighten the workload of radiographers. In addition, a high knowledge base among the users of intelligent machines is essential for the development and correct application of AI. The human side remains necessary for further optimization in clinical practice and for future developments. Therefore, optimization is achieved by deploying smart technologies and by merging of knowledge obtained by man and machine, creating opportunities for a "knowledgeable" CT scanner. Ultimately, this may lead to a symbiosis between man and machine.

DUTCH SUMMARY (NEDERLANDSE SAMENVATTING)

Computertomografie (CT) scans worden ingezet om meer inzicht te verkrijgen in ziektebeelden. Sinds de introductie van de techniek begin jaren 70 van de vorige eeuw, zijn er vele technologische ontwikkelingen geweest binnen de CT, met name op het vlak van scansnelheid, resolutie en stralingsdosisreductie. Hierdoor is het aantal parameters en diverse keuzemogelijkheden bij het instellen, vervaardigen en uitrekenen van de CT-beelden sterk toegenomen. Daarnaast zijn deze parameters vaak aan elkaar gerelateerd, waardoor het lastiger is deze individueel aan te passen en de invloed van de aanpassingen op de beeldkwaliteit en dosis te begrijpen. Hierdoor is optimalisatie van CT-scans voor de individuele patiënt vaak een uitdaging. Kunstmatige intelligentie (in het Engels: *artificial intelligence (AI)* genoemd) en geavanceerde software zouden kunnen bijdragen aan het "slimmer" maken van CT-scanners (in het Engels: *the "knowledgeable" CT-scanner* genoemd). Dit maakt het mogelijk om het scan- en reconstructieproces meer te automatiseren, standaardiseren en reproduceerbaar te maken. De CT-scanner ondersteunt hierbij als het ware de uitvoerders van CT-scans in het maken van beslissingen, het accuraat uitvoeren van een CT-scan en het analyseren van beelden. Dit proefschrift beschrijft de prestaties en nauwkeurigheid van verschillende technologische ontwikkelingen binnen de keten van een CT-onderzoek. Hierbij worden de ontwikkelingen op het gebied van patiëntpositionering, het scannen van een patiënt en het aanpassen van het contrast voor een individuele patiënt en de beeldreconstructie uitgelicht. Daarnaast wordt de invloed van de technologische ontwikkelingen op het optimaliseren van een patiënt specifiek CT-onderzoek belicht.

In **deel I** (**Hoofdstuk 2)** worden aan de hand van een literatuurstudie de ontwikkelingen van de afgelopen 50 jaar en hun invloed op de stralingsdosis en beeldkwaliteit beschreven. In de beginjaren van CT werden vooral technologische ontwikkelingen doorgevoerd om de scantijden te verkorten, terwijl later de focus meer op optimalisatie van het scanprotocol lag. In eerste instantie werd een CT-scan uitgevoerd met een stationaire scannertafel, terwijl de röntgenbuis rond de patiënt van positie veranderde door een combinate van translatie en rotatie. De scantijd bedroeg enkele minuten en de "plakdikte" van het beeld was ongeveer 5-10 mm. De introductie van spiraal CT aan het eind van de jaren tachtig van de vorige eeuw zorgde voor nieuwe mogelijkheden, zoals het verder verkorten van de scantijd waardoor een CT-scan van de longen na één ademteug in zijn geheel vervaardigd kon worden. Een andere doorbraak kwam eind jaren negentig met de introductie van *multi-detector* CT waarbij er meerdere rijen met detectoren naast elkaar geplaatst zijn. Hierdoor werd het mogelijk langere afstanden te scannen in dezelfde tijd, dan wel dezelfde afstand in kortere tijd. Doordat de detectoren ook steeds kleiner werden, werd het mogelijk om een hogere resolutie te behalen en

werd het mogelijk om bijvoorbeeld gedetailleerde beeldvorming van de bloedvaten te verrichten. ECG-gecorreleerde beeldreconstructie maakte daarbij afbeeldingen van de kransslagaders mogelijk. De introductie en verdere ontwikkelingen in automatische dosismodulatie zorgde voor een verdere optimalisatie van de dosis en beeldkwaliteit. De introductie van *dual source* CT (DSCT) en detectoren met een nog groter bereik in de longitudinale richting verminderde niet alleen de scantijden nog verder, maar maakte ook respectievelijk spectrale (*dual energy*) beeldvorming en dynamisch scannen mogelijk.

Binnen het proces van optimaliseren van een CT-scan is de invloed van de gebruiker toegenomen en tegelijkertijd zijn geautomatiseerde tools geïntegreerd om hierbij helpen. Er is een verband tussen stralingsdosis en beeldkwaliteit voor veel acquisitie- en reconstructieparameters, waardoor het ingewikkelder wordt om ze individueel aan te passen en te begrijpen. Vooral als ze deel uitmaken van geautomatiseerde algoritmen en in de nabije toekomst waarschijnlijk worden aangestuurd door kunstmatige intelligentie. Uiteindelijk zullen technologische verbeteringen en geautomatiseerde tools, gecombineerd met aandacht voor o.a. de menselijke kant door de medisch beeldvormend deskundige (MBB'er), leiden tot de optimale scanprocedure.

Deel II richt zich op de beoordeling van de nauwkeurigheid van geautomatiseerde patiëntpositionering met behulp van een 3D-camera. Een juiste (centrale) positionering van de patiënt in de CT-scanner is o.a. nodig voor het optimaal functioneren van automatische dosismodulatie en van de buisfilters (de zogenaamde "*bowtie* filters"). De hoogte van de CT-tafel wordt idealiter zo ingesteld dat het isocentrum van de scanner precies samenvalt met het isocentrum van de patiënt; de zogenoemde optimale tafelhoogte. Als een patiënt hoger of lager dan het isocentrum van de scanner gepositioneerd is, dan wordt de patiënt op de planningsröntgenfoto (vervaardigd voorafgaand aan iedere CT-scan) vergroot of verkleind weergegeven. Hierdoor wordt de stralingsdosis die door de automatische dosismodulatie wordt toegepast, verhoogd of verlaagd, wat kan leiden tot respectievelijk een suboptimale beeldkwaliteit of een onnodige dosisverhoging. Het instellen op de optimale CT-tafel hoogte (en dus de positie van de patiënt in de scanner) is in sommige gevallen lastig voor de MBB'er. Recent is automatische patiëntpositionering beschikbaar gekomen met behulp van een 3D-camera die is gekoppeld aan de CT-scanner. Voorafgaand aan een CT-scan wordt een foto gemaakt middels het 3D-camera systeem. Op basis van deze foto wordt een 3D-model van de patiënt gemaakt en is het mogelijk om de juiste positie van de patiënt in de CT-scanner te bepalen. Het doel van ons onderzoek was om de prestaties en nauwkeurigheid van dit systeem te beoordelen. Verder is deze vergeleken met handmatige positionering door een MBB'er. In **Hoofdstuk 3–5** worden de resultaten besproken van ons onderzoek naar geautomatiseerde patiëntpositionering middels het 3D-camera systeem. De resultaten behaald

bij volwassen patiënten zijn gepresenteerd in **Hoofdstuk 3**. De mediane afwijking van de optimale tafelhoogte, voor alle lichaamsdelen samen, was 13,2 mm (*interquartile range* (IQR): 17,0) voor patiënten (n=423) gepositioneerd door MBB'ers en 6,1 mm (IQR: 7,0) voor patiënten (n=254) op de CT-scanners uitgerust met een 3D-camera (p<0,05). Hieruit werd geconcludeerd dat de 3D-camera in staat is om patiënten accuraat te positioneren. Daarnaast toonde de 3D-camera minder extreme afwijkingen van de optimale tafelpositie dan gezien werd bij de groep patiënten gepositioneerd door MBB'ers. Het algoritme dat gebruikt wordt voor de 3D-modellering van de patiënt is voornamelijk getraind op datasets van volwassen patiënten. Vanwege het verschil in lichaamsverhoudingen was het algoritme nog niet geoptimaliseerd voor pediatrische patiënten (kinderen). Om het algoritme te verbeteren is er een additionele algoritmetraining uitgevoerd. Hierna zijn de prestaties van de 3D-camera bij kinderen onderzocht (**Hoofdstuk 4**). Optimale positionering van kinderen kan flink uitdagend zijn. Niet alleen door de grote variatie in lichaamsverhoudingen, maar ook door het gebruik van fixatiemiddelen. Deze worden voornamelijk ingezet bij hele jonge kinderen die minder coöperatief zijn en met meer kans op beweging. Om beweging te beperken wordt er vaak gebruik gemaakt van fixatiemiddelen zoals een speciaal voor CT onderzoek ontwikkelde babywieg of een vacuümkussen. De conclusie van ons onderzoek was dat positionering met behulp van een 3D-camera zorgt voor een nauwkeurige positionering, vooral in gevallen waarbij er geen fixatiemiddelen gebruikt worden. Het positioneren van patiënten in een fixatiemiddel is mogelijk met een 3D-camera, maar de evaluatie van de nauwkeurigheid werd beperkt door de kleine steekproefomvang. MBB'ers spelen sowieso een belangrijke rol bij het positioneren van patiënten met fysieke beperkingen of niet-coöperatieve patiënten.

In **Hoofdstuk 5** worden de resultaten gepresenteerd van het onderzoek naar de invloed van een inademing of uitademing op de nauwkeurigheid van de voorgestelde patiëntpositionering middels een 3D-camera. De resultaten van dit onderzoek lieten zien dat er een verschil in optimale tafelhoogte is voor een inademing en uitademing (p<0,05). Het onderzoek toonde aan dat het benaderen van de optimale tafelhoogte het best bereikt kan worden wanneer het camerabeeld en de daaropvolgende CT-scan worden verkregen in dezelfde ademhalingstoestand. Daarnaast wordt aanbevolen om het 3D-beeld in uitademing te maken bij het vervaardigen van CT-scan van de thorax (borstkas) waarbij zowel een inademing als een uitademing scan nodig is.

Deel III (**Hoofdstuk 6–8**) richt zich op de invloed van technologische ontwikkelingen binnen het acquisitie- en reconstructiegedeelte van een CT-onderzoek en het geven van aanbevelingen voor het optimaliseren van scans met behulp van deze ontwikkelingen. In **Hoofdstuk 6** is de optimalisatie van een cardiovasculair scan bij kinderen beschreven. Hierbij zijn mogelijkheden voor acquisitie- en reconstructieprotocol

optimalisatie, het belang van goede patiëntpositionering, contrastinjectie en timing en de mogelijke effecten op de stralingsdosis en beeldkwaliteit benoemd. Ondanks de uitstekende ruimtelijke en temporele resolutie is een CT-scan vaak niet de eerste keuze voor thoracale en cardiovasculaire diagnostiek bij kinderen. We beschreven hoe kennis van recente verbeteringen in DSCT enkele van de belangrijkste nadelen van CT, zoals de stralingsdosis, hebben verminderd. Tevens maakt DSCT het mogelijk om de complexe anatomie goed in beeld te brengen; wat weer verder kan helpen in het bepalen van het behandelbeleid. Optimalisatie van CT-scans bij pediatrische patiënten wordt dan ook voornamelijk behaald door de kennis en kunde van een heel team, bestaande uit de MBB'er, radioloog en klinisch fysicus. Scan- en reconstructieparameters die gebruikt worden voor volwassenen 'gewoon kopiëren' naar scanprotocollen voor kinderen wordt dan ook niet aangeraden.

In CT-scans wordt vaak gebruik gemaakt van gekwantificeerde beelddata. Als er aanpassingen gedaan worden in de manier van scannen of reconstrueren, dan heeft dit invloed op de resultaten. In **Hoofdstuk 7** wordt een nieuwe reconstructiemethode beoordeeld die gebruikt wordt bij het kwantificeren van kalk (calcium) in de kransslagaders. De meest gebruikelijke manier voor het kwantificeren van verkalkingen in de kransslagaders of coronaire slagaders is de Agatston coronaire calcium score (CACS). Middels deze score is het mogelijk om aan de hand van de gemeten hoeveelheid calcificaties een risico inschatting te maken op coronaire hartziekten. Recente richtlijnen houden (nog steeds) vast aan een buisspanning van 120 kVp in combinatie met een reconstructiemethode die gebruik maakt van gefilterde terug projectie (*filtered backprojection,* FBP). Volgens de richtlijnen van de "S*ociety of Cardiovascular Computed Tomography"* kan een iteratieve reconstructietechniek met 100 kVp-acquisitie gebruikt worden, mits deze gevalideerd is in het eigen instituut. Er is echter een belangrijk argument voor het gebruik van een lagere, of zelfs patiënt specifieke, buisspanning: de noodzaak om de stralingsdosis te verlagen door optimalisatie. Echter, het verlagen van de buisspanning in CACS kan ten koste gaan van inconsistente calcium scores omdat CT-nummers, uitgedrukt in Hounsfield-eenheden (*Hounsfield units,* HU), energieafhankelijk zijn. Door de invoer van een nieuwe reconstructietechniek, de zogenoemde "calcium bewuste beeldreconstructie", is het mogelijk om CT-nummers van calcium te reconstrueren die zouden zijn gemeten bij 120 kVp. Hierdoor zou het mogelijk moeten zijn om beelden te verkrijgen met een verlaagde stralingsdosis, terwijl de Agatston-score en het potentieel van de risico inschatting behouden blijven. Ons onderzoek toonde aan dat, dankzij de "calcium bewuste beeldreconstructie" techniek, nauwkeurigere CT-nummers en vergelijkbare calcium scores behaald werden als bij de standaard buisspanning van 120 kVp. Echter, er werd minder consistentie waargenomen bij kleine verkalkingen met een lage dichtheid. Automatische verlaging van de buisspanning resulteerde daarnaast in een dosisverlaging tot 22%.

Met de introductie van de spiraal CT en het steeds langer worden van de detector in de lengterichting van de patiënt, nam het zogenaamde "overstralingsgebied" (*overranging*) toe. Hierdoor nam ook de stralingsdosis voor de patiënt toe. Deze stralingsdosis kan gereduceerd worden met een dynamische collimator voor de röntgenbuis. In **Hoofdstuk 8** is de werkzaamheid van zo'n collimator in een derde generatie DSCT-scanner onderzocht, waarbij er ook bekeken is of deze beter presteerde dan de dynamische collimator in de tweede generatie DSCT-scanner. De resultaten toonden aan dat de verbeterde dynamische collimator ongeveer 50% van de overkoepelende dosis blokkeert. In vergelijking met de scanner van de tweede generatie is de verbeterde dynamische collimator beter in staat om de *overranging* dosis af te schermen, ook als er gebruik gemaakt moet worden van een hoge scansnelheid.

CONCLUSIES

Technologische ontwikkelingen, zoals de 3D-camera en nieuwe beeldreconstructietechnieken, helpen de gebruiker om een CT-onderzoek te optimaliseren voor een individuele patiënt. Nauwkeurige positionering met behulp van de 3D-camera heeft potentiële voordelen bij het optimaliseren van de stralingsdosis en de beeldkwaliteit. Een 3D-camera lijkt dan ook een consistente diagnostische nauwkeurigheid te bieden. Bij het positioneren van zowel volwassenen als kinderen geldt dat MBB'ers een belangrijke rol blijven spelen, vooral als het gaat om uitdagende patiënten zoals niet-coöperatieve patiënten.

Optimalisatie van een CT-scan zal bereikt worden door het implementeren van technologische ontwikkelingen en door de ontsluiting van de door mens en machine verkregen kennis, ondersteund door slimme technologieën. Als het ware door het "intelligenter" (*"knowledgeable"*) maken van een CT-scanner. Slimme oplossingen zoals AI moeten worden omarmd, omdat ze een belangrijke rol kunnen spelen bij het helpen van medische zorgverleners. AI-gestuurde beeldacquisitie kan bijvoorbeeld helpen om de acquisitieprocedure te automatiseren en de huidige manier van werken opnieuw vorm te geven. Mogelijk verlicht dit ook de werklast. Daarnaast is kennis over de werking van "intelligente" machines essentieel voor gebruikers om te zorgen voor verdere ontwikkeling en correcte toepassing van AI. Over het algemeen leveren de ontwikkelingen nauwkeurigheid, efficiëntie en de mogelijkheid om de blootstelling aan straling te verminderen. De menselijke kant blijft echter noodzakelijk voor het verder optimaliseren van processen in de klinische praktijk en bij toekomstige ontwikkelingen. Optimalisatie wordt daarom bereikt door het inzetten van slimme technologieën en door het samenvoegen van door mens en machine verkregen kennis, waardoor kansen ontstaan voor een "intelligente" CT-scanner. De ontwikkelingen gepresenteerd in dit

proefschrift tonen aan dat de eerste stappen in het proces tot een "perfecte symbiose tussen mens en machine" zijn gezet, maar dat nog vele stappen zullen (moeten) volgen.

LIST OF PRESENTATIONS AND PUBLICATIONS

Presentations and publications

2005
- Educational presentation on RSNA, Chicago: "Automated tube current modulation: Just switch it on, or is there more to it?!"

2010
- Educational presentation on ECR, Vienna: "Triple rule out, what's the fuss all about? Full thorax CT angiography on the Second generation dual source CT: an evolutionary road"

2011
- Educational exhibit on ECR, Vienna: „Ready? Set. Go! Low contrast agent and radiation doses with artifact free, high speed CTA of the aorta"

2011
- Educational exhibit on RSNA, Chicago: "Implementation of New CT Applications in Daily Practice in Order to Improve Workflow and to Take Full Advantage of the Available Dose Reduction Techniques without Compromising Diagnostic Image Quality" ***(Certificate of Merit)***

2012
- Educational presentation on RSNA, Chicago: "You just received an important CT update, what do you do? Guidelines on how to deal with redefined tube current modulation (TCM) curves"
- Interview "CARE kV Allows a Reduction of Radiation Dose" published in SOMATOM Sessions of Siemens Healthineers, RSNA 2012 edition – Issue 31.

2013
- Educational presentation on ECR, Vienna: "128-slice dual source CT in pediatric CT: technological improvements, dose reduction and challenges in robust protocol"
- Scientific presentation on ECR, Vienna: "Improved CT detector technology with less electronic noise: potential for dose reduction?"
- Educational presentation on RSNA, Chicago: "Multi Planar Reformations (MPR) and Three-dimensional (3D) imaging with 128-slice multidetector CT of head and spine injuries in the emergency room: a pictorial review"

2014
- Oral presentation on ESPR, Amsterdam: "Cardiovascular and Thoracic Imaging in Babies and Toddlers – Tips, Tricks & Traps"
- Educational presentation on RSNA, Chicago: "Third Generation Dual Source Scanner for Pediatric Thoracic and Cardiac CT: Technological Improvements and Challenges in Robust Protocol Design" ***(Certificate of Merit)***

2015
- ECR – Refresher course "CT from A to Z – Tips and Tricks for CT optimisation"

2016
- "Cardiovascular Imaging in Pediatric Patients Using Dual Source CT" in JCCT, October 2015 (doi: 10.1016/j.jcct.2015.10.003)
- "Niet de laagste, maar de juiste dosis" - First published on http://sie.ag/1LL6Eor and edited in second publication on https://www.mit-online.nl/niet-de-laagste-maar-de-juiste-dosis/

2017
- ECR - Refresher course "Safety in CT: dose minimisation and beyond"
- "Efficacy of a dynamic collimator for overranging dose reduction in a second- and third-generation dual source CT scanner" in European Radiology, January 2017 (DOI: 10.1007/s00330-017-4745-8)
- Book chapter "Computed Tomography" in "The gentle way: the art of paediatric imaging" publiced by Euopean Society of Radiology (ISBN: 978-3-9504388-2-6)
- Master thesis presentation – Inholland university of applied sciences "De rol van dynamische 4DCTA in popliteal artery entrapment syndrome (PAES)" (in Dutch).

2018
- ECR - Refresher course "Optimising Computed Tomography: Optimising Radiation Dose and Image Quality"
- SCCT 2018 – Texas "Automated Patient Positioning in Cardiac CT: Accuracy of a 3D Camera Body Contour Detection System and Analysis of Optimal Patient Position"
- Radiologendagen "De Rol van Dynamische 4DCTA in Popliteal Artery Entrapment Syndrome (PAES)" and "Automated Patient Positioning in CT: Accuracy and Effect on Radiation Dose of a 3D Camera for Body Contour Detection"
- NVMBR Jaarcongres: "De Rol van Dynamische 4DCTA in Popliteal Artery Entrapment Syndrome (PAES)" and "Automated Patient Positioning in CT: Accuracy and Effect on Radiation Dose of a 3D Camera for Body Contour Detection"
- Parkstad CT Symposium "4D Imaging met CT"
- "Accuracy of automated patient positioning in CT using a 3D camera for body contour detection" in European Radiology, October 2018 (DOI: 10.1007/s00330-018-5745-z)
- CT at Sea - Helsinki: "Optimising CT – Optimising Radiation Dose and Image Quality"
- Interview "3D Measurement Camera and the Personal Approach in Radiology" published in SOMATOM Sessions of Siemens Healthineers, RSNA 2018 Edition – Issue 38

2019 · Organization and presentation Nederlands CT Netwerk - Pediatric CT Congres, Rotterdam "Pediatrie: CT Scan Technieken"
· ECR – Scientific oral presentation "Coronary Calcium Scoring in CT with a Calcium-aware Image Reconstruction Technique: Dose Reduction by Lowering X-ray Tube voltage"

2020 · "Dose reduction for CT coronary calcium scoring with a calcium-aware image reconstruction technique: a phantom study" in European Radiology. 2020. European Radiology, 30(6), p. 3346-3355
· "Automated patient positioning in CT using a 3D camera for body contour detection: accuracy in pediatric patients" in European Radiology. 2020. DOI: 10.1007/s00330-020-07097-w.
· "Technological developments of x-ray computed tomography over half a century: User's influence on protocol optimization" in European Journal of Radiology. 2020. https://doi.org/10.1016/j.ejrad.2020.109261

2021 · Book chapter "CT bij kinderen" in "Computer Tomografie" (in Dutch). Online publication expected mid 2021.

2010 - 2017 Several contributor to www.DSCT.com as expert member in the field of Computed Tomography education

As co-author:

- de Weert TT, de Monye C, Meijering E, et al. Assessment of atherosclerotic carotid plaque volume with multidetector computed tomography angiography. Int J Cardiovasc Imaging. 2008;24(7):751-9.
- Vermeule W, Booij R, et al. How "Tiny" Problems Get Solved: Improvements in Pediatric CT with the Introduction of a Second Generation Dual Source CT (conference paper RSNA 2009).
- Dijkshoorn ML, van Straten M, Booij R, et al. Understanding Radiation Dose and Dose Determining Parameters in Multidetector CT (conference paper RSNA 2010).
- De Roode E, Dijkshoorn ML, Booij R, et al. CT Image Quality: Beyond the Choice of kV and mAs (conference paper RSNA 2010).
- Dijkshoorn ML, Booij R, et al. Understanding Contrast Enhancement in Multidetector CT (conference paper RSNA 2010).
- Siebelt M, van Tiel J, Waarsing JH, et al. Clinically applied CT arthrography to measure the sulphated glycosaminoglycan content of cartilage. Osteoarthritis Cartilage. 2011;19(10):1183-9.
- Ouhlous M, Dijkshoorn ML, Booij R, Moelker A. Dual-Source CT of Cardiac and Extracardiac Anomalies in Newborns (conference paper RSNA 2011).

- Odink A, Rossius M, Booij R, Schaefer-Prokop C, Hartmann I. Lung Perfusion Defects on Dual-Energy Computed Tomography (DECT): Review of Morphology and Differential Diagnosis" (conference paper RSNA 2011).
- Dijkshoorn ML, Booij R, et al. Understanding Kilovoltage in Multidetector CT (conference paper RSNA 2012).
- Lip-Pauwels W, Dijkshoorn ML, Booij R, et al. Optimizing 3-Phase Liver CT in Hepatocellular Carcinoma: Achieve better lesion depiction and reduce radiation dose and contrast media (conference paper ECR 2012).
- van Tiel J, Siebelt M, Waarsing JH, et al. CT arthrography of the human knee to measure cartilage quality with low radiation dose. Osteoarthritis Cartilage. 2012;20(7):678-85.
- Saru RG, Dijkshoorn ML, Booij R, et al. Pulmonary Blood Volume Imaging with Dual Energy Computed Tomography in Pediatric Patients with Congenital Heart Disease: State of the Art (conference paper RSNA 2013).
- Dijkshoorn ML, Booij R, van Straten M. Optimization of soft-tissue imaging in CT with the aid of additional tin filtration (conference paper RSNA 2015).
- Maaskant L, Booij R, et al. Dual Energy Computed Tomography in post-(T)EVAR patients: advantages of the Virtual Non-Contrast CT and the Iodine Overlay Measurements (conference paper RSNA 2015).
- Maaskant L, Booij R, et al. Dual Source Dual Energy CTA for the Detection of Endoleaks after (Thoracic) Endovascular Aneurysm Repair (conference paper RSNA 2016).
- Lubbers MM, Kock M, Niezen A, et al. Iodixanol versus Iopromide at Coronary CT Angiography: Lumen Opacification and Effect on Heart Rhythm-the Randomized IsoCOR Trial. Radiology. 2017:162779.
- De Groen JJ, Booij R, Dijkshoorn ML, van den Berg A. Exploring the Pros and Cons of Post-Processing in Contrast-Enhanced Dual-Energy Neck CT Scans (conference paper ECR 2018).
- Dijkshoorn ML, Booij R, van Straten M. There is metal in my scan volume, what should I do with my scan protocol? A practical guide to cope with metal in dual source CT scans (conference paper ECR 2018).
- Van der Werf N, Booij R, Budde RPJ, Leiner T, Willemink MJ, Greuter MJW. CT tube voltage independent reconstruction of coronary calcium scores at varying heart rates: a dynamic phantom study (conference paper SCCT 2020).

PHD PORTFOLIO

1. PhD training		
	Year	**Workload (Hours/ECTS)**
General courses		
- Biomedical English Writing and Communication	2017	3.0
- Research Integrity	April 2018	0.3
- Statistics	2017	2.0
- BROK ('Basiscursus Regelgeving Klinisch Onderzoek')	Maart 2018	1.5
Specific courses (e.g. Research school, Medical Training)		
- Excel 2010 Workshop: Basic	2017	0.3
- Excel 2010 Workshop Advanced	2017	0.3
- Systematic literature review + Endnote Workshop	2017	1.0
- Photoshop and Illustrator	2019	0.3
Seminars and workshops		
- Training "Vakinhoudelijke artikelen beoordelen" NVMBR	2016	20 hours
- "Webinar AI op de radiologie" Siemens Healtineers	2020	2 hours
Presentations		
- Zie (inter)nationale conferences	2017-2020	
(Inter)national conferences		
- 1. RSNA 2017 (scientific poster presentation)	2017	1 ECTS
- 2. ECR 2018 (RC course)	2018	1 ECTS
- 3 SSCT Texas (poster presentation)	2018	1 ECTS
- 4. Radiologendagen (two oral presentations)	2018	2 ECTS
- 5. NVMBR CT symposium (two oral presentations)	2018	2 ECTS
- 6. Talk @ CTatSea2018 in Helsinki, Finland	2018	2 ECTS
- 7. Seminar master MIRO Haarlem	2018	2 ECTS
- 8. Parkstad CT Symposium Heerlen	2018	2 ECTS
- 9. Kinder CT Congres (organization and presentation)	2019	2 ECTS
- 10. ECR 2020 (Online congress; RC course)	2020	1 ECTS
Other		
- Several obligated e-learnings and practical training like BLS, Coaching, patient safety, etc.	2017-2020	2 ECTS

2. Teaching		
	Year	**Workload (Hours/ECTS)**
Lecturing		
- Masterclass "CT(A) Thoracic and Cardiac imaging in Child and Adult at Emrin and Inholland	2017-2020	135 hours
- Post-graduate courses at Emrin and Fontys	2017-2020	120 hours
- CT Technique courses for Bachelor CT students at Zorgacademie Rotterdam	2017	10 hours
- Clinical courses at Erasmus MC	2017-2020	40 hours
- E-learning lecture + multiple choice questions ESR "Education on Demand"	2018	10 hours
- Post-graduate course CT in Curaçao	2020	70 hours
Supervising practicals and excursions, Tutoring		
- Radiographers (students) in scientific presentations and teaching courses (practicals and educationals)	2017-2020	70 hours
Teaching experience		
• Setting up learning units and objectives of the theoretical and practical learning programme of Computed Tomography for the InService education of radiographers at the Zorgacademie Erasmus MC, Rotterdam		2007
• Teacher of Computed Tomography in clinical practice at the Erasmus MC for radiographers, physicians, radiologists and (medical) students		Since 2007
• Teaching postgraduate education in multislice CT at Emrin and providing masterclasses in CT(A) Thorax and CTA Cardiac (adult & child).		2011-2018
• Providing In-company training in almost every CT aspect preferred		Since 2013
• Teaching at Master Medical Imaging and Radiation Oncology in multislice CT at InHolland university of applied science, providing lessons in CT(A) Thorax and CTA Cardiac (adult & child)		Since 2015
• Invited lectures in CT at the St. Elizabeth ziekenhuis/ Curaçao Medical Center provided by Fontys Hogescholen.		2020
• Invited lecturing at CT Learning in CT(A) Thorax and CTA Cardiac pediatrics		2020

Supervising Master's theses

- Lifelong learning programme Erasmus subprogramme. Multiple thesis guidance (2008-2010):
  - o "Reduction of dose to the female breast with the use of partial and tube current modulated (X-CARE) CT examinations: a phantom and patient study overview"
  - o "The effects of different adaptations of AEC system on patient dose and image quality varying patient size"
  - o "Evaluation and recommendations on image quality and dose with the use of partial CT scanning"
- Afstudeerscriptie MBRT Fontys Hogescholen: "Low voltage, high advantage" door Khang Vu, Korstiaan Spruijt, René Charan (juni 2011)
- Afstudeerscriptie MBRT Inholland Hogescholen: "Low dose, high advantage!?" door Marlies van der Geer, Roeli Zandvliet, Mariëlle Brusse (augustus 2012)
- Afstudeerscriptie MBRT Fontys Hogescholen: "Toepassingen van verschillende sterkten van de mAs-aanpassingscurve" door Merel Albers (juni 2012)
- Afstudeerscriptie MBRT Fontys Hogescholen: "Toepassingen van verschillende sterkten van de mAs-aanpassingscurve bij een CT-onderzoek van volwassen thorax-fantomen" door Barbara Brörmann (juni 2012)
- Afstudeerscriptie MBRT Inholland Hogescholen: "Metaalartefactreductie in het KNO gebied" door Alle Minnema (augustus 2014)
- Afstudeerscriptie Communication and multimedia design, Avans university of applied sciences te Breda: "Fixation in Computed Tomography" door Katie Verschueren (mei 2020)

Other

International Congress participations:

2005 RSNA (Chicago)
2007 SOMATOM World Summit (Berlin)
2009 SOMATOM World Summit (Valencia)
2010 ECR (Vienna) and ISCT (San Francisco)
2011 ECR (Vienna)
2011 RSNA (Chicago)
2012 RSNA (Chicago)
2013 ECR (Vienna)
2013 RSNA (Chicago)
2014 ESPR (Amsterdam)
2014 RSNA (Chicago)
2015 ECR (Vienna) invited lecture
2016 ECR (Vienna) invited lecture
2017 RSNA (Chicago) scientific presenter
2018 ECR (Vienna) invited lecture
2019 ECR (Vienna) scientific presenter
2020 ECR (Vienna) invited lecture (online congress)
(Co-)author of several publications and educational/scientific contributions and regular contributor/speaker at (inter) national symposia like Parkstad (two oral presentations October 2, 2015; one oral presentation October 5th 2018), Dag van Marc (February 10, 2015), NVMBR jaarcongres (2014, 2015, 2018), Radiologendagen (2018), ECR, and RSNA
Leading organization member of the "Pediatric CT Congres" as owner of Nederlands CT Netwerk, January 12, 2019, Rotterdam

Awards and honors

- Certificate of Merit at RSNA, Chicago, Dec. 2011
- Education award 2011, Erasmus MC, Rotterdam, Dec. 2011
- Winner of the international Right Dose Excellence Award 2013, category "Trauma", Siemens Right Dose Image Contest, Chicago, Dec. 2013
- Certificate of Merit at RSNA, Chicago, Dec. 2014
- Employee of the year, Erasmus MC, Rotterdam, Dec. 2016

Reviews

Reviewer for NVMBR, Digital Magazine "MBB'er in Beeld" sinds 2016
Reviewer for Journal of Cardiovascular Computed Tomography (JCCT) October 2016
Reviewer for European Radiology January and June 2020
Reviewer for European Journal of Radiology October 2020

Committees

June 2016 – October 2017	EFRS expert committee member for Medical Imaging (represent: Computed Tomography)
	Contributor to EFRS European Paediatric Dose Collection project (EPDC)

Funding

Individual project agreement (IPA) with Siemens Healthineers: Projects regarding the 3D camera supported workflow at the CT scanner

DANKWOORD

ACKNOWLEDGEMENTS (DANKWOORD)

Beste lezer,

Dank voor het lezen van mijn proefschrift! Of ben je stiekem hier begonnen ☺? Dan wil ik je alsnog uitnodigen om de andere delen van dit boek te lezen. Al is het maar de discussie en de Engelse of Nederlandse samenvatting. Maar zonder gekkigheid…De inhoud van dit boekje was niet tot stand gekomen zonder de hulp van diverse mensen. Mijn dank is dan ook groot! Een aantal wil ik hieronder in het bijzonder bedanken.

Allereerst mijn promotor. Professor Krestin, graag wil ik u bedanken voor het mogelijk maken om als eerste radiologie laborant (MBB'er) in Nederland te mogen promoveren. Ik herinner mij ons gesprek na het kerstfeest van 2012 nog goed. U was direct bereid een PhD traject te steunen, maar u gaf ook terecht aan dat ik eerst maar eens moest proberen een artikel te schrijven. Kijken hoe ik dat proces, met kans op diverse tegenslagen, zou vinden. De gevolgde master en het daaropvolgende PhD traject heb ik als buitengewoon interessant en leerzaam ervaren. Mijn dank aan u is groot!

Professor Prokop, ik ben bijzonder vereerd dat u deel uitmaakt van mijn promotiecommissie! Uw naam was een van de namen waar ik eind jaren negentig van de vorige eeuw als MBB'er op de CT-scan mee in aanraking kwam. Uw boek "Computed Tomography of the Body" heb ik dan ook veelvuldig ingekeken. Dank voor het verder aanwakkeren van mijn "liefde" voor CT.

Professor van der Lugt, beste Aad, ik vind het prachtig om te zien hoe je bent uitgegroeid tot hoogleraar! Ik waardeer het heel erg dat je altijd even tijd neemt om samen te zitten bomen over mijn ambities of ideeën, dan wel even wat te overleggen. Bedankt!

Professor Tiddens, beste Harm, dank voor het deelnemen aan de kleine promotiecommissie. Onze samenwerking gaat inmiddels alweer meer dan tien jaar terug. Je bent altijd geïnteresseerd geweest in de mogelijkheden van CT en vooral ook in hoe we de meeste informatie uit de plaatjes kunnen halen. Ik hoop nog jaren met je te kunnen werken!

Hartelijk dank ook aan de leden van de grote commissie: Prof.dr. Wiro Niessen, prof.dr. Natasja de Groot en dr. Marcel Greuter voor de bereidheid om met mij van gedachten te wisselen over dit proefschrift.

Mijn copromotoren, dr. ing. Marcel van Straten en dr. Ricardo Budde. Jullie zagen het zitten om een MBB'er te gaan begeleiden tijdens het PhD-traject. Ik wil jullie dan ook danken voor jullie inzet en de uitstekende begeleiding! Ik heb erg genoten en veel geleerd van deze periode en dat is voornamelijk jullie verdienste. Dank!
Beste Marcel (van Straten), we ontkomen er op de afdeling niet aan omwille van de duidelijkheid je voornaam te vergezellen van een achternaam. Als fysicus van onze afdeling hadden we al nauw contact en deze samenwerking is alleen maar intenser geworden tijdens mijn PhD traject. Ik heb veel respect voor je nauwkeurigheid en je geduldig gegeven (en soms standvastige) feedback. Natuurlijk waren al die rode markeringen in een manuscript niet altijd leuk; ze waren wel effectief en scherp. Ik kijk ernaar uit om onze samenwerking verder te continueren en verder uit te bouwen.
Beste Ricardo, jij bent medeverantwoordelijk voor het kickstarten van dit PhD traject. Na het behalen van een *certificate of merit* (RSNA 2014) stelde jij voor dat ik het *educational* eens in een artikelvorm zou proberen te gieten. Dit resulteerde uiteindelijk in mijn eerste paper als "eerste auteur". Ook jij was altijd scherp, had goede feedback en mede middels jouw suggesties zijn de papers naar een hoger niveau getild. Dank!

Mijn paranimfen Joyce Kazmierczak en Marcel Dijkshoorn! Onze goede band gaat al terug naar het begin van mijn carrière in het Dijkzigt! Jullie zijn veel meer geworden dan collega's. Wat hebben wij mooie tijden beleefd: Rock Werchter, Pinkpop, diverse concerten, verjaardagen, uitgaan en ga zo maar verder. Laten we hopen dat we in het "Post-COVID-tijdperk" weer vele mooie momenten met elkaar gaan beleven.
Lieve Joyce, jij bent ondertussen al vele jaren een vriendin. Ondertussen niet alleen meer van mij, maar ook van Sandra en de kinderen (tante Joyce). Mijn waardering en respect voor jou is groot. Je hebt genoeg voor je kiezen gehad en bent meer dan een sterke vrouw. Ik ben dan ook verheugd dat je in Gedeon een toffe gozer en fijne partner hebt gevonden! Dank voor de persoon die je bent! Mij rest nu alleen nog maar het volgende woord: Proost!
Marcel! Ook jij bent al weer twee decennia meer dan een collega. Ik heb altijd genoten van onze momenten al discussiërend over de CT. Zelfs tijdens privé momenten kwam dat mooie woord (CT) altijd wel een keer (of honderd) ter tafel. Ik heb in jou een gelijke (lees: vakidioot) gevonden! Maar ook zonder gesprekken over de CT is het natuurlijk gezellig met je. Ik hoop dat we nog vele jaren samen het gebied van CT mogen blijven ontdekken en wie weet kunnen we zelfs de weg plaveien voor verdere ontwikkelingen en implementaties!

Niels van der Werf, eigenlijk kan ik met een woord af: "Mand!"

Maar ja…dat is weer zo kort. Je weet dat ik daar niet van houd ☺. Een paar jaar geleden kwam je bij ons op de afdeling werken. Ik heb altijd genoten van onze (helaas de laatste tijd schaarse) koffie momenten. Even bijkletsen over thuis en natuurlijk over die … kalkjes. Ik heb de momenten van sparren en analyseren en scannen en analyseren en scannen en… als waardevol, maar ook als gezellig ervaren. Een steekje onder water en het terug plaatsen ervan, dan wel een woordgrap waren aan jou wel besteed. Dank voor je hulp, dank voor je samenwerking en dank voor je gesprekken. Laten we er nog vele mooie jaren van maken. Wie weet wat de nabije toekomst brengt … ☺.

Mijn CT-collega's, Annelies, Anneke Hopman, Anneke Koch, Annemarie, Alle, Daan, Danielle van der Zande, Danielle Viallé, Donna, Edwin, Erwin, Floor, Joël, Kelly, Maarten Dirks, Maarten Kremer, Marieke, Martin, Pauline, Richard, Rufi, Sylvia, Tony, Thomas Brands, Thomas de Man, Wilma en Wouter, bedankt voor jullie (in)directe steun tijdens dit traject. Zonder jullie hulp had ik nooit zoveel inclusies gehad. Dank voor jullie medewerking. Jullie zijn een geweldig stel hardwerkende, leuke en fijne collega's! Weet dat ik altijd open sta om eens van gedachten te wisselen over het schrijven van een wetenschappelijk artikel, dan wel om mijn ervaringen van mijn master en het PhD traject te delen.

Natuurlijk wil ik ook mijn dank uitspreken aan onze medisch technici CT: Robbert en Renald. Dank voor jullie technische ondersteuning!

Jolanda Wisselo, jou wil ik bedanken voor de vele fijne gesprekken en steun. Daarnaast was het erg leuk om samen met Marcel en jou het "Pediatrisch CT-congres" in Blijdorp namens het "Nederlands CT Netwerk" te organiseren! Ik ben blij dat ik je destijds hebt "weggekaapt" uit het Haga ☺. Ik hoop dat we nog vele jaren samen zullen werken om de kennis binnen onze CT-unit te behouden en verder te kunnen uitbreiden.

Dank ook aan al mijn andere collega's van de afdeling Radiologie & Nucleaire Geneeskunde! Het was altijd leuk als iemand vroeg hoe het ervoor stond en wat mijn plannen waren voor na het PhD traject. Of de vraag of ik dan "eindelijk eens rustig aan ga doen na de PhD" (het antwoord is dus nee). Lieve Leni, dank voor je begrip als je nachtzuster was en je mij op bepaalde momenten midden in de nacht liet doortypen of fantoom scans liet maken. Dank!

Jolanda Meijer, ik heb je aardig wat "lastig" gevallen met (te lange) mails en gesprekken m.b.t. een carrière als MBB'er met een master of een PhD. Ik heb de (koffie en café/restaurant) gespreksmomenten hierover, met name op de RSNA en ECR, erg gewaardeerd. Ik ga er alles aan doen om zoveel als mogelijk uit mijn "post-PhD carrière" te halen!

Monique de Waard, jou heb ik ook aardig "gestalkt" en gesproken over "wat kan een MBB'er met een PhD". Onze gesprekken hierover, maar ook over allerlei contracten of privézaken, heb ik als prettig en fijn ervaren. Dank je wel! Ik hoop dat we nog vele jaren zo verder kunnen werken.

Professor Vernooij, lieve Meike. Met jou heb ik hele fijne gesprekken gehad. Al toen we (tijdelijk) kamer genoten waren in het Ca-gebouw beantwoorde je met alle geduld mijn vele vragen. In de afgelopen jaren bleef je geïnteresseerd of bereidt tot een gesprek. Dank je wel!

Beste Daniel, ik kon je altijd benaderen met vragen. Vaak gingen ze over statistiek, maar ik heb ook genoten van onze andere gespreksonderwerpen, zoals "hoe pak je dat aan; een PhD?! Jouw tips hebben mij meer inzicht gegeven over hoe ik dit traject moest starten. Daarnaast heb ik alle respect voor hoe je jouw onderzoeksgroep leidt en ben ik blij met mijn toevoeging aan de "Vascular Imaging Group" meetings.

Collega's van het imagingbureau: dank voor jullie hulp bij het anonimiseren van de CT-data van de honderden patiënten. Laurens, dank voor alle hulp en support bij het activeren van mijn account voor de Resto-server. Renée, Milja, Leontien en alle anderen: Dank!

Dear Andreas Wimmer, Ulrike Haberland, Matthias Senn and many others at Siemens Healthineers. It was, and still is, a pleasure to work with you! I really love debating and discussing with you about the "future of CT". Thank you for all the years as a collaboration partner and I hope the next years will be even more fruitful! Vielen Dank!
Michiel de Bruijn en Peter Melger, ik ken jullie inmiddels ook al meer dan twintig jaar. De samenwerking met Siemens Nederland is natuurlijk ook geweldig en ik geniet van onze gesprekken, met name over de toekomst van CT. Aan beide: succes in jullie nieuwe rol binnen Siemens Healthineers en ik ben ervan overtuigd dat we elkaar nog genoeg zullen zien en spreken.

Ton Everaers, ik heb genoten van onze koffiemomenten op Na25! Het was altijd goed om bij te praten, dan wel te horen dat mijn muziek smaak helemaal geen herrie is, maar gewaardeerd wordt! Dank voor het aandragen van andere bands en dank voor je hulp bij het creëren en aanpassen van de figuren voor mijn eerste publicatie. Ik maak nog steeds gebruik van je CT-afbeelding!

Berend, je bent dan al enige jaren niet meer werkzaam, maar als "unithoofd CT" was jij het die destijds een balletje opgooide bij professor Krestin of het niet mogelijk zou zijn dat een laborant/MBB'er zou promoveren. Jij hebt altijd een open blik gehad en ging een uitdaging niet uit de weg. Bedankt voor je enthousiasme en het "kick starten" van het promotie avontuur!

Heren van Symposium Parkstad: Armand en Kris. Kris! Onze samenwerking en gezellige app-gesprekken ervaar ik als een teken van wederzijds respect en daarnaast buitengewoon leuk! Wie weet zitten we gauw een keer met onze zoons op Spa naar het eerste F1 kampioenschap van Max te kijken! Armand, dank voor de mooie samenwerkingen en gesprekken van de afgelopen jaren. Dat er nog vele zullen volgen!

Dank aan de medewerkers van de NVMBR en met name Sija: dank voor je mail wisselingen die we hadden over wat de meerwaarde van een MBB'er met een PhD zou kunnen zijn.

Brechtje en Sabine, jullie vraag om naar Curaçao te gaan voor een post-hbo-cursus CT overviel mij even. Ik heb echter een geweldige tijd gehad daar en ben jullie dankbaar voor hoe alles is gelopen. De samenwerking was fantastisch! Dank ook voor jullie lieve mails en gesprekken aangaande het verloop van mijn PhD.

Thom Roding en Marcel Hakkert, tijdens mijn master of tijdens mijn lessen als gastdocent waren jullie altijd fijne gesprekpartners en toonden jullie oprechte interesse in mijn vorderingen. Ik hoop dat er gauw weer een tijd aanbreekt om elkaar weer in het echt te zien en wie weet weer een seminar bij te wonen! Beste Jelle, dank voor je begeleiding en sturing tijdens mijn master. Ik heb je wijze raad gebruikt tijdens mijn PhD en ik hoop dat dit boekje hiervan een bewijs is. Beste Geert de Vries, dank nogmaals voor de begeleiding bij mijn scriptie en ik wens jou alle succes toe met het zelf afronden van je PhD! Beste Freia, dank voor de fijne mailing de afgelopen tijd en het altijd goed regelen van de diverse bijeenkomsten.

Beste Anne, dank voor de lange samenwerkingen die we hadden op het gebied van post-hbo CT! Ik heb de gesprekken met je over de ontwikkelingen als MBB'er als bijzonder nuttig en leuk ervaren. Ik wens je nog alle goeds toe!

Beste Roos, jij bent nog zo een persoon die ik veel heb "lastig" gevallen…Ik wil je danken voor je geduld met mij, je hulp en natuurlijk voor het doorlezen van de *introduction*, *discussion* en de *summary*. Het heeft mede de definitieve versie vormgegeven. Dank!

Mayjean, super dank voor het checken van diverse tekst onderdelen en de tips! Het heeft zeker bijgedragen aan de verhoging van de leesbaarheid van de tekst!

Channah, dank voor je bereidheid om de drukproef door te nemen. Jij hebt de puntjes op de "i" gezet. Dank!

Medewerkers van Optima, dank jullie wel voor jullie werk! Ik ben super blij met dit resultaat. Erwin, jij bent diegene die vier A4'tjes met ideeën voor de cover en de lay-out kon omzetten naar het prachtige resultaat dat voor je ligt. Ik ben er super blij mee! Dank je wel!

Lieve vrienden, oud-collega's en familie, hier is het dan! Het boekje waar ik al die jaren aan heb gebikkeld is af. Dank voor jullie support!

Roelof, vriend van het eerste uur! Letterlijk zelfs! Ik ken je al 40 jaar. Man, wat een geweldige jeugd heb ik met je beleefd. Onze eerste keer uitgaan, de keren stappen die daarop volgde, de eerste kus van een meisje: wat hebben wij toffe gesprekken gehad. Vaak midden in de nacht met MTV aan of "*Bottom*" en na een bord shoarma, friet met frikandellen en natuurlijk de Grolsch beugel uit de vriezer (wel de timer zetten op 45 minuten!). Diverse ups-and-downs in ons leven: jou kan ik vertrouwen en op jou kan ik bouwen. Je bent een fijne vriend. Helaas woon je nu wat verder weg (al is het nog geen Spanje), maar je bent altijd bereikbaar voor een luisterend oor of een goed gesprek. I love you man!

Roeland: hier is het dan!! Mijn eerste boek! In de middelbare schoolperiode hebben we leuke gesprekken gehad over een boek schrijven. Welke hoofdpersonen erin moesten komen, wat hun namen zouden zijn… Nou…de hoofdpersonen in dit boek zijn dus iets anders dan ik destijds dacht. Ik hoop dat je plezier beleeft aan het lezen van dit boek.

Erik en Mirella, of het nu spelletjes avond was, F1 kijken, of op visite bij jullie op de camping: Gezellig was het altijd! Een aangename afleiding tijdens deze periode. Dat er nog vele mooie dagen en avonden zullen volgen. "Huppethee!"

Mijn vader, moeder en grote zus. Lieve pa, jij bent de liefste vader die ik mij wensen kan. Je staat altijd voor ons klaar, je bent lief en erg begaan met iedereen. Hoe jij bent omgegaan ten tijde van ma haar ziekte vind ik bewonderenswaardig. Heen en weer naar de Daniel den Hoed, de vele bestralingen, je stond altijd voor haar klaar. Lieve pa, ik hou van je en ik hoop dat je nog vele jaren gezond en wel bij ons blijft!

Lieve ma, ondanks dat je dit nooit zult lezen, wil ik het woord aan je richten. Zonder jou en pa zou ik nooit geworden zijn zoals ik ben. En dat bedoel ik zeker positief! Je was een lieve moeder die mij altijd steunde en stimuleerde bij alles wat ik wilde ondernemen. Lieve ma, ik mis je nog iedere dag. De afbeelding in "het oog van de CT -scanner" aan het begin van het "Dankwoord" is een eerbetoon aan jou.
Lieve Mirella, wat is het fijn dat we af en toe samen kunnen lunchen in het Erasmus MC. Even bijkletsen over thuis en werk. Je bent een fijne zus en een lieve schat. Ik houd van je!

A special thanks to The Editors, Nirvana, Foo Fighters, Daft Punk (Tron Legacy!!), Tool and Radiohead! Your music pulled me through all the difficult moments!

Last, but not least: Mijn gezin! Lieve, lieve Sandra, woorden kunnen niet beschrijven hoeveel ik van je houd en wat je betekent voor me. Je bent een ontzettende schat en een lieve moeder. Sorry voor al dat eindeloze getik (of geram) op dat toetsenbord als ik naast je in bed zat te werken aan mijn master en PhD. Of die tientallen keren dat ik midden in de nacht zachtjes probeerde naar bed te sluipen (met zoeklicht) na een avondje doorwerken aan een artikel. I love you!

Lieve Julia en Timo, ondertussen zijn jullie tieners! Interesse voor de inhoud van dit boekje is nog een "ver van jullie bed show", maar wie weet mag het op de Engelse boekenlijst? Weet dat ik onwijs veel van jullie houd en ik erg van jullie geniet. Jullie zijn de liefste kinderen die ouders zich kunnen wensen. Liefs, papa.

Mocht ik iemand vergeten zijn persoonlijk te noemen: mijn excuus!

Dan sluit ik dit mooie traject af met de volgende woorden: Werk hard. Durf te dromen. Durf paden te betreden die onbegaanbaar lijken. Durf jezelf uit te dagen! Of zoals Michael Jordan het mooi verwoord heeft: "*You have to expect things of yourself before you can do them*". Het harde werken wordt vast en zeker een keer beloond.

Lange dagen en aangename nachten! En …vergeet niet nog even op zoek te gaan naar de Easter eggs in o.a. de cover ☺.

Ronald Booij
December 2020
Rotterdam

ABOUT THE AUTHOR

Education	
1997-2000	Erasmus MC In-Service Education Radiographer
2003-2004	Postgraduate Computed Tomography
2006-2007	Postgraduate in supervisor in health care
2014-2017	MSc (Master Medical Imaging & Radiation Oncology)

Professional Experience
Since 1997: Department of Radiology and Nuclear Medicine, Erasmus MC, Rotterdam, The Netherlands, specialist in CT technology, CTA, pediatric, cardiac, bringing CT innovations to the clinic.

Ronald Booij was born on April 17, 1980 in Rozenburg, The Netherlands. After graduating the HAVO at the Angelus Merula in Spijkenisse in 1997, he started the in-service education Radiographer at the Dijkzigt hospital (now Erasmus MC). Already during the second year of his education, he fell "in love" with Computed Tomography (CT) and he became a certified radiographer in 2000. He obtained postgraduate degrees in CT (2004) and in "supervisor in health care" (2007). It was also from 2007 that he became teacher in CT at the in-service education at Erasmus MC. In 2009 he became the coordinator of Research & Innovation of the unit CT. From 2011, he became teacher of several postgraduate education in CT in The Netherlands and a regular contributor to (inter)national conferences. He was a EFRS expert committee member for medical imaging, representing CT. In April 2017 he obtained the degree of Master of Science (MSc) in medical imaging & radiation oncology at the Inholland university of applied sciences in Haarlem, The Netherlands. Subsequently, he started his PhD project at the Erasmus MC Rotterdam, entitled: the "knowledgeable" CT scanner under supervision of professor Gabriel Krestin (head of Radiology & Nuclear Medicine department) which resulted in this thesis.

Ronald married Sandra Voogdt on September 15, 2006 and they have two children: Julia (February 2008) and Timo (December 2009).